Stability and Protection Enhancement of Power Systems using SMES and SFCL Considering High Penetration of Renewable Energy Sources

Doctor of Philosophy Dissertation

Stability and Protection Enhancement of Power Systems using SMES and SFCL Considering High Penetration of Renewable Energy Sources

再生可能エネルギー源が大量普及した電力システムにおける SMES と SFCL を用いた安定性と保護の強化

Emad Abdelnabi Mohamed Younis

(Student ID: 16595506)

A dissertation presented for the degree of Doctor of Philosophy in

Electrical Engineering

Department of Engineering

Graduate School of Engineering

Kyushu Institute of Technology

Japan

March 2019

再生可能エネルギー源が大量普及した電力システムにおける SMES と SFCL を用いた安定性と保護の強化

イマド アブデルナビ モハメド ユニス

(学生番号: 16595506)

指導教員　三谷康範

博士学位論文

九州工業大学　工学府　　工学専攻

平成 31 年度

Emad Abdelnabi Mohamed Younis
Kyushu Institute of Technology
Department of Electrical and Electronics Engineering
Tobata, Kitakyushu, Fukuoka, Japan
q595506a@mail.kyutech.jp

A record for this book is available from the Kyushu Institute of Technology Academic Repository in Publication Data Thesis (http://kyutech.repo.nii.ac.jp).

Dedicated to my parents,

My wife (Asmaa), my daughters (Hana & Haya) and son (Yousif)

My parents, Brothers, Sister, teachers, friends and

Those who take pleasure in my prosperity and

Been there for me during the times of nonlinearities

With my love and respect

The doctoral dissertation supervisor and chair of the doctoral dissertation approval committee:

Yasunori Mitani, PhD
Professor, Department of Electrical and Electronic Engineering
Graduate School of Engineering, Kyushu Institute of Technology
Tobata, Kitakyushu, Fukuoka, Japan

The members of doctoral dissertation approval committee:

Masayuki Hikita, PhD
Professor, Department of Electrical and Electronic Engineering
Graduate School of Engineering, Kyushu Institute of Technology
Tobata, Kitakyushu, Fukuoka, Japan

Masaki MITO, PhD
Professor, Department of Basic Sciences
Graduate School of Engineering, Kyushu Institute of Technology
Tobata, Kitakyushu, Fukuoka, Japan

Masayuki Watanabe, PhD
Associate Professor, Department of Electrical and Electronic Engineering
Graduate School of Engineering, Kyushu Institute of Technology
Tobata, Kitakyushu, Fukuoka, Japan

The committees have examined the dissertation entitled "Stability and Protection Enhancement of Power Systems using SMES and SFCL Considering high Penetration of Renewable Energy Sources" presented by Emad Abdelnabi Mohamed Younis, A candidate for the degree of Doctor of Philosophy and hereby certify that it is worthy of acceptance.

Acknowledgments

I am deeply indebted to my supervisor, ***Prof. Yasunori Mitani***, for his constant support. This research would not have been possible without the support and help. I thank him for supervising my research work continuously and providing me with valuable advice and expert guidance. Words cannot express my gratitude to him for his patience, helpful, tirelessly offered invaluable assistance, support, and guidance.

My deep gratitude is also due to ***Prof. Masayuki Hikita***, ***Prof. Masaki MITO***, and ***Prof. Masayuki Watanabe***, who served as my supervisory committee members, for their continuous support, guidance, and comments, during the period of my study. The author extends many thanks and appreciations to ***Dr. Yaser Qudaih*** for his technical guidance, thoughts, and support.

It is a pleasure to acknowledge the scholarships, awards and support the author received from the Egyptian government, ***Egypt cultural affairs and missions sector***, Ministry of higher education.

Special thanks go to my colleagues, and staffs at Kyushu Institute of Technology and anyone helped me to know at any place or at any time. Finally, the author offers his deepest personal gratitude to his parents and family for the strength that keeps me standing and believing that this research would be possible, more interest and success.

Emad A. M. Younis

March 2019

Preface

Recently, the new renewable energy resources (RERs) share has been rapidly risen in the electrical networks. The main vastly widespread RERs sources are wind and solar photovoltaic (PV). They are considered economically for supplying energy to electrical grids and suitable for power generation in remote areas where the grid is not available. However, the intermittent energy generations from these sources because of weather changes, causes fluctuations in power flow and frequency in the power systems. Furthermore, the high penetration levels of wind and solar energies have led to reduce of microgrid (MG) inertia. Consequently, increase the voltage and frequency fluctuations, which affect directly on the MG stability, reliability, and protection. Moreover, the RERs exchange electrical power to MGs through power electronic inverters, which cause higher power fluctuations than the traditional synchronous generators. These problems threaten the MG system security and could lead to complete blackouts as well as damages to the system equipment. To protect the MGs from threats related to these challenges, this thesis proposes different techniques handling the stability and protection coordination issues due to the integration of RERs.

This thesis studies and presents the solutions for the stability and protection issues for MGs with high penetration of RERs. Firstly, the application of the superconducting fault current limiter (SFCL) is utilized to limit the high fault current levels and enhance the low voltage ride-through (LVRT) capability of wind turbine (WT) in Chapter 3. However, the fluctuation due to high penetration of wind and PV generations is another challenge due to the integration of RERs. The SFCL integrating could not solve this problem. Hence, a coordination of an optimized PID controller based new swarm intelligence algorithm as a load frequency controller (LFC) with the dynamic contribution of the superconducting magnetic energy storage (SMES) is presented to maintain the stability and enhance power quality of power systems in the presence of violent changes of loads or high penetration of the RERs in Chapter 4.

From another side, in cases of a large generation loss disturbance or high integration levels of RERs, the conventional power reserve may not be enough to return the stable condition of the system frequency. Hence, the emergency control and protection schemes plan may be followed. Therefore, this thesis presents a new intelligent coordination of SMES and the digital over/under frequency relay (OUFR) to protect the MG in emergency cases with very large frequency variations. In addition, this coordination avoided the mal-operation of the digital frequency relays in Chapter 5. The efficiency of the proposed methods are verified using a large-scale power system such as the Egyptian power system (EPS) in Chapter 6.

Contents

List of Figures

CHAPTER (4)

CHAPTER (5)

CHAPTER (6)

List of Tables

List of Symbols

δ	Power angle
ρ	Air density
P_w	Wind power
υ	Wind speed
A	Area covered by the rotor
C_p	Coefficient of performance of the turbine
λ	Flux linkage
ω_s	Synchronous speed
ω_r	Rotor angular speed
R	Rotor resistance
A_{sc}	Superconducting film cross sectional area
A_i	The core cross-section area
A_w	The window cross-sectional area
A_{sc}	Superconducting film cross sectional area
R_{sc}	Superconducting film resistance
ρ_{sc}	Superconducting film resistivity
L_{sc}	Superconducting film length
J	Current density
J_c	Critical current density
J_{c77}	Critical current density at 77 K
T	Temperature
T_c	The critical temperature
C	Specific heat capacity in $J/m^3.K$
E_c	Critical Electric field value at critical current density Jc
E_o	Depend on material processing conditions $0.1 \leq Eo \leq 10$
ρ_k	Maximum resistivity of superconducting film
ρ_{sc}	Superconducting film resistivity
ΔT	Increment in the temperature
Δt	Time increment
μ_r	The relative permeability of the iron core material
α	Depend on material processing conditions $5 \leq \alpha \leq 15$
β	Depend on material processing conditions $2 \leq \beta \leq 4$
P_{LN}	The power losses in the liquid nitrogen
i_{sh}	The shunt resistor current
t_i	Time of the fault occurrence
t_f	Time of the fault clearing
E_k	Kinetic energy
E_{SFCL}	The energy loss of superconductor
R_{crow}	Crowbar resistance
R_s	Stator resistance
Δf	Frequency deviations
K_p	Proportional controller variable gain
K_I	Integral controller variable gain
K_D	Derivative controller variable gain
K_{smes}	SMES gain

T_{smes}	SMES time constant
D	Microgrid damping coefficient
H	Microgrid system inertia
T_g	Time constant of governor
T_t	Time constant of turbine
ΔP_{ACE}	Regulating the system frequency
ΔP_m	Change in Mechanical power
ΔP_g	Governor power deviation
ΔP_C	Regulating the system frequency
ΔP_d	Change in demand power
R	Droop constant
T_{WT}	Time constant of wind turbines
T_{PV}	Time constant of solar system
V_U	Maximum limit of valve gate
V_L	Minimum limit of valve gate
K	Integrator threshold time
f_{max}	Maximum frequency limit
f_{min}	Minimum frequency limit
T_1	Valve time constant of non-reheat plant
T_2	Steam valve time constant of reheat plant
T_3	Water valve time constant hydro plant
T_d	Dashpot time constant of hydro plant speed governor
T_h	Time constant of reheat thermal plant
T_w	Water starting time in hydro intake
ΔP_L	Load variation
β	Frequency bias factor
m	Fraction of turbine power (intermediate pressure
R_1	Governor speed regulation non-reheat plant
R_2	Governor speed regulation reheat plant
R_3	Governor speed regulation hydro plant
P_{n1}	Nominal rated Power output for non-reheat plant
P_{n2}	Nominal rated Power output for reheat plant
P_{n3}	Nominal rated Power output for hydro plant
ΔP_{c1}	Regulating the system frequency of non-reheat plant
ΔP_{c2}	Regulating the system frequency of reheat plant
ΔP_{c3}	Regulating the system frequency of hydro plant
$best_g$	The global best solution
$best_p$	The best light source position
ε_1	Random samples were drawn from Gaussian stochastic
$\varepsilon_2, \varepsilon_3$	Random numbers within the interval [0,1]
x_j^{max}	the upper limit
x_j^{min}	The lower limit
2g/G	the social factor
1-g/G	the cognitive factor
r_1, r_2	Random number within the interval [0, 1]
n_p	Number of pathfinders moths
μ_t	Variation coefficient
$\boldsymbol{\sigma}_j^t$	Dispersal degree

List of Acronyms

CH4	Methane
CO2	Carbon dioxide
RER	Renewable energy resources
PV	Photovoltaic
MG	Microgrid
LVRT	Low voltage ride-through
HVRT	High voltage ride-through
RoCoF	Rate of change of frequency
WT	Wind turbine
PMSG	Permanent magnet synchronous generator
DFIG	Doubly-fed induction generator
SR	Solar radiation
EPS	Egyptian power system
SC	Superconductor
RSFCL	Resistive superconducting fault current limiter
SMES	Superconducting magnetic energy storage
LFC	Load frequency control
OUFR	Over/under frequency relay
MSA	Moth swarm algorithm
PI	Proportional-Integral
PID	Proportional-Integral-Derivative
SM	Synchronous machines
EDC	Economic dispatching control
ESS	Energy storage system
MPPT	Maximum power point tracking
DG	Distributed Generation
GHG	Greenhouse gas
PCC	Point of common coupling
MGCC	Microgrid central controller
FCL	Fault current limiter

VSC	Voltage source converter
IGBT	Insulated-gate bipolar transistor
PWM	Pulse width modulation
PCS	Power conversion system
UC	Ultra-capacitors
UPS	Uninterruptible power supply
CDM	Coefficient Diagram Method
EV	Electric Vehicles
MPC	Model Predictive Control
LP	Linear programming
QP	Quadratic Programming
IP	Interior point algorithm
GA	Genetic algorithm
SOC	State of charge
CB	Circuit breakers
STATCOM	Static synchronous compensator
FSIG	Fixed-speed induction generator
FACTS	Flexible AC transmission system
HTS	High temperature superconductor
FRT	Fault-ride through
SVC	Static var compensator
TCR	Thyristor-controlled reactor
TSC	Thyristor switched capacitor
TCSC	Thyristor-controlled series compensation
DVR	Dynamic voltage restorer
MERS	Magnetic energy recovery switch
BFCL	Bridge fault current limiter
UPQC	Unified power quality conditioner
UCS	Unified compensation system
RSC	Rotor side converter
GSC	Generator side converter
BSCCO	Bismuth strontium calcium copper oxide

AESO	Alberta Electric System Operator
LN2	Liquid Nitrogen
SCIG	Squirrel cage induction generator
PLL	Phase-locked loop
GUI	Graphical user interface
MFs	Membership functions
COG	Center of gravity
WPG	Wind power generator
GRC	Generation Rate Constraints
WPGS	Wind Power Generation System
TSR	Tip-speed ratio
AVR	Automatic Voltage Regulator
PSS	Power System Stabilizer
FDM	Forward Difference Method
BDM	Backward Difference Method
FMU	Frequency Measuring Unit
FDE	Frequency detection element
IED	Intelligent electronic device
EEHC	Egyptian Electricity Holding Company
CSP	Concentrated Solar Power
NECC	National Energy Control Center
ISE	Integral of squared-error
MgB2	Magnesium diboride
ANFIS	Adaptive neuro-fuzzy interference system

Chapter 1

Introduction

1.1 Introduction

The world relied on fossil fuels, such as petrol, coal, diesel, and natural gas to generate energy for thousands of years. However, the rapid growth of electrical loads especially industrial plants and human activities, resulting in excessive using of fossil fuels. This caused a significant shortage of these energy sources. Furthermore, the burning of fossil fuels caused climate change and global warming due to emissions of harmful gases, such as methane (CH4) and carbon dioxide (CO2). Therefore, the governments all over the world move toward alternatives. The most important alternatives are renewable energy resources (RERs). The generation of electricity from RERs is not necessary only for the shortage of other energy sources and satisfies the increased demand of energy but also for avoiding the emission of oil gases and lower impact on the environment [1- 4].

Recently, the new renewable energy resources (RERs) share has been rapidly risen in the electrical networks due to several merits, such as being clean and unpolluted, renewability and they do not need for expensive maintenance. The main vastly widespread RERs sources are wind and solar photovoltaic (PV). They are considered economically for supplying energy to electrical grids and suitable for power generation in remote areas where the grid is not available. Globally, the penetration levels of renewable energy sources into the electrical grid power systems are growing exponentially [5]. For instance, the annual growth rate of wind energy generation has been sharply increased reaching of 17.02% from 2014 to 2015, with expected increased worldwide capacity of 2000 GW by the year 2030 [6]. In addition, the yearly growth rate of photovoltaic (PV) generation has been largely increased reaching of the total generation of 227 GW in 2015 compared with a total generation of 177 GW in 2014. It is expected that PV generation continues increasing and achieving between 1760 to 2500 GW by the year 2030 [6]. In accordance, a vast improvement in renewable power technologies has been achieved. An increased attention has been given to large-scale RERs that help to increase power densities and to decrease the cost of the generated kilowatt-hours [7]. Therefore, RERs plays a significant role in supporting electrical grids and self-healing capability of utility grids. However, the high

penetration level of RERs in power systems, especially in microgrids (MGs) has made the voltage stability, frequency stability, power quality, short circuit levels, existing protection schemes, energy balancing, and power leveling of the principal interests for research and industry. This is to guarantee stable performance after integrating of high RERs and during other network disturbances such as faults and violent changes of loads [8-10]. To protect the electrical networks from threats related to these problems, there should be rigorous technical requirements, such as: (i) low voltage ride-through (LVRT), (ii) control of active/reactive power response during and following disturbances, (iii) frequency regulation support, (iv) voltage regulation capability [11].

1.2 Technical Challenges and Impacts of RERs

The intermittent nature of RERs made their integration into the electrical grid more challenging. The technical challenges and issues related to the ability of RERs to work effectively as part of the industry nowadays and reducing the variability of the RERs output. Furthermore, RERs must meet the technical requirements regarding frequency, voltage, and protection of faulty parts to isolate them quickly from the network. The technical issues due to integrated of RERs are:

1. Power quality
    a. Frequency and voltage fluctuations
    b. Harmonics
2. Power fluctuation
    a. Longtime power fluctuation
    b. Small time power fluctuation
3. Storage systems
4. Protection issues
5. Optimal allocation of RERs
6. Islanding detection.

Due to the increasing tendency of connecting high penetration of RERs in electrical grids, the utility is concerned, as some problems threaten the network in terms of power quality issues, voltage and frequency regulation, stability, and reliability. The random nature of RERs causes power fluctuations, which influenced the stability and power quality issues negatively [12]. Furthermore, the high RERs integration affects the tie line overloading. If the location of the

RERs is away from the main load centers and synchronous generators, this may require augmentation for the network and need to increase the interconnections to avoid the constraints of power flow. Furthermore, if an unexpected sudden reduction in large RERs occurs, it may lead to challenges of overload issues in the interconnection lines. This will require new control and monitoring techniques in the future to specify in advance the expected performance of power systems regarding such events.

1.3 Wind Power Generation

Among all RERs, the development of wind power today's is impressive, The wind energy has been given global concerns due to their high power generations up to 10 MW in a single wind turbine, low cost of generated kWh, and environmentally friendly. Therefore, wind energy systems are suitable for high penetration levels of RERs that may lead to a full replacement of conventional energy sources [13]. However, there are still unresolved issues for wind energy integration, especially in the area of frequency regulation enhancement. Whereas, replacing conventional synchronous generating units with wind turbines, the frequency response will be influenced due to wind speed variations. Consequently, the rate of change of frequency (RoCoF) will increase. This may lead to load shedding or blackouts especially in islanded microgrids (MGs), which have a lower inertia than the large system. Hence, the frequency stability will be decadent in these situations [14].

The ability of wind turbines (WTs) to match the new grid codes is greatly affected by the WT type and its technology. Fig. 1.1 shows the different types of wind generators [15].

- **Fixed-speed induction generators (FSIGs) (Type 1):** FSIGs are the most basic utility-scale wind turbines generators in operation. This type uses the squirrel-cage induction machines, which is directly linked to the grid. Although the fact that it is simple in design, reliable, and the cheapest technology among the other generator types [16], FSIG absorbs more reactive power from the grid during faults which leading further voltage dip on the system. Therefore, this type cannot meet the requirements of the international grid codes. To improve the operation and LVRT capability of FSIG, a comprehensive review of several methods dealing with this WT type has been accomplished in the next chapter.

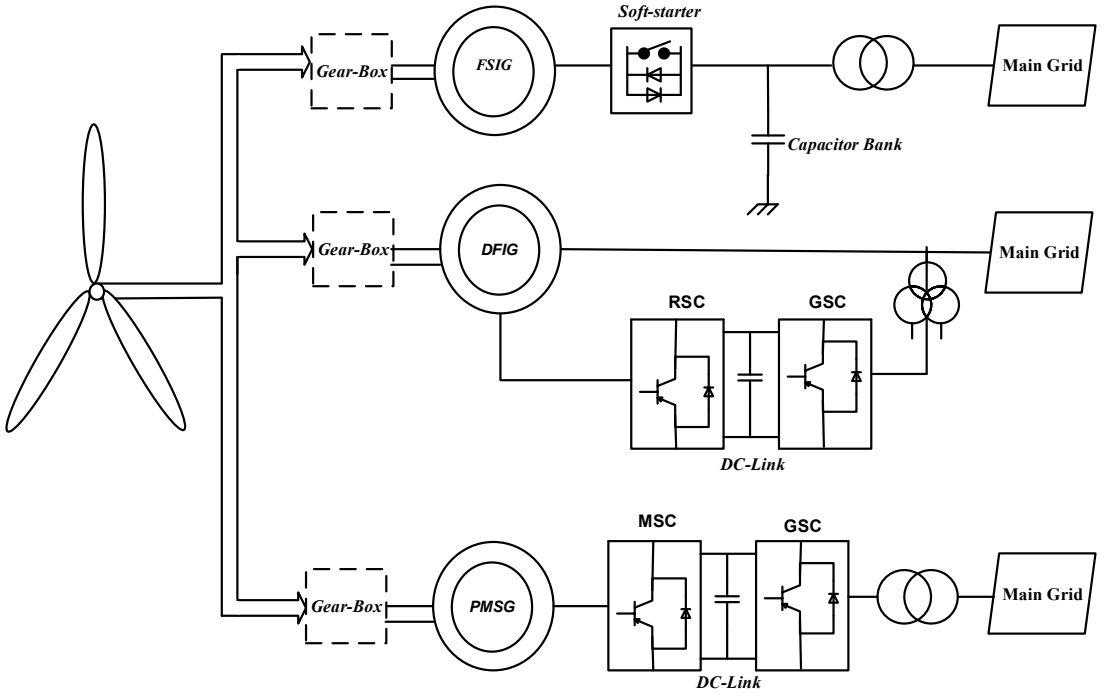

Fig. 1.1 Types of wind turbine generators

- **Permanent magnet synchronous generators (PMSGs) (type 2):** this type Features with low maintenance requirement and it has a back-to-back AC/DC/AC, converter, which is decoupled completely from the grid. Therefore, it has better LVRT capability [17]. However, this type faces a **problem** of varying the values of the dc-link voltage and rotor speed over the limits due to the unbalance between the mechanical input power and the electrical output power. This happens during a fault or extreme loads and may lead to force the WT to disconnect from the grid.

- **Doubly-fed induction generators (DFIGs) (type 3):** the DFIGs have been most preferred selection for the wind farms all over the world because they have the ability to operate at different rotor speeds and control the exchange of active and reactive power with the grid. However, DFIG suffers from some problems especially grid faults because when they are connected into the grid, the frequency and terminal voltage depend on the AC source of the power system [18]. When the grid is exposed to a fault, the stator current increases and consequentially high currents are induced in the rotor and the converter, resulting in damage to the DFIG converters. The most common solution for this problem is the use of the conventional Crowbar system; it is connected with the rotor terminals through electronic switches to cut off the converters from the generator. This method is very

effective in limiting the high currents in the rotor during the fault but the DFIG changes to a squirrel cage machine, which draws reactive power from the grid which may lead to further decrease in the grid voltage [19].

1.4 Photovoltaic Power Generation

PV systems are made from semiconductors that allow solar radiation to be converted directly into electricity. The essential ingredient for PV technology is the solar "cell". Multiple PV cells are connected to form a PV "module". Modules range in power output from about 10 W to 300 W. A PV system has the following components, as shown in Fig. 1.2 [20]:

1. One or more PV modules which are connected to an inverter,
2. Inverter to convert the DC current to AC current, and
3. ESSs such as batteries with charging and discharging controller.

PV systems can be divided into two basic groups, as shown in Fig. 1.3 of PV system types (a) off-grid (b) on-grid [21]:

1. off-grid, that is PV systems not connected to the network
2. on-grid, that is PV systems connected to the network.

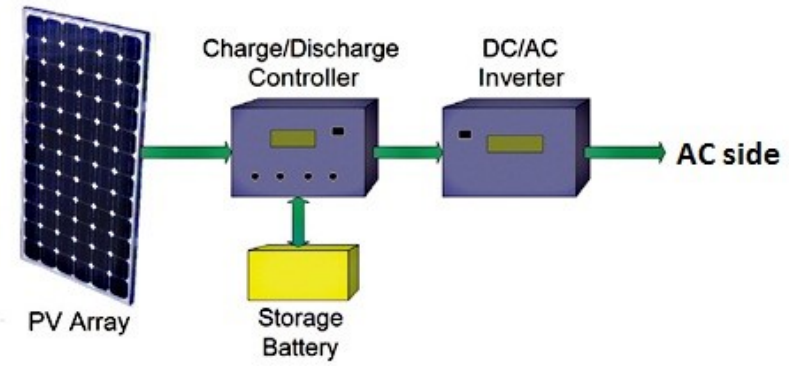

Fig. 1.2 Main components of PV system

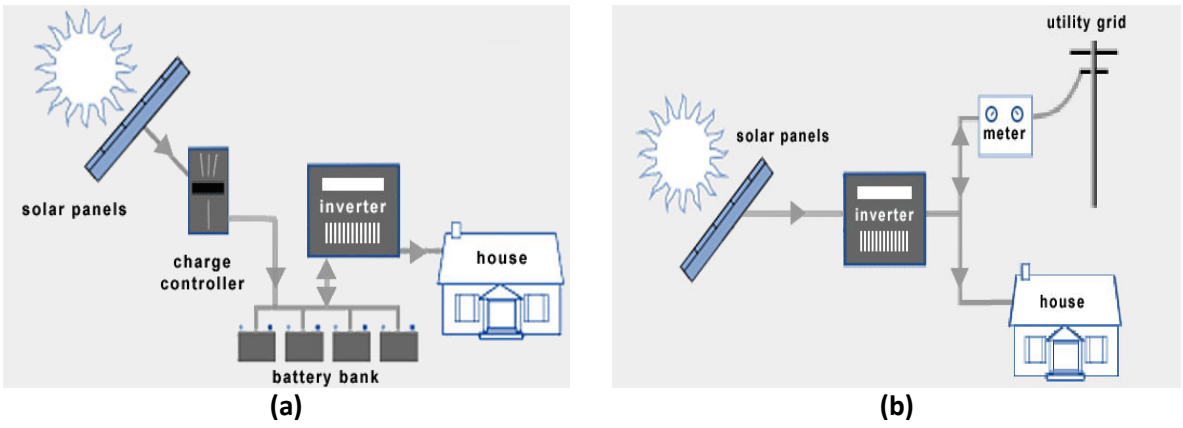

Fig. 1.3 Photovoltaic system types (a) off-grid (b) on-grid

PV systems are Different from the conventional generation systems that they do not have rotating parts. Hence, PV systems have no inertia. Moreover, PV generations are safe, clean, and highly reliable, less maintenance and its operation is cost-effective in remote areas. On the other hand, the PV output power is highly sensitive to solar radiation (SR), which may cause large variations in the output power in case of sudden change, in its value. This happens when the PV rises quickly to its maximum value depending on the inverter operation after the sunrise. Furthermore, a significant drop in the PV output occurs when the clouds start to cover the PV location. This drop may reach below 10 % of its maximum output. Similarly, this process occurs again when the clouds move away from the PV area. The penetration level of PV power generation also influences the SR. If the PV penetration in power systems is high, the value of SR decreases suddenly and may cause a voltage drop, which affects the operation of protection devices. In contrast, if the PV output increases due to an increase in the SR, this may cause overvoltage, which can cause equipment damage and protection malfunctions. The severity of these challenges issues depends on the penetration level of PV generation units and their locations.

1.5 Problem Definition

It is clear from the aforementioned discussion that the stability and protection of power systems represent crucial factors for the existing and future extension of RERs in electrical power systems especially MGs. According to field experience surveys, the wind and PV generations possess the highest integration challenges of RERs in MGs due to the intermittent energy generations from these sources because of weather changes, causes fluctuations in power flow and frequency in the power systems. Furthermore, the high penetration of wind and PV has several impacts on the performance of the islanded MG such as the reduction of system inertia; consequently, increase the voltage and frequency fluctuations. Furthermore, the RERs exchange electrical power to MGs through power electronic inverters, which cause higher power fluctuations than the traditional synchronous generators. Therefore, if the RERs penetration becomes larger, the islanded MGs might become insecure as the stabilizing in system frequency and voltage is difficult in that situation. Moreover, there will be unbalanced between the generation and load due to the variable nature of RERs. These changes lead to the appearance of challenges for the conventional control and protection systems such as nature transient variations in MG. These variations are highly affected by the operation mode of MG whether grid-connected or stand-alone.

On the other hand, the high penetration of RERs influenced the fault current by changing its value and direction. Consequently, there will be a mis-coordination of the protective devices, which leads to a mal-operation for these protective devices. In addition to the selection and coordination of conventional protective relays became more complex due to the frequent bidirectional power flow in connection feeders of MGs to utility grids. Moreover, for large integration of wind power, low voltage ride through (LVRT) is now required in most power systems. Therefore, many studies have developed different control strategies to deal with these challenges. However, in case of large frequency deviations, which might follow by an additional generation or load events leading to imbalances in active power during the fault periods, the control technique is unable to restore the system frequency. In that situation, the emergency control and protection must be used to return the system frequency to its steady-state condition. Therefore, this thesis will study the frequency stability and protection coordination issues of the islanded MGs and the large Egyptian power system (EPS) considering high RERs penetration.

1.6 Research Objectives

Motivated by the abovementioned stability, reliability, and protection challenges due to high integration of RERs in power systems, the scope of this thesis is concerning to accurate assessment and considerable enhancement of the stability and security of different-scales power systems. This is by developing and implementing models to enhance the control and protection requirements for interconnection of wind and PV power plants in power systems that are considered the high penetration of the RERs and the violent changes of loads. In this context, the advanced methods for active/reactive power capability, protection plan, and control requirements have been proposed.

The research has presented the application of superconducting (SC) power devices, such as the resistive superconducting fault current limiter (RSFCL) and superconducting magnetic energy storage (SMES) into the design and optimization of a bulk level of RERs. The work presented in this dissertation is expected to provide results that can be used to explore and develop SC technology for integrating very high levels of RERs. The RSFCL have the unique property of being able to automatically switch from low impedance to high impedance rapidly as a result of the high current, which make them especially suitable for the current limiting application. It drew more interest especially after the discovery of high-temperature SC materials. Moreover, SMES is capable of storing electrical energy in the magnetic field generated by DC current

flowing through it. The direct storage of electrical energy in the field of SC coil allow access time in the range of milliseconds, while duration and the number of charge/discharge cycles have no influence on the lifetime of SMES. Further, charge/discharge efficiency is very high (up to 90%) fast response capability and no deteriorations. Therefore, the dynamic contribution of SMES with a new optimized PID controller-based a new Swarm intelligence to compensate the system frequency deviations (Δf) has been presented.

From another side, the system stability is often related to different disturbances, while in case of faults or large disturbance, the effect on the power system is influenced significantly. Therefore, the protection response must be quickly and accurately to ensure the safe operation of power systems. Hence, it is meaningful to study and analyze the coordination between the control action and protection scheme instead of only focusing on the control subsystems, which addressed in many previous literatures. Therefore, this thesis presents a new intelligent coordination of the digital protection scheme based on the digital over/under frequency relay (OUFR) and conventional/digital load frequency control (LFC) to protect the power systems against high-frequency variations due to high RERs integration or sudden load changes. Moreover, study the direct impacts of integrating SC power devices on this coordination.

The contributions and significance of this thesis can be highlighted as follows:

1. Investigate the different impacts of high PV and wind penetration to identify the problems of frequency fluctuation in power systems.
2. Investigate the impacts of high PV and wind penetration during different disturbances and faults.
3. Developing a reliable model of the RSFCL to protect the power system from the in-feed currents due to high RERs penetration and enhance the low voltage ride-through (LVRT) capability of the wind turbine.
4. Apply of an efficient recent optimization method of moth swarm algorithm (MSA) technique to optimally fine tuning of the RSFCL parameters.
5. Developing a novel optimized decentralized nonlinear controller base on new swarm algorithm for both MG system and the EPS.
6. Study the coordination of SMES and the new optimal controller based-MSA for compensating the system frequency deviation.
7. Developing the design of the digital OUFR to protect the power systems during large disturbances or faults.
8. Presenting a new intelligent coordination of the digital OUFR and conventional/digital

load frequency control (LFC) to maintain the dynamic security of different-scale power systems due to high integration of RERs.

9. Study the different impacts of superconducting power devices on the presented coordination of digital protection and control for emergency cases.

1.7 Research Outlines

The Thesis is divided into seven chapters. The outlines of these chapters are as follows:

In chapter one, an introduction to the essential needs and benefits of the RERs is presented. Moreover, the weaknesses and threats regarding the penetration of RERs into MGs including instability, protection coordination, energy balancing, malfunction operation of LVRT, reduction of network inertia are highlighted. In addition, problem definition, research motivations, and thesis outlines are introduced as well.

Chapter two introduces a literature review regarding the control, stability, and protection of electrical MGs with high penetration of RERs. The chapter also summarizes various research work carried out for the challenges and solutions of operating power systems with very high level of RERs into power system and its impacts on emergency control and protection coordination.

In chapter three, changing the fault current level and direction is a great challenge due to the integration of RERs in MGs. Therefore, this chapter presents the application and accurate mathematical electro-thermal derivations of the optimized resistive superconducting fault current limiter (RSFCL) to limit the negative impact of RERs integration. Moreover, the RSFCL can protect the wind turbine from tripping during faults by enhancing the LVRT of the wind generators. Furthermore, it decreased the activation of the conventional control scheme for the wind power generator. To validate the effect of RSFCL on the dynamic performance of the wind turbine, it is compared with the Crowbar protection scheme.

In chapter four, the fluctuation due to the high penetration of wind and PV generations is another challenge due to the integration of RERs. The RSFCL integrating could not solve this problem. Hence, the conventional LFC technique is presented first to handle the problem of high penetration of RERs in MGs. It succeeded to restore the system frequency in case of small frequency deviations. However, in case of large frequency deviations, the LFC cannot maintain the system frequency. Therefore, this chapter proposes a new optimized PID controller-based new moth swarm algorithm (MSA). The MSA method is developed through simulation of simplified social models, which is one of the most modern swarm intelligence algorithms. This

controller is coordinated with the dynamic contribution of the superconducting magnetic energy storage (SMES), which is used in this study as frequency stabilizer, (i.e., auxiliary secondary control) for more damping out the system frequency oscillations. Finally, A comparative study of optimal PID controller, conventional SMES, and SMES based on optimal PID has been carried out to validate the effectiveness of the proposed coordination regarding the peak undershoot, peak overshoot, and settling time.

Chapter five discusses the impacts of integration of the superconducting (SC) power devices on the protection schemes performance with high penetration of RERs. SMES exchanges power with the grid during charging/discharging process, which may lead to mal-operation for the protective relays. This chapter presents firstly a specific design of the digital over/under frequency relay (OUFR). This relay operates for both conditions of over and under frequencies to trip necessary generations or loads after the failure of the combined response of the primary and secondary controls to avoid market failure and to stop further frequency decline. Then, the coordination of the new optimized PID controller based swarm intelligence and the OUFR is presented. Finally, study the effects of SC devices integration on the performance of the proposed coordination. Furthermore, an improving OUFR is proposed to solve this problem.

In chapter six, to verify the effectiveness and feasibility of the proposed methods used in this thesis, a large-scale power system such as the Egyptian power system (EPS) is tested under the same disturbance cases. This system consists of three dynamics subsystems; hydro, reheat and non-reheat power plants with the integration of RERs.

Chapter seven summarizes the thesis outcomes, concludes the significance of this research, discusses the results, and finally makes recommendations for the future works.

1.8 Summary

This chapter provides an introduction on the essential needs and impacts of RERs on the power systems. Background and motivation are emphasized. The research objectives and contributions are described and the outline of this thesis is explained.

Chapter 2

Background and Literature Review

2.1 Introduction

The electrical power system generation has the accountability to guarantee that sufficient power is supplied to the electrical loads, both reliably and economically. The continuous and random changes in load during the power system operation affect the quality of power supply. Also, renewable energy resources (RERs) such as wind and photovoltaic (PV) power generations are significantly affected by climate changes that may cause fluctuations in the frequency and voltages of power systems. These disturbances may change from small to large ranges, which must be adjusted following theses changing conditions without losing the synchronism of machines. The non-synchronism will lead to power system instability problems with different forms. Hence, power system stability and control are required to ensure the balance condition between generation and load. Load frequency controller (LFC) is considered as one of the most important control strategies in power system which maintains the system frequency and power variations at their standard values, in order to ensure the reliability of electric power [22].

From another side, Due to the high level of installation of wind and PV generations in electrical power systems, the short circuit current will increase due to the extra contribution of these sources as shown in Fig. 2.1. The additional short-circuit currents may lead to malfunction or damage the switchgear [23-24]. Furthermore, disturbing the protection and control coordination, which make the traditional protection methods based on voltage, current, and frequency protection will not work successfully. Therefore, it is required to develop smart protection and control techniques to ensure high reliability of electrical power systems by increasing resiliency against component failures or natural disasters such as hurricanes and earthquakes. These disasters affect the power system networks with system faults, which not only limited to the physical damage of power systems, but power quality disturbances also take place and may cause severe power outages. Some large outages are initiated by a single event that gradually leads to cascading outages and eventually to the collapse of the entire system. They are very complex as a sequence of failures lead to a blackout in a large

area of grid. Recent cascading failure happened in Hokkaido, Japan during September 2018 due to an earthquake destroyed several towers of transmission lines and three coal -fired units and the power supply suddenly plunged. Hence, the electrical frequency dropped rapidly to 46.12 Hz as shown in Fig. 2.2 [25]. A serial reaction resulted in hydraulic power and wind power generators coming to a stop within a minute. 3.1 million kilowatts nearly of demand power was lost due to the quake, which leads to complete blackout [25] and left 2.95 million household in Hokkaido in the dark. In order to maintain the system security during the occurring of the unpredictable natural events, this thesis will present a new coordination of digital protection scheme, control techniques and SMES to ensure high reliability of electrical power systems by increasing resiliency against these natural disasters.

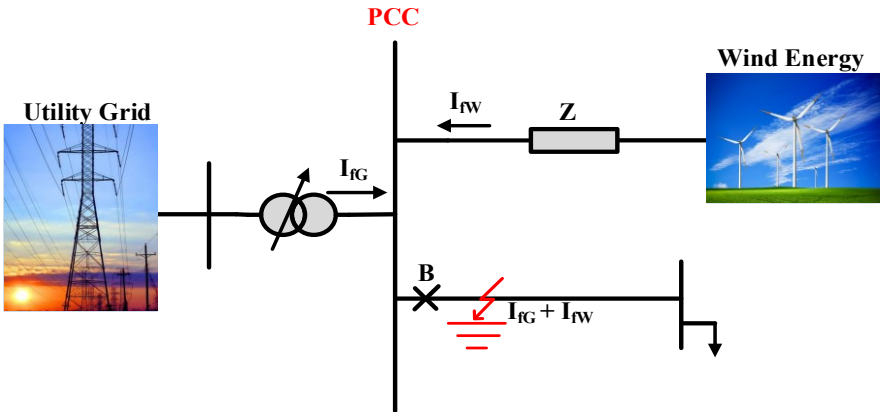

Fig. 2.1 Equivalent circuit of a faulted distribution network

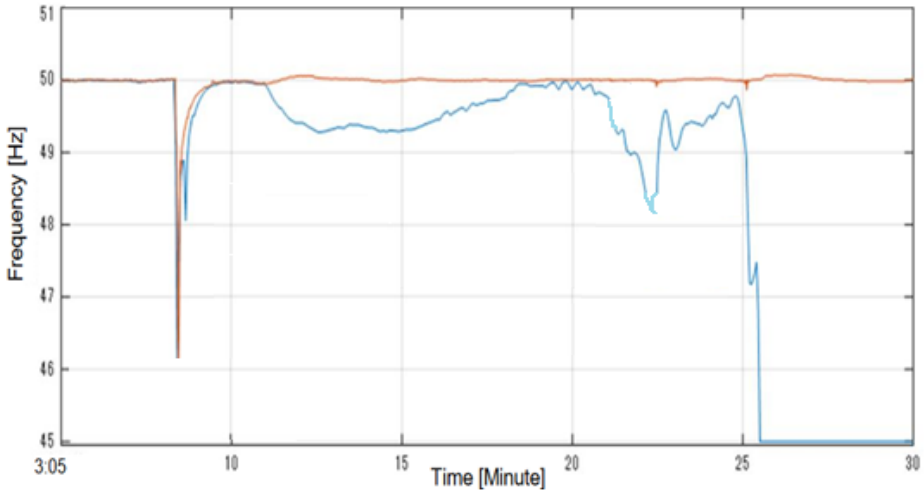

Fig. 2.2. Sequence of Events of the Hokkaido Earthquake to the Blackout [25]

2.2 Theoretical Backgrounds

2.2.1. Power System Stability

Power System Stability is the ability of a power system that enables it to restore a state of operating equilibrium after being subjected to any disturbance [26]. The power system response to any variation in system parameters can be controlled to maintain its stability utilizing a number of devices for control, protection, and monitoring. If the power system stability has been lost, the speed of generators' rotors accelerates, the bus voltage decreases, and the frequency deviates. Power system stability issues fall under many phenomena, which classified as shown in Fig. 2.3 to angle stability, voltage stability, and frequency stability. These phenomena may occur in a short or long term in case of a small or large disturbance in the power system.

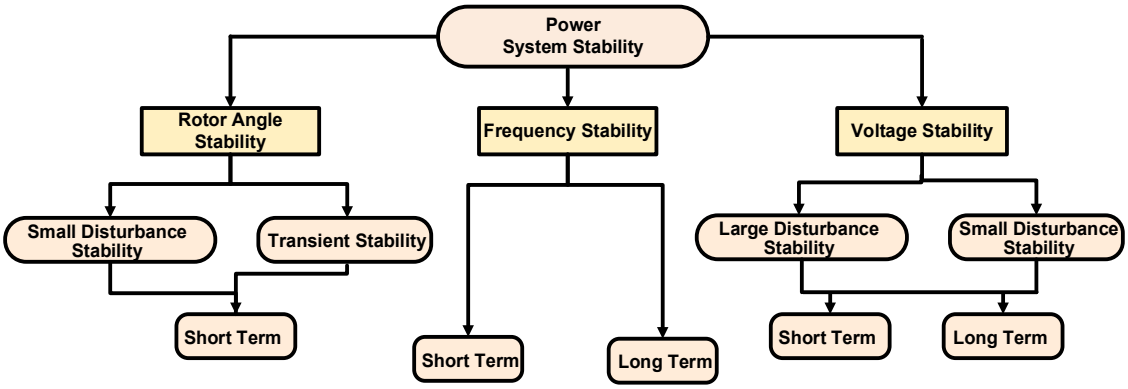

Fig. 2.3 Classification of power system stability

2.2.1.1. Voltage Stability

It is the aptitude of a power system to preserve steady voltages at all nodes within the system when subjected to a small or large disturbance. It depends on the balance of active and reactive power between load and generation. Hence, when the load is increased, load power also will increase and voltage and power are controlled. Voltage instability happens once the requested reactive power increases due to a disturbance results in increasing the reactive power capacity from the generation source. A doable outcome of voltage instability is the loss of loads , or tripping of transmission lines and alternative parts by their protecting systems leading to cascading outages. Consequently, a loss of synchronization of some generators may occur from these outages [27]. This is also namely voltage collapse, which is more complex than the voltage instability leading to very low unacceptable values of voltage profile.

The voltage stability is one of the most important factors that affect RERs stable operation especially wind farms. The high penetration of wind generation into the grid makes the voltage

stability more important due to the intermittent of random speed and their characteristics. Therefore, the impact of wind integration on reactive power requirements is an interested area of RERs integration studies and power system operators.

2.2.1.2. Rotor Angle Stability

The angle stability characteristics are complex and nonlinearly. It alludes to the ability of synchronous machines (SM) of an interconnected power system to stay in synchrony after being subjected to a disturbance. It depends on the aptitude to keep or restore equilibrium between electromagnetic torque and mechanical torque of every SM within the system [27]. It depends on two types of torques, which are the damping torque and the synchronizing torque. If a scarcity of synchronizing torque occurred, results in a periodic instability while an oscillatory instability occurred in case of lack of damping torque.

2.2.1.3. Frequency Stability

Frequency stability alludes to the aptitude of a power system to sustain steady frequency following a severe system disturbed leading to a significant imbalance between generation and consumption [26]. It mainly depends on how to keep or restore the equilibrium in a short time between production and consumption with minimum involuntary loss of load. In case that the consumption is larger than the generation, the kinetic energy stored in SM is used to maintain the balance condition but the rotational speed of the SM decreases. Consequently, the system frequency decreases leading to a loss of generation. These causes unbalance between the generation and load. The primary control tries in that case activating the reserve units to compensate the requested load demand for increasing the system frequency. The primary control can solve the problem only during the first 30 seconds after occurring of disturbance, After this time, the secondary control such as load frequency control (LFC) will return the system frequency to its initial value.

In this thesis, the most important issues are the intermittent and uncertainty of the RERs especially related with the active and reactive power. Hence, this work focuses more on the frequency stability and voltage stability of small power systems such as MGs and large power system such as the Egyptian power system (EPS).

2.3 Frequency Stability and Control Problem

There is a strong relation between the frequency and balance between production and consumption. This requires that all generation units have the ability to operate and maintain synchronism continuously within the allowable limits around the rated frequency. Moreover,

there must be sufficient generators units, which can quickly support loads during the variations in frequency through a central control or a dispatcher. This is to regulate the frequency and reduce the frequency difference to zero. Hence, the difference between mechanical and electrical torques governs the rotor acceleration of a generator. Therefore, to maintain a constant speed, mechanical input and electrical output powers need to be continually matched. The frequency control is divided into three main levels: primary control, secondary control such as load frequency control (LFC), and tertiary control as depicted in Fig. 2.4. The aim of all control actions is:

- To maintain the desired megawatt output power of a generator matching with the changing load.
- To assist in controlling the frequency of larger interconnection.
- To keep the net interchange power between pool members, at the predetermined values.

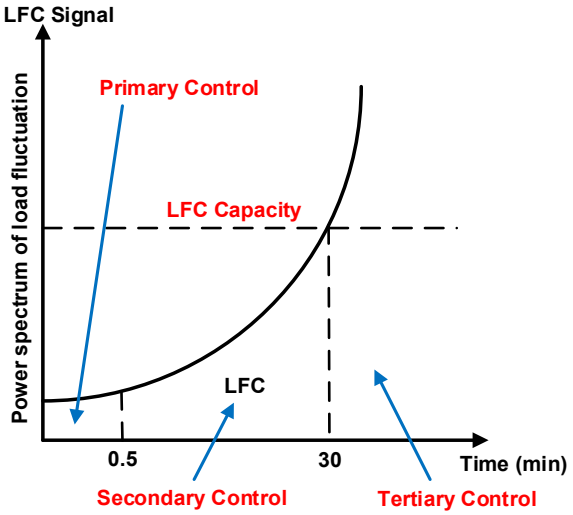

Fig. 2.4 Frequency control levels [6]

2.3.1. Primary control

Disturbances such as load variations or losses of generation units are translated into frequency changes. In order to stabilize the frequency at a new value, the primary control is implemented through governor control installed in each generating unit starts within seconds of a disturbance. The governing systems of the turbines drive the generators to change their output power, depending on the frequency deviation, until either the balance between turbines' output power and the load is restored or the primary control reserves are depleted. The main role of the primary control is to stabilize the frequency system but not return the frequency to its nominal value [28].

2.3.2. Secondary control

The secondary control, which is called the supplementary control such as LFC is used for the frequency fluctuation of a period of about thirty minutes. It automatically controlled reserves to restore the frequency to its nominal value by changing the valve reference positions of the generating units [29, 30].

2.3.3. Tertiary control

Tertiary control refers to the economic dispatching control (EDC) of units (i.e. the manual activation of power reserves by the system operator). Tertiary control actions on (30 minute-to-hours) time scale [28].

To improve the frequency control of power systems-based high penetration of RERs, a control method depending on controlling the energy storage of an energy storage system (ESS) is recently adopted [31].

2.4 Integration of RERs into Power System

2.4.1. Impact of RERs on Stability and Frequency Regulation of Power System

The continuous and fast demand for new electricity sources all over the world and widespread concerns about global warming pushes the governments toward RERs. The RERs have a great interest in the investment and development fields [32, 33]. The replacement of traditional generating units with a large amount of RERs especially wind turbines and PV cells leads to the appearance of new crucial challenges for the existing control systems, protection systems, and power system stability. These issues related to replacing the conventional generation units with RERs will intensely affect the frequency response due to the variations in wind and PV outputs. Not only the RoCoF changes but also the frequency magnitude deviation is increased following an outage of generation units [34]. Moreover, the high penetration level of the RERs reduces the frequency lower than the threshold value. This may cause load shedding or even lead to several cascaded blackouts in the electrical power systems due to the imbalance between the electrical load and power supply. The frequency stability will be highly decadent in case of more replacement of conventional generation units with RERs, especially in the islanded grids, which have lower inertia than the large power systems [35, 36]. Therefore, the impacts of RERs on the power system operation and control can no longer be disregarded. The intermittent of RERs influence the grid operation and increases the uncertainty of energy sources, which badly affects the grid reliability [37]. Furthermore, the prevalence of harmonics and reduction of system inertia due to the application of power electronic converters should be added to the predatory effects of the RERs integration in power system [38].

The reactive power support of wind generation is a major interest of power system operators and researchers. This is because there are types of wind turbines, which absorbs more reactive power from the grid during faults, leading further voltage dip on the system and cause voltage instability issues [39, 40]. Regarding the inertia aspect of view, the conventional generators differ from the wind turbine in the active power. Some studies proved the redesigned internal control of wind turbine can emulate a virtual inertia response for frequency stability, but it does not put in practice for power systems [34, 36]. Furthermore, the rotor angle stability is affected by reactive power support of wind turbines and this property can be suitable in severe low voltage events and diminish the separation of the synchronized units [41].

If the replacement of conventional generators with RERs increased, the power system inertia becomes lower. This leads to a higher quantity of RoCoF in case of a frequency drop, and hence needs a faster reaction from generation units, which are contributing in the LFC action. The rise of RoCoF value is the result of lower inertia rather than higher active power deficit [38, 42]. Consequently, the resultant load shedding may delay the recovery process of the power system or even blackout. Therefore, the initial RoCoF in the presence of the RERs may no longer be a suitable indicator of the mismatch between load and generation as without integration of RERs [43]. Normally, the variable speed wind turbines do not inherently contribute in the LFC to support the grid during disturbances due to two main reasons. Firstly, the application of the converters decouples their rotor inertia from grid frequency (low or no inertial response) [44]. Secondly, the operating point of variable speed wind turbines is typically set at maximum power point tracking (MPPT) to develop maximum power from the wind generator. Therefore, they are unable to inject more power to the grid in case of further active power requirement [44]. In order to provide the variable speed wind turbines with LFC capabilities similar to conventional synchronous generators, necessary LFC control loops need to be implemented inside the power electronic converters and the spinning reserve should be procured in the variable speed wind turbines by shifting their operating point from MPPT to a suboptimal point with lower efficiency. Under any circumstances, the variable speed wind turbines are merely able to release the power up to 1.2 times of their rated power transiently during the events due to the limited MVA of their power electronic converters, whereas the synchronous machines may support the grid up to 2-3 times of their apparent power capacity in the transient state [43,44].

Typically, the spinning reserve around 5-10% of variable speed wind turbines nominal power is considered in literature [37, 42]. In power systems with a high penetration rate of wind generation, the total available reserve in the whole network may not be sufficient to overcome

the entire range of severe contingencies especially the events with a high level of active power shortage resulting from islanding events. Reduction of total inertia is one of several wind generation outcomes, which remarkably affects the dynamical behavior of the power system [43]. During disturbances, the high RoCoF value causes a rapid decline of the system frequency. It is one of the low system inertia consequences, which needs a fast response of control actions. Eventually, the high integration level of RERs into the electrical grid leads to appear the following issues, which influence the dynamic behavior of the power system:

- The prevalence of harmonics due to power electronic converters leads to lower power quality.
- Reduction in system inertia due to using power electronic converters.
- Mis-coordination for existing protective devices.
- Bidirectional power flow in feeders.
- The high value of RoCoF (i.e. steeper frequency decline).
- The uncertainty of energy sources.
- Lack of or no spinning reserve in RERs due to the MPPT.
- Wrong estimation of active power shortage, which leading to overload shedding or dispatching.

2.4.2. Impact of RERs on Protection Systems

With a large penetration of RERs in power systems, not only power quality and stability related issues would appear but also may lead to problems, such as reverse power flow, change the short circuit current levels and directions. As a result, there will be many problems, such as false tripping of protective relays and circuit breakers, generate blind zones of detection for protection devices, unwanted grid islanding, and re-closers are out of synchronism. This leads to changes in the setting of the existing protection systems [45, 46]. To solve these problems in the presence of high level of RERs, the sequence of protective actions during fault must be modified as follows. Firstly, trip the feeder side circuit breaker; trip the renewable energy source connected to this feeder; then reconnect the faulty feeder using the re-closer; finally reconnect the RER after recovery of normal operation of voltage and frequency [47]. This process brings a large amount of extra work.

On the other hand, the augmentation in fault currents levels leads to a voltage reduction at the RERs terminals, which may lead to disconnection of large RERs. Hence, the changes in voltage profile during short circuits might also cause problems for the RERs, especially for wind turbines. The aspect of grid code for a power system includes wind farm is called the fault ride-

through (FRT) capability. The FRT requirements reveal that the RERs need to remain connected to the network during a disturbance to provide active and reactive power to the electrical grid and has the ability to come back to its normal operation quickly after ending of the disturbance. The low-voltage ride-through (LVRT) related to the voltage dip and the high-voltage ride-through (HVRT) related to the voltage swell are two aspects of the FRT.

Since wind farms use widely the induction generators, they absorb the reactive power from the grid to provide active power under the normal conditions. This wind type is not able to control the terminal voltage. Hence, the operation under this circumstance for a long time during a fault, the generators speed may exceed the limits or overcurrent happens, which may lead to disconnecting the wind turbine through protection devices. Therefore, the investigation of LVRT of a wind turbine is essential [48]. The HVRT is related to the voltage swell, which caused by a single-line-to-ground fault or sudden load outage. The first grid code for the HVRT is developed by Australia for wind turbines. It requires the wind generator to withstand 130% of the rated voltage for a time of 60 ms with enough current for recovery [49].

2.5 Microgrids Introduction and Concept

Microgrids (MGs) are small-scale of low voltage power supply's networks, which are destined to provide power generation in remote areas where the grid is not available. MGs are considered as the building block of smart grids [50]. As the solution of MGs is capable of facilitating wide penetration of renewable energy resources (RERs), distributed generations (DGs) and energy storage systems into power systems, reducing power loss and greenhouse gas (GHG) emissions in power systems, increasing the security and reliability of energy supply to users, for these reasons, MGs have been gaining more and more attention recently.

MG is an interconnected group of domestic loads, DGs such as gas turbines, PV, fuel cell, wind farms, microturbines, and energy storage devices, such as energy batteries, flywheels, and capacitors as shown in Fig. 2.5. This combination of a different kind of generation is configured in a way to ensure continuous power supply to the load without interruption. MGs are designed to lower cost, increase the efficiency, and help the environment. In other words, MGs are distribution systems that would change the idea of being passive to be active networks by distributing decision making and control, in addition, the power flows are bidirectional.

The intermittent nature of RERs such as wind speed and sunshade influences the output of these sources. Therefore, energy storage plays a basic role in the construction of MGs. Storage devices help in diminishing the cost of the power in the peak loads case [51].

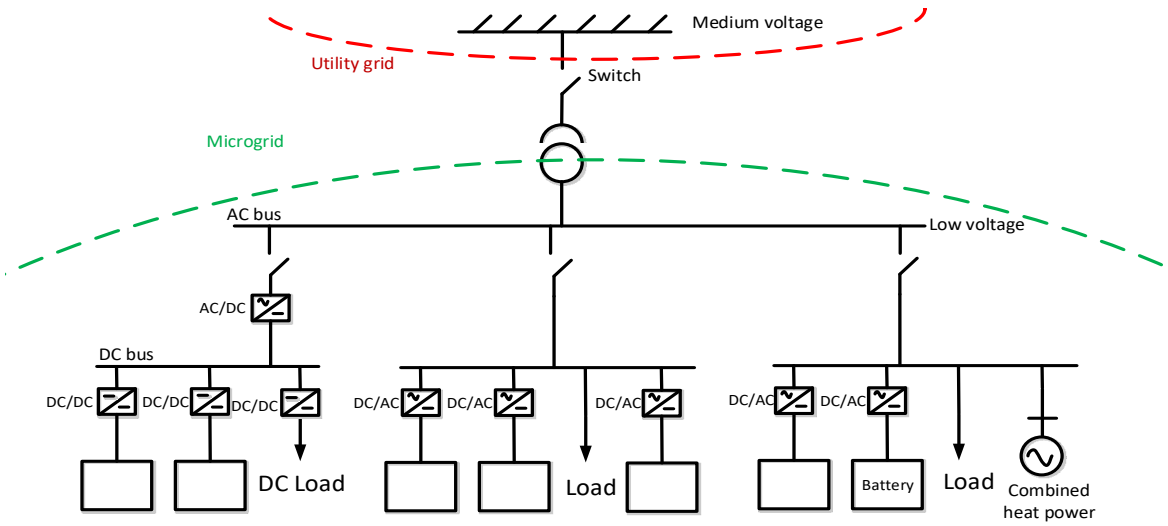

Fig. 2.5 A basic microgrid system

Using the modern control abilities and automatic operation technologies allow MGs connect to the upstream distribution network in order to operate when isolated from the utility grid in case of faults or severe disturbances, thus increasing the quality of supply. Consequently, this helps in avoiding the cascading failures. Thus, MGs are designed to overcome issues like blackouts and lose of stability. MGs can be attached to the utility in grid-connected mode and islanded mode easily in case of faults in the utility. The MG control should be designed to manage MGs that in the distribution networks with RERs/DGs. In the grid-connected mode, MGs obtain electrical power from both utility grid and local micro-generation. In this mode, the control system monitors and controls the voltage, power, and the frequency for both, utility and MGs. Moreover, the micro-generations operate in the current-control mode where they can maintain power exchanges between the MG and the utility grid. But at the isolated operation (e.g., faults, blackouts, voltage drops, frequency drops), MGs can disconnect from the utility grid through a static switch in about a cycle. In this mode, micro-generations operate in the voltage-control mode as they should regulate the MG voltage and share with electrical loads. Also, MGs should have enough generation sources to provide the demand of load at least to meet the requirement of the sensitive loads [52].

The power balance between the MGs generation and domestic loads is considering one of the most important requirements. Where the exchange of electrical power between MG and the utility grid is occurred to match the power balance during the grid-connected mode. While during the islanded mode, MGs should match the balance between production and domestic loads by increasing/decreasing the micro-generation or by load shedding process [53].

2.6 Reasons for Microgrids

The traditional arrangement of a large modern power grid offers many benefits. Large generating units are often economical and operate only with a relatively small range of personnel. A high-voltage transmission network allows the generator reserve demand to be decreased, the first generation will be developed economically at any time, and large energy to transport giant distances with limited electrical losses. The distribution network is often designed for one-way power flow and sized to accommodate customer loads only. However, over the previous years, ranges of influences have been combined to guide towards MG schemes. Reasons that encourage MGs are:

- Reduction in CO2 gaseous emissions.
- Rational use of energy.
- Deregulation or competition policy.
- Diversification of energy sources.
- National power requirement.
- Short construction times and lower capital costs of smaller plants.
- The closing of generation units to loads, which reduces the transmission cost.

2.7 Microgrid Operation

The main operational modes of the MG are the grid-connected mode and the islanded mode. In the grid-connected mode, the MG is connected to the utility grid and all the system feeders are closed using a static switch, and the MG can provide the overflowing power to the main grid. Fig. 2.6 shows a grid-connected mode, where the MG is connected to the utility grid at the point of common coupling (PCC).

In the islanded mode, the static switch is open and the utility grid does not supply power to the MG. This mode result when the utility subjected to faults or instability events. In this case, the MG should have enough generation units to meet the needs of the load. Once the abnormal event in the utility grid has cleared, MGs could be connected again.

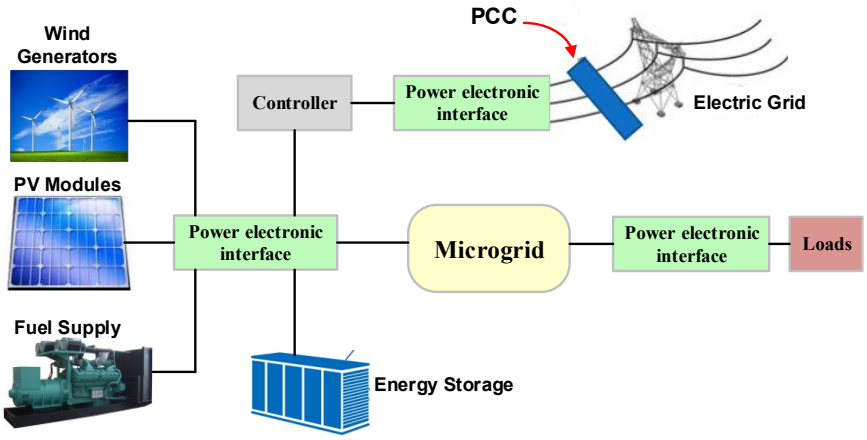

Fig. 2.6 Point of common coupling in a microgrid

2.8 Microgrid Control

Nowadays, as the high penetration of RERs in MGs is growing worldwide due to their reliable, sustainable and environmentally friendly, it increases the complexity of control, protection and communication of RERs in MGs. Hence, the MG control and operation is one of the irreplaceable issues for MG development. Control system of MGs should be designed to manage MG in both grid-connected and islanded modes using the MG central controller (MGCC) and built-in distinct devices of RERs or both of them. MG control should allow an increasing number of distributed generators without a change in the present operation. Furthermore, control should make the MG be capable of islanded and reconnected to the utility grid without making power flow problems to the loads.

Most of RERs and energy storage systems (ESS) are controlled using power electronic control circuits. These power electronic circuits' interfaces distinguish with a generation type and feeders. Regarding the elements of RERs in the MGs, the MG depends on inverters and converters, which operates as a voltage source or current source. Fig. 2.7 shows a simplified model, which contains a power source, DC –link, and voltage source inverter, connected to the MG through a feeder. The inverter can control the output values of the micro-generation, such as the frequency, voltage, active power, and reactive power. The vector relationship between the inverter voltage (V) and the voltage at MG side (E) with the feeder's reactance (X) determines the exchanging of active and reactive power (P, Q) flow from the micro-generation to the MG [54].

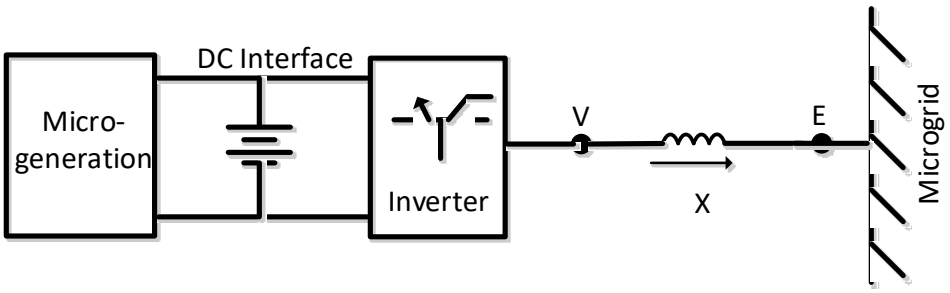

Fig. 2.7 Basic control of active and reactive power

The relationship between active and reactive power of a micro-generation is shown in equation (1). For small change, the active power is dependent on the power angle (δ) and the reactive power is dependent on the voltage magnitude. These relations used to create the main feedback control loop for the (P) and (E) control via regulation of (Q) flow.

$$P = \frac{3}{2}\frac{E \cdot V}{X}\sin\delta \tag{2.1}$$

$$Q = \frac{3}{2}\frac{V}{X}(V - E\cos\delta) \tag{2.2}$$

$$\delta = \delta_V - \delta_E \tag{2.3}$$

where, δ_V and δ_E are the angles of V and E, respectively.

It is clear that if the frequency decreases, micro-generations will increase their production (P) increases, the frequency will decrease, and vice versa, as seen in equation (2.4). Further, the relationship between (V) and (Q) similarly as seen in equation (2.5).

$$\omega - \omega_0 = -R_P(P - P_0) \tag{2.4}$$

$$V - V_0 = -R_Q(Q - Q_0) \tag{2.5}$$

where, R_P and R_Q are the frequency and voltage droop coefficients, respectively. ω_0, V_0, Q_0, P_0 are the nominal values of frequency, voltage, active power, and reactive power, respectively. Based on equations (2.4) and (2.5), the feedback loops are designed for the control of P, Q, f, and V of MG. Therefore, the interconnected RERs with different droop characteristics can follow and precise the load demand change to return the frequency and voltage of an MG to nominal values. MGs can be controlled based on several types of control loops, which are

divided into four types: local control, secondary control, emergency control, and global control [52].

2.9 Microgrid Protection Issues

The switching between the grid-connected and islanded modes is to ensure the power to be continued to the loads without interruptions, but it is very difficult for the conventional protection schemes to protect the MG in isolated mode. If a fault current occurred in islanded mode, the protection system might not discover the faults. Hence, the protection system could not be adjusted to operate for the two MG modes. For example, the trip time of the current-time relay type may be very large in case of isolated MG. Therefore, innovative protection schemes for the network with both operation modes should be explored. Furthermore, The MGs contains power electronic devices for the RERs and distributed generation. These generation sources are modeled in a different way in both operational modes. It should be modeled as a constant power source in the grid-connected mode, while voltage with variable internal impedance in the isolated mode. Hence, it is required an adaptive protection scheme in that case for adapting the network changes. Over the last years, several protection schemes for MGs have been presented as shown in Fig. 2.8.

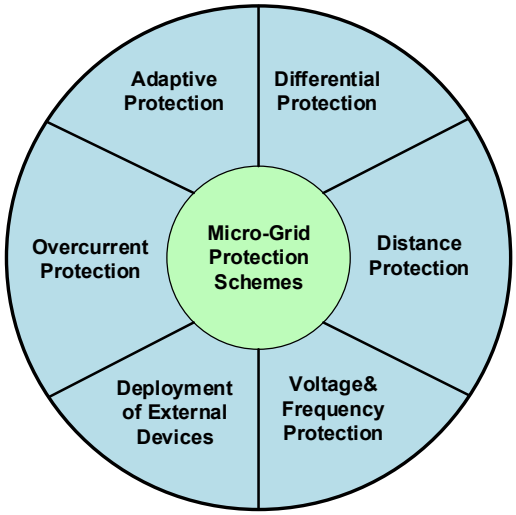

Fig. 2.8 Existing microgrid protection schemes

- **Adaptive protection schemes:** In this protection scheme, an automatic setting readjustment of relays would activate when the MG disconnect or reconnect to the main grid. This protection type is an online system, which can edit the protective response to change the requirements quickly via external signals or control actions.
- **Distance protection schemes:** In this protection scheme, the distance relay measures the impedance of a protected line up to a predetermined point for the distance measurement.

This relay is designed to activate only for faults that happen between the relay assignment and the selected measurement point. But the distribution line of the MG is not long. Hence, it is unfavorable for the relay setting, so the distance protection is not applicable to the MG.

- **Voltage and Frequency protection:** The frequency protection and voltage protection are mainly used within the stability control equipment. Hence, they rarely used alone in the utility grid. They could be used only as a main protection at the grid tie point for the anti-islanding condition.
- **Differential protection scheme:** This protection scheme has the merit of fast response. It can take an action within 5ms. The differential protection can be adapted to both grid-connected mode and islanded mode. This making this protection system is appropriate for MGs. However, it suffers from its need for the high requirement of communication channels.
- **Overcurrent protection scheme:** This protection scheme is the most known in distribution networks. It usually used as a backup protection for MG, not main protection due to some reasons, such as in case of multiple micro-generations in the MG, the power flow can be bidirectional and the new energy sources are equipped with fault current limiters (FCLs). These FCLs can last the fault current for a short period. Furthermore, the short-circuit current differs greatly under both grid-connected mode and islanded mode of the MG; overcurrent protection cannot be adopted to guarantee the response, sensitivity and selecting accuracy for the two operating modes.
- **Deployment of external devices:** As stated earlier, the big problem of large fault current level differs between the grid-connected mode and the islanded mode faced the MG operation. Hence, it is very necessary to develop an adequate protection scheme appropriate for both MG operation modes. These protection techniques depend on a change of the fault current level during the switching between the grid-connected mode and isolated mode. These protection schemes can be divided into two groups: the First one is the FCLs, which can reduce the level of the short circuit current of the aggregated contribution of many generation sources to avoid the exceeding the design limits of system equipment. The second one is using the energy storage devices, such as batteries and flywheels, which can provide a supplementary fault current level to the network. This is due to the fact of MG about the short circuit current level is limited to twice/triple times of the rated value [54].

2.10 Technical challenges in Microgrids

There are two main challenges must be taken into consideration when planning the MG protection system that enables the MG to work properly in the grid-connected and islanded operation modes. First, the RERs contains power electronic devices. The output currents of these power electronic devices are limited values approximately double the rated current; hence the contribution of currents from the RERs during fault might not be enough to trip the conventional overcurrent protection. The fault current levels are very high in the grid-connected mode compared to that in the isolated case. Therefore, if the fault is in the main grid, the protection system should isolate the MG from the main grid as quickly as necessary to protect the MG loads. In the case of MG fault, the protection system should isolate the smallest part of the MG when clears the fault. Second, the high cost of using numerical relays, such as distance and differential relays and new current limiting devices makes it difficult to use these relays in MG protection. Therefore, new incorporating and coordination of an adaptive protection system with the control system is still a good idea in the research and operational frameworks to avoid the problems related to the sensitivity, such as undetected faults or delayed tripping and selectivity, such as false or unnecessary tripping.

2.11 Need for Energy Storage

MGs face several problems during its operation due to the large time constants of micro-generation, such as wind and PV, Also due to the changes of supply and load, and during the switching from grid-connected mode to islanded mode. A temporary fast response power supply is used to regulate the frequency and voltage within the available limits of the network. However, this is effective only for the conventional generator units as they have sufficient high kinetic energy, which able to compensate the fluctuations. For RERs, the kinetic energy possessed to power fluctuations is low in MG. Hence, a fast response storage device is required to provide the appropriate amount of power to make a balance between supply and demand in the islanded mode and to make the MG be ready and stable for the upcoming disturbances [56] mitigate the additional intermittency and fast ramps at higher penetration of intermittent RERs. In addition, the storage systems can support the frequency control and phase angle of the MG when reconnecting with the main electrical grid [57].

There are many types of energy storage devices, which can store large amounts of electrical power. They are classified into mechanical, electrochemical, chemical, electrical, and thermal types [58]. For mechanical and electrochemical, such as battery system and flywheel, the

response is slow to compensate power fluctuations. Furthermore, the battery system and flywheel have low efficiency and short lifetime [59].

On the other hand, the Superconducting magnetic energy storage (SMES) is an advanced discover from the superconductivity application. It can store electrical power in the form of a magnetic field in a large superconducting coil (SC) [60-63]. The direct storage of electrical energy in the field of a superconducting coil allow access time in the range of milliseconds, while duration and the number of charge/discharge cycles have no influence on the lifetime of SMES. Moreover, charge/discharge efficiency is very high [64, 65].

At first, the SMES is used instead of the pumped storage systems for leveling the load [66]. Hence, large storage capacities from ESSs are considered primarily. A significant research and development were carried out over a quarter century, beginning in the early 1970s. The electrical energy department and the Institute of electric power research in Australia supported this work. Regarding the international level, Japan had a significant program for about twenty years, and several European countries participated at a modest level.

- **Benefits of SMES**

1. The power quality of electrical sensitive loads is enhanced with SMES, which can supply carryover energy in case of voltage sags and generation outage.
2. Improving load leveling between the RERs and the distribution networks.
3. SMES does not depend on any chemical process and no toxin like batteries. Hence, it is environmentally beneficial.
4. SMES has nearly infinite cycling capability and high dynamic range; hence, it can improve the transmission line performance and capacity. In addition to a recovery rate of nearly 100%.
5. It can enhance the frequency regulation during generation outage as well as improving the dynamic stability of the power system.
6. It is used as VAR compensation (dynamic voltage support).
7. RERs are intermittent generation and depend on weather conditions. SMES could support both RERs by smoothing their output and shifting the generated power in durations.

- **Merits of SMES**

1. The direct storage of electric energy in the field of a superconducting coil allows access times in the range of milliseconds.
2. The duration and number of charge/discharge have no influence on the lifetime of SMES.
3. Further, a charge/discharge efficiency of up to 95% can be obtained.

4. The SMES unit is highly efficient due to its low power loss.
5. Electric currents in the coil encounter almost no resistance and the unit has no moving parts.

The major disadvantage of SMES is the high cost of designing its construction [67]. However, with the technology improvement and discovering new superconducting materials, the predicted cost of SMES unit is likely to drop down to 25% of the existing cost [68]. Another drawback of SMES is the SC's sensitivity to temperature. Small changes in temperature can cause the unstable condition for the SC and lose energy in heat form since the superconductor state value depends on the cryogenic temperature. In addition, the cooling system can cause parasitic losses inside the system. All the disadvantages mentioned above mostly pertain to possible technical problems, so designers should be able to mitigate them with accurate designs.

The SMES structure is shown in Fig. 2.9. It consists of a voltage source converter (VSC) using an insulated-gate bipolar transistor (IGBT), transformer, DC-DC chopper using IGBT, power conversion system (PCS), pulse width modulation (PWM), DC link capacitor, and large inductance as a superconducting coil (SC). The VSC consists of two IGBT devices to diminish the harmonics and it is linked with the DC-DC chopper by a DC-link capacitor. The SC is charged from the grid during the normal operation to a set value. After the SC charged, it conducts current supporting the electromagnetic field. During the SMES operation, the SC must be through immersed in liquid Helium at 4.2 K in an insulated vacuum cryostat to maintain it in the superconducting state. Whenever there is a fluctuation in the system power during a disturbance, the discharging start immediately through the PCS to the utility grid. The control system restores the power system to an equilibrium condition and the SC charges again to its initial value. In addition to technical consideration, the economics of ESSs are also essential to be considered. The overall benefits of the system must be calculated accurately if the authorities are to know whether installing and running the system is feasible.

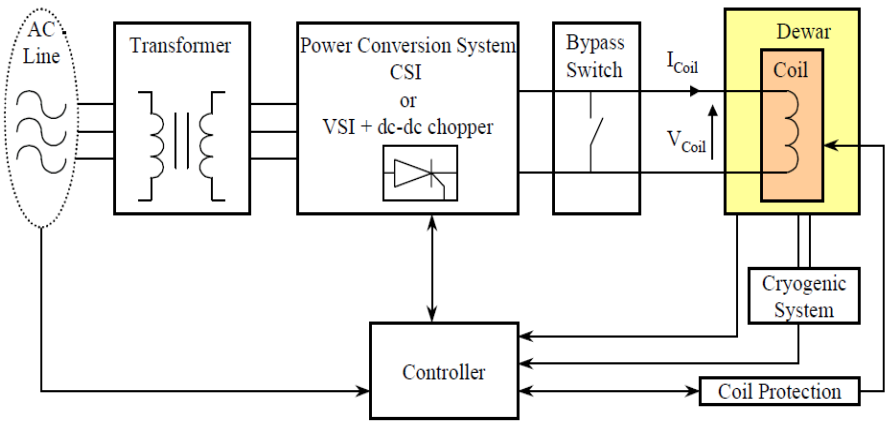

Fig. 2.9 Components of a typical SMES system

Therefore, the selection of ESSs should be cost-effective in all aspects. According to [69], the estimated cost in US$ per kW for each ESS: flywheel ESS has the highest cost, ranging from 500 to $6,000/kW followed by a pumped hydro system at a maximum cost of 1,600$/kW. SMES has a medium cost that lies at $1,000/kW. The ultra-capacitors (UC) cost per kW is relatively cheap, which may make UC a suitable connection to small-to-medium scale kW systems. Battery ESS also has a competitive cost per kW, as it lies in the range of $350 to $1,000/kW. In fact, it is already used widely in the uninterruptible power supply (UPS) system. The economic consideration of connecting the ESSs to the power system must include close estimates of all economic aspects in order to achieve the most cost-effective combinations. For example, developers may discover that using a hybrid of two or more ESSs might be better for certain power system after they conduct all calculations for the related generating and load systems.

In this research, the extra power is stored by SMES for future needs when the generation is higher than the demand for a grid-connected mode in the typical MG. The stored power is used to supply the load or stabilized the system when there is any shortage/loss of generation or the utility grid during the islanded mode. For the isolated operation, SMES is used to stabilize the MG from instability and collapse in the presence of violent changes of loads or outage of generations. Furthermore, a modified controlled SMES to mitigate the frequency and voltage fluctuations of the MG considering the high penetration of RERs is adopted and will be compared with optimal PID controller and conventional SMES.

2.12 Literatures Review

A wide range of research and development in the field of integrating RERs with power systems and the potential effects on the frequency and voltage fluctuations were done in the past. This section presents the relevant literature review done to carry out this research work.

In past, several cascaded blackouts happened in electrical power systems due to frequency instability in case of the imbalance between the electrical load and power supply or N-1 contingency [70]. Nowadays, this problem increased after the growth of the RERs, which have several impacts on the performance of the power systems especially MGs as the reduction of system inertia. Consequently, increase the voltage and frequency fluctuations [71]. Furthermore, the RERs exchange electrical power to MGs through power electronic inverters, which cause higher power fluctuations than the traditional synchronous generators. In addition, the high penetration of RERs leads to an increase in the short-circuit capacity of the power

system. Therefore, if the RERs penetration becomes larger, the islanded MGs might become insecure as the stabilizing in system frequency and voltage is difficult in that situation [72, 73]. Moreover, there will be unbalanced between the generation and load due to the variable nature of RESs. These changes lead to the appearance of challenges for the conventional control and protection systems such as nature transient variations in MG. These variations are highly affected by the operation mode of MG whether grid-connected or stand-alone [74, 75]. On the other hand, the selection and coordination of conventional protective relays became more complex due to the frequent bidirectional power flow in connection feeders of MGs to utility grids [76, 77]. Therefore, several studies have developed different control strategies to deal with these challenges. However, in case of large frequency deviations, which might follow by an additional generation or load events leading to imbalances in active power during the fault periods, the control technique is unable to restore the system frequency. In that situation, the emergency control and protection must be used to return the system frequency to its steady-state condition.

Load frequency control (LFC) is considered as one of the most important control strategies in a power system which maintains the system frequency and the power variations at their standard values. In previous decades, LFC problem has a great interest and several studies to enhance the power system operation, control, and stability. In this context, many control strategies were applied to the LFC of the MGs and interconnected power systems such as a fuzzy controller, neuro-fuzzy control, and artificial neural network controller [78-81]. These methods seem to be efficient to deal with this problem. However, they suffer from 1) their long computation time; 2) complex procedures; 3) its proper design depends mainly on the designer experience, and they have high cost compared with the conventional controllers. Moreover, Authors in [81] discussed the robustness of the Coefficient Diagram Method (CDM) controller including energy storage system (ESS) such as Electric Vehicles (EV) in his control strategy in a small power system. In addition, the same issue has been studied for the modern power system [83]. However, the structure of this control technique is complicated, as it required more steps to get its parameters. Mohamed et al. [84] used Model Predictive Control (MPC) based LFC for both single and multi-area interconnected power system.

On the other hand, the proportional–integral (PI) and PID are the most popular in industrial applications due to some merits such as its simple design and lower cost and wide stability margin [85]. However, these controllers suffer from the system non-linearity and the sensitivity to the variation of system parameters. Therefore, there are numerous studies have been used in order to optimize the parameters of these controllers for the LFC of different power systems.

Some designers used the conventional methods such as linear programming (LP) [86], Interior point algorithm (IP) [87], and Quadratic Programming Method (QP) [88]. However these methods suffer from stagnation, may be trapped in local minima. In addition, they need numerous iterations to guarantee that the solution is converged. Hence, these techniques are computationally intensive. While, many recent heuristic optimization algorithms were used for solving this problem, such as genetic algorithm (GA) [89], Fruit Fly Optimization [90], Firefly algorithm [91], and particle swarm optimization [92]. Indeed, Most of previous LFC approaches were for the interconnected power systems, which are linear, simple structure, and depends mainly on the conventional synchronous generators [89-92]. Some few studies deal this problem in MGs and wind energy conversion systems such as [93] studied the LFC for interconnected power system concerning wind turbines. Praghnesh et al. in [94] studied the effect of the dynamic contribution of DFIG for a two-area interconnected hydrothermal power system. Furthermore, in [95], the LFC problem take into account the uncertainty of the wind energy conversion system and the problem is solved using the symbiotic organisms search algorithm.

Due to the intermittent nature of the RERs, the problems of the voltage and frequency fluctuations increased and the power generated cannot follow the load demand effectively, thus several studies proposed the Energy Storage System (ESS) as a new LFC scheme as frequency stabilizer to enhance the MG stability. The main goal of using energy storages in MG systems is to keep the active power of the MG in stable point by mitigating the renewable power fluctuation, shaving the load peak, and leveling the load, as illustrated in [96-98]. Furthermore, some studies presented single or hybrid ESS and mentioned that the performance is enhanced [99, 100]. And recently, a coordination of self-adaptive wavelet decomposition method and a two-level power reference signal distribution technique have been used as a hybrid ESS to alleviate the wind power variations in [101]. Moreover, a Novel coordinated control strategy using model predictive control for power scheduling with different ESSs is presented in [102]. In addition, Heuristic optimization algorithms using particle swarm optimization method was also introduced for real-time implementation [103]. Shi et.al [104] introduced a power fluctuation index, which used for ESS control. Recently, some authors proposed a control technique for ESSs taking the state of charge (SOC) into account such as Dang et. al. in [105] proposed the SOC feedback control technique for ESS activating pitch control. However, this method is not proper for responding to the sudden deviation of wind power fluctuation, which is commonly happening. Another one in [106] considers SOC by proposing a method that divides the control region for the ESS. In this method, the mitigating of wind power fluctuations

is solved only by ESS without any action from a wind turbine. This can lead to the capacity-related problems of ESS and diminishes its lifetime. Pingping et al. [107] have presented the energy storage in electric vehicle battery as an auxiliary LFC technique.

The superconducting magnetic energy storage (SMES) is considered one of the very important ESS technologies where it is preferred with RERs. It is better than other ESSs as it has a shorter time delay during charging and discharging process, higher efficiency, and longer lifetime [108]. Moreover, the bidirectional flow of both real and reactive powers can be achieved from the SMES coil according to the status of an electrical power network, which increases the ability of the applied control and enhances reliability and accessibility of the power network [109]. Many studies illustrated the application of SMES with wind power generation (WPG). Some of them presented the impact of SMES in improving the transient stability in presence of doubly fed induction generator (DFIG)-based wind turbine [110, 111]. Regulating the PCC voltage, active power, and reactive power transfer between the grid and fixed speed SCIG type by using SMES is reported in [112]. Authors in [113] analyzed and proposed the impact of SMES unit installed in the distribution system equipped with DFIG and SCIG wind turbine on voltage sag and swell events. Gaber et al. in [114] have discussed the superconducting magnetic energy storage (SMES) as a new supplementary LFC scheme.

Due to the high integration of the RERs in the existing MGs, they share in increasing the fault current levels during short circuits conditions. This makes the electric power systems have become more complicated, fault current levels are becoming larger than the capability of the existing circuit breakers (CBs). The ESS devices cannot solve this type of problems. Therefore, limiting the fault current is a potentially good option for mitigating the RERs impact on the power system. Fault current limiters (FCLs) can keep the existing CBs and delay their replacement due to RERs integration, and maintain the coordination of the original protective relays even with high RERs penetration. Consequently, the voltage at the terminals of RERs could stay at a relatively an acceptable level without large voltage dip and can keep the RER connected in the grid, which called the LVRT capability. In the last decades, conventional techniques have been used to overcome this problem and enhance the LVRT capability of RERs, such as series reactors, current-limiting fuses, and high-impedance transformers [115]. However, some of these alternatives may create other problems, such as loss of power system stability, high cost, and increase in power losses [116]. Some studies presented the conventional Crowbar system to improve the LVRT capability of wind turbines [117]. It is connected with the rotor terminals of the doubly-fed induction generator (DFIG) through electronic switches to cut off the converters from the generator. This method is very effective

in limiting the high currents in the rotor during the fault. However, the DFIG changes to a squirrel cage machine, which draws reactive power from the grid which may lead to a further decrease in the grid voltage [118]. To overcome these disadvantages, several control techniques needed [119, 120]. Recently, some researchers used a modified Crowbar type named the Outer Crowbar which is connected in series with the DFIG instead of being connected to the stator windings [121]. Static synchronous compensator (STATCOM) is used widely for power compensation but it can only control the reactive power and increase voltage dip after the occurrence of fault [122, 123].

Many techniques have been presented recently to deal with the enhancement of LVRT capability of the fixed-speed induction generator (FSIG) based-wind turbine. Hossain et al. used the fast pitching technique of the turbine blades [124] and Moghadasi et al. presented the application of flexible AC transmission system (FACTS) devices [125]. A comparative study on different methods for enhancing the FSIG has been presented in [126]. This study proved that the pitch control method is the most economical one, but its dynamic response is very slow because of the mechanical design constraints. In addition, this study stated that the installation of ESSs and FACTS devices have a high capital cost due to utilizing of power conditioning systems.

Also, the improving of LVRT capability of permanent magnet synchronous generator (PMSG) has been analyzed and presented in [127-130]. In [127], a coordination of fuzzy logic control (FLC) and fast pitch controller has been presented for enhancing the wind turbines performance under the severe disturbances. Another technique allows the augmented wind energy to be retained in the wind turbine shaft inertia during the fault [128, 129]. However, these methods have a slow dynamic response and cannot contribute alone for LVRT support although they are cheap solutions. The authors in [130] used the well-known braking chopper for the PMSG. This method has a simple control to consume the extra power and also it is not expensive. However, the total cost of braking choppers in a large wind plant will dramatically increase. In addition, this method suffers from the poor power quality of wind turbine output since the braking chopper dissipates the power. On the other hand, many control methods are suggested for the PMSG operation during faults. In [129, 131], the authors used the linear proportional-integral (PI) controller and pulse width modulation (PWM). The specific problem is that a linear PI controller is considered for normal voltage levels, which in turn lead to high currents at diminished voltage levels during the fault. The nonlinear control methods are introduced to improve the classical current control method [129, 112], but most of them are complex and

very sensitive to system parameters for practical applications and need proper tuning of control [133].

Recently, attention has been devoted to the superconducting fault current limiter (SFCL). Superconductors have the unique property of being able to automatically switch from low impedance to high impedance rapidly as a result of the high current, which make them especially suitable for the current limiting application. SFCL is in principle a completely passive device and has fail-safe characteristics, thereby making it a better choice for fault current limiting. In [134], the authors presented SFCL as a self-healing device to control the short circuit current levels in distribution and transmission networks. After discovering new materials of high-temperature superconductors (HTS), the use of SFCL becomes more applicable [134, 135]. Hence, SFCL has many merits, such as nearly zero impedance at normal conditions, fast response to the fault current, recovering automatically, and faster performance in damping excessive fault current.

From another side, in cases of a large generation loss disturbance or high integration levels of RERs, the conventional power reserve may not be enough to return the stable condition of the system frequency, the emergency control and protection schemes plan may be followed, such as over/under frequency load shedding must be used to restore the system frequency. Some studies handled the frequency protection problems such as; Laghariet et al. [136] applied an intelligent computational technique for load shedding of the power system under faulted conditions. Moreover, Komsan et al. [137] discussed the same issue using the rate of change under frequency relay to improve the load shedding scheme in MG systems. Further, W. Freitas et al. [138] presented a comparative study of the rate of change of frequency (RoCoF) and vector surge relays for distributed generation applications. However, they faced a very hard task in relays coordination as their design may not detect the islanded conditions within the required time. Furthermore, Jongchan et al. [139] developed a design for protection coordination between load shedding scheme and synchronous generator protection. William et al. [140] presented how the microprocessor-based protective relays are used to offer both control and protection functions for MGs. Also, the use of digital relays with communication systems presents a solution for these problems [141], but its cost is high in some cases. Jose Vieira et al. [142] proposed the coordination of RoCoF and over/under frequency relays (OUFRs). However, this coordination did not compensate the frequency fluctuations within the allowable frequency limit due to the action of the relay is energized when the system frequency become out of the allowable limit. Such a problem can be overcome by designing the proposed

coordination of frequency stability using digital LFC and digital OUFR, which will be presented in this thesis.

2.13 Summary

A literature review regarding the power system control, stability, and protection of electrical power systems considering high penetration of RERs have been presented. The impact of RERs integration on control and protection of power system is discussed. Afterward, the definitions, basic concepts, and technical challenges of MGs issue are addressed. The MG operation, control, and its application are presented.

Chapter 3

Application of Superconducting Fault Current Limiter in Microgrid Systems

3.1 Overview

Due to the high penetration level of wind farms in the electrical grids, many grid connectivity issues interested and must be highlighted such as the improvement of Fault-ride through (FRT) capability of grid-integrated doubly fed induction generators (DFIGs) based wind-turbine. This chapter presents an introduction of the recent approaches, which are employed to enhance the low voltage ride through (LVRT) capability of the wind turbines. Then, presenting a positive approach using a resistive superconducting fault current limiter (RSFCL) to minimize the fault current, enhance the FRT capability of DFIG, preserve DC-link voltage level and improve the power system quality under abnormal conditions. To achieve these objectives, the thermal modeling of the RSFCL is developed and its impact on the dynamic performance of DFIG is studied by using MATLAB/Simulink. The proposed scheme performance has been compared with the Crowbar system to confirm its validity.

3.2 Introduction

Disturbances, which occur on the wind power system, can lead to voltage dip situation at wind turbine terminals because of the high fault current. To deal with this problem, the wind turbines should be tripped with circuit breakers instantly when the fault appears and the voltage at their terminals reduced to 80%. The tendency toward the integration of high RERs plants shares in the increase in fault current levels, as well as voltage reductions at the terminals of RERs, which lead to disconnection a large RERs. Consequently, the power system operation is affected seriously. Thus, new grid code requirements concerning the grid voltage support, which is called LVRT capability, are regularly being developed [143-145]. This LVRT reveal that RERs need to stay connected during the disturbance scenario to provide real and reactive power support to the power system.

The LVRT has been defined by many international codes, such as the Danish code for wind turbines connected to the grid [146]. It is shown in Fig. 3.1(a). Based on this code, if the voltage remains at the level greater than 20% of system voltage for a period less than 0.5 s, the wind

turbine should be connected to the grid. Wind turbines are only forced to disconnect from the grid when the voltage profile falls into the Area B. Furthermore, some other codes require high penetration of wind turbines to contribute to the voltage restoration of the power system by injecting sufficient reactive power during the fault and the recovery period, while maintaining the operating point above the area B of Fig. 3.1(b).

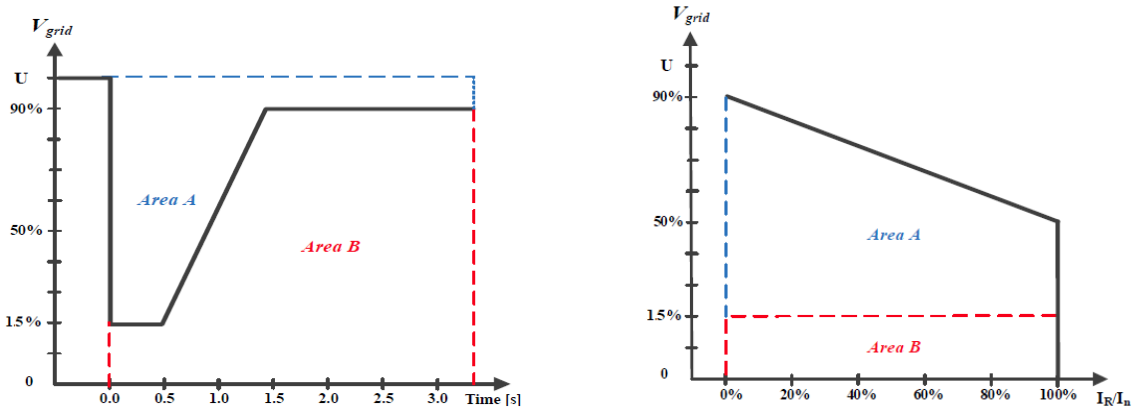

Fig. 3.1 Danish grid codes (a) LVRT requirement. (b) Reactive power support requirement

There are many auxiliary devices to provide an adequate dynamic voltage support and enhance the LVRT capability of wind turbines. The major categories of LVRT methods for the wind turbines are depicted in Fig. 3.2. Depending on the connection configuration, these methods can be classified into series-connected solutions, shunt-connected solutions, and hybrid-connected solutions.

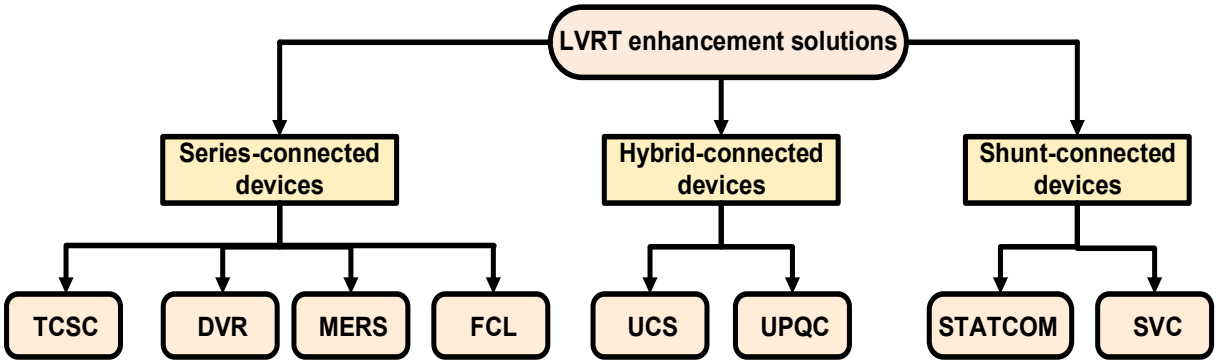

Fig. 3.2 Methods for LVRT capability enhancement

3.2.1. Shunt-connected solutions

These techniques are widely used to provide a fast steady state and transient voltage control at the connection point. These methods proved that they the most effective solution for the wind turbine connection with a grid to be appropriate for the recent international grid codes. This is because the output current of these devices can be adjusted to control the voltage or reactive power injected into the system.

The static var compensator (SVC) is a member of flexible AC transmission system (FACTS) family for reactive power compensation, which is most widely used in power systems. It consists of thyristor switched capacitors in shunt with the thyristor-controlled reactor (TSC-TCR). The TSC provides a step change of connected shunt capacitance, while the TCR provides continuous control of the equivalent shunt reactance. The SVC can be operated to provide reactive power control or closed-loop AC voltage control [147]. The main problem of SVC is to inject an uncontrollable reactive current dependently on the grid voltage [148]. Hence, the current injected by the SVC reduces linearly with the voltage drop and consequently, the injected reactive power reduces quadratically. In [148], the PI controller has been used to control the firing angle of the thyristors of the TCR and TSC during and after a fault. However, the tuning of the PI controller didn't achieve a simplistic method. Koessler et al. proposed a tuning technique for the transient gain to reduce the SVC response [149]. However, this method leads to a slower voltage recovery after the fault and exceeding the LVRT requirements.

Static synchronous compensator (STATCOM) is another shunt device, which can support the voltage stability by providing a controllable reactive current due to a reduction in the grid voltage. It consists of three devices, i.e. DC link energy storage capacitor, voltage source converter, and connection transformer. The main advantage of the STATCOM compared to SVC is that the compensating current is independent of the voltage level of the connecting point and thus the compensating current is not reduced as the voltage drops [148]. This advantage is very important nowadays that the new grid codes will require wind turbines to supply reactive power in a variable manner depending on network request and voltage level. However, regarding the LVRT, the most relevant feature of the STATCOM will be its ingrained capability to increase the transient stability margin by injecting a controllable reactive current independently of the grid voltage.

3.2.2. series-connected solutions

These techniques are relatively simple solutions with less current injection comparing with shunt connected methods. They are used to regulate the voltage or limit the fault current effectively, which in turn enhance the voltage and transient stability of power systems.

The thyristor-controlled series compensation (TCSC) is one from the series connected methods. It controls the power flow of the grid lines to increase the power system stability and damp the power fluctuations [150]. It consists of three components: capacitor banks, bypass inductor, and forward-biased thyristors. The ability of TCSC to limit the fault current and control the unbalanced voltage of wind turbines is presented in [151]. Moreover, this device may be useful

for enhancing the LVRT of wind farms, which are located far away from the PCC, such as offshore wind farms [152].

The dynamic voltage restorer (DVR) is another series connected device, which injects a suitable voltage into the requested bus in order to keep the generator voltage constant at PCC with the same phase as the grid. DVR might have a sufficient energy storage capacity to generate the missing voltage at the wind turbine terminal during the voltage dip. Several types of research have been presented to mitigate the voltage dip and recovery with DVR to restore the terminal voltage of wind turbine to the operating point within the shaded area of the LVRT code [153, 154]. However, the DVR is required to absorb the extra active power, which is generated by the wind generator during the fault in order to keep the dc-link voltage at the determined level. Thus, this is the main drawback of the DVR, as it must have energy dissipation capabilities.

Furthermore, Wiik et al. used the magnetic energy recovery switch (MERS), which is a variable series compensator between the transformer of the wind farm and the grid to enhance the LVRT capability of wind turbines by controlling the reactive power and voltage at the terminals of wind turbines [155, 156]. MERS consists of four reverse conductive semiconducting switches and a DC capacitor similar to the single-phase full-bridge inverter with a smaller dc capacitor.

Recently, the utilizing of fault current limiter (FCL) is increased with the high levels of fault currents due to the high penetration of RERs into power grids. Several types of FCL have been used recently, such as transformer coupled bridge fault current limiter (BFCL), a resonant circuit, reactors, solid-state FCL, and superconducting fault current limiter (SFCL) [157, 158]. These previous FCL studies have proven the ability of FCLs to improve the LVRT capability and the transient stability of the wind power systems, especially the BFCL and SFCL. Firouzi et al. [159] and Jafari et al. [160] presented the BFCL with a discharging resistor. The resistor is in parallel with a semiconductor switch are connected in series with a dc reactor of the BFCL to control the short circuit current by controlling the dc reactor current. This technique suppresses the instantaneous voltage drop and enhances the transient behavior of wind turbines at the fault instant without delay, which is the main merit of this FCL type over the other LVRT methods. However, this approach needs a special and costly transformer to connect the three-phase diode bridge in series into the power system, in which primary voltage rating of the transformer must be almost equal to the transmission line voltage to maintain the desired level of voltage within the fault duration [161].

The SFCL is a self-healing device since it doesn't need any control action due to its automatic transition from non-superconductivity to the superconducting state. It suppressed the fault

current immediately from the first peak of current and diminishes the voltage drop at the wind turbine terminals, leading to enhancement of the LVRT curve [162, 163]. This innovating FCL device introduces an exclusive feature that cannot be obtained by conventional current limitations.

3.2.3. Hybrid-connected solutions

Some researchers used series-shunt (hybrid) topologies to improve the LVRT capability of wind turbines. One of these methods is the unified power quality conditioner (UPQC), which is an integration of series and shunt VSC, has been commonly used to improve the voltage sag, voltage unbalance, harmonics, dynamic active and reactive power regulation [164, 165]. Furthermore, Moghadasi et al. propose a novel combination of resistive SFCL and UPQC in order to improve power quality problems and fulfill grid code requirements [166]. However, the capital cost is very higher than any other solutions devices because of the use of two converters and costly SFCL.

Huang et al. introduced in [167] a novel technique of combined series and shunt methods, which is called unified compensation system (UCS), to improve fault ride-through (FRT) capability for wind turbines. This technique used one converter to provide both series and shunt compensation. It operates like a STATCOM in the normal operation to support reactive power regulation via its shunt connection, while, it instantaneously switches from shunt-connection to series-connection during the fault instant to compensate the voltage and maintain the stator voltage at the rated value.

3.3 LVRT Improvement of Wind Turbines Using RSFCL

In this section, an optimal resistive superconducting fault current limiter (RSFCL) is proposed as a self-healing equipment in order to enhance the LVRT capability of the DFIG based-wind turbine. In addition, preserve DC-link voltage level and improve the power system quality under abnormal conditions. To ensure the validity of the proposed technique, the thermal modeling of the RSFCL is developed and its impact on the dynamic performance of DFIG is studied by using MATLAB/Simulink. The proposed scheme performance has been compared with the popular crowbar system to confirm its validity.

3.3.1. DFIG-Based Wind Turbine Model

DFIG is a variable speed wind turbine and its configuration is a wound-rotor induction machine. Fig.3.3 illustrates the main construction of DFIG. It has two voltage-source converters being connected to the rotor and the grid. The first one is the rotor side converter (RSC) which controls the power factor and the second is the grid side converter that is used to control the

DC-link voltage. The DC-link capacitor which connects the two converters back-to-back is used to reduce the voltage ripple. By these two converters, the rotor currents can be controlled, by controlling the rotor voltages through a PWM strategy. Wind kinetic energy is straight converted to a mechanical power through a wind turbine. A gearbox is connected with the wind turbine to adjust a rotational speed of the DFIG. The output power of a wind turbine is written as:

$$P_w = 0.5\, C_p\, A\rho v^3 \tag{3.1}$$

Where ρ is the air density, v is the wind speed, A is the area covered by the rotor and C_p is the coefficient of performance of the turbine.

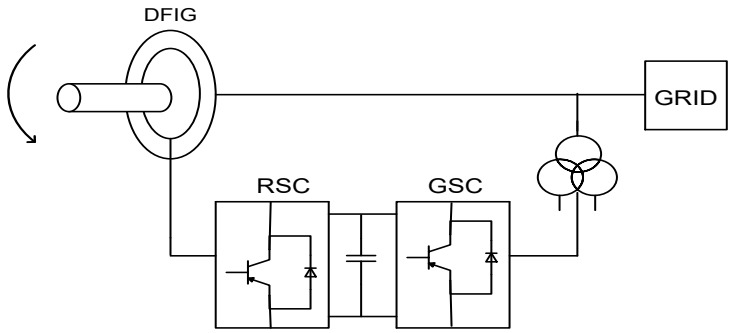

Fig. 3.3 Construction of DFIG

In order to investigate the actual behavior of the DFIG, dynamic equation needs to be considered for more realistic observation. From the point of view of the control of the machine, the d-q representation of an induction machine leads to control flexibility; Fig. 3.4 and Fig. 3.5 show the equivalent circuit of the DFIG in the d-q frame. The dynamic behavior of the DFIG in the synchronous reference frame can be represented by the Park equations provided all the rotor quantities are referred to the stator side. The stator and rotor voltages are expressed as follows:

$$v_{ds} = R_s i_{ds} - \omega_s \lambda_{qs} + \frac{d\lambda_{ds}}{dt} \tag{3.2}$$

$$v_{qs} = R_s i_{qs} + \omega_s \lambda_{ds} + \frac{d\lambda_{qs}}{dt} \tag{3.3}$$

$$v_{dr} = R_r i_{dr} - (\omega_s - \omega_r)\lambda_{qr} + \frac{d\lambda_{dr}}{dt} \tag{3.4}$$

$$v_{qr} = R_r i_{qr} + (\omega_s - \omega_r)\lambda_{dr} + \frac{d\lambda_{qr}}{dt} \tag{3.5}$$

Where λ is the flux linkage, ω_s is the synchronous speed, ω_r is rotor angular speed and R is the resistance.

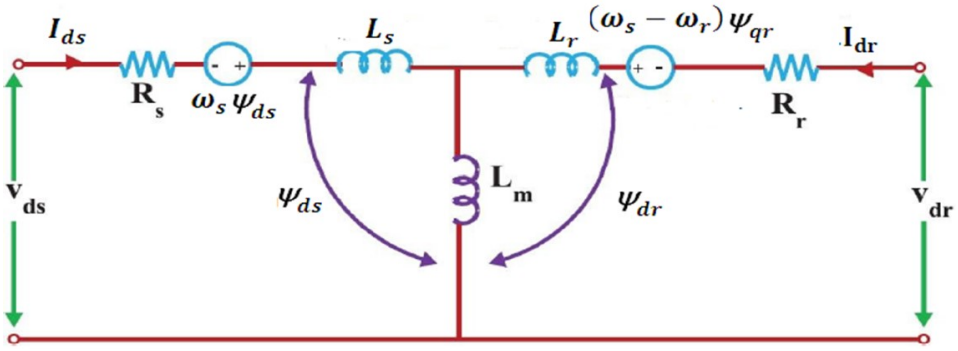

Fig. 3.4 Dynamic d-q equivalent circuit of DFIG (d-axis circuit)

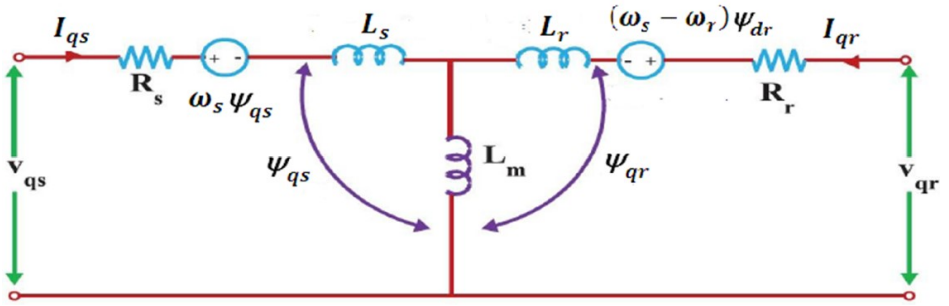

Fig. 3.5 Dynamic d-q equivalent circuit of DFIG (q-axis circuit)

3.3.2. BSCCO SFCL Model

Practically, high temperature superconducting (HTS) FCLs have been classified into the resistive, inductive, and hybrid types [168–170]. Among these types of SFCLs, the RSFCL can protect the system against the fault current immediately by a considerable increment in the resistance. RSFCL is not structurally complex, compact size, simple operation and very effective in power system stability [171]. RSFCL also can be switched to the normal operation condition autonomously after barricading the fault current. Hence, the damping performance of RSFCL is recognized as multi-sided cooperation between the fault current magnitude values, thermal properties, and the variable resistance of the HTS substrate.

RSFCL unit is modeled in SIMULINK as a controlled voltage source, its value depends on the total resistance of the superconducting (SC) film and shunt resistance and on the current value. RSFCL is connected in series with the line, which has to be protected. Fig. 3.6 shows a unit structure of RSFCL, which is based on the switching from SC state to normal state with bismuth strontium calcium copper oxide (BSCCO). It is one of the advanced high temperature superconducting (HTS) materials that have the ability to work around 77 K and hence less costly in cooling systems comparable with conventional superconductors which work near 4K. The specification data of the superconducting materials are shown in appendix A.

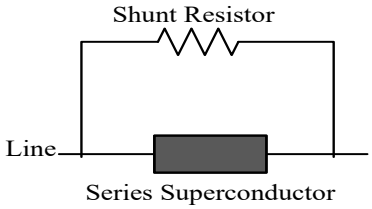

Fig. 3.6 A unit structure of RSFCL

The limiting resistance of the superconductor depends on the cross-sectional area and length of material as shown in the following equation:

$$R_{sc} = \rho_{sc} \frac{\ell_{sc}}{A_{sc}} \tag{3.6}$$

Where R_{sc}, ρ_{sc}, ℓ_{sc} and A_{sc} are the resistance, the resistivity, the length and cross-section area respectively.

The resistivity of the Bi-2212 SC material depends on three main parameters, the current, the magnitude and direction of the external magnetic field applied to the SC material and the temperature. SC resistivity varies over three possible states, which are a superconducting state, flux flow state and normal state (resistive state) [172].

- For $T < T_c$ and $J < J_c$

$$\rho_{sc} \cong 0 \tag{3.7}$$

- For $T < T_c$ and $J > J_c$

$$E(J,T) = E_o \left(\frac{E_c}{E_0} \right)^{\beta/\alpha(77k)} \frac{J_c(77K)}{J_c(T)} \left(\frac{J}{J_c(77K)} \right)^{\beta} \tag{3.8}$$

$$J_c(T) = J_c(0) \left(1 - \frac{T}{T_c} \right)^{\gamma} \tag{3.9}$$

$$E = \rho \, \mathrm{J} \tag{3.10}$$

Equation (3.11) below has been derived by simply substituting for $J_c(T)$ from Equation (3.9) into Equation (3.8). Then use Equation (3.10) to estimate the resistivity of the superconducting tube in the "flux-flow" state.

$$\rho_{sc}(\mathrm{J},\mathrm{T}) = \mathrm{K} \left(1 - \frac{\left(\mathrm{J}^2 \right)}{\left(1 - T/T_c \right)} \right) \tag{3.11}$$

where: $$K = E_o\left(\frac{E_c}{E_0}\right)^{\beta/\alpha}\left(\frac{1}{J_{c0}\times(J_{c77})^{\beta}}\right) \quad (3.12)$$

- For $T > T_c$

$$E(J,T) = \rho(T_c).\frac{T}{T_c}J \quad (3.13)$$

$$\rho_{sc} = \rho(\mathrm{T_c})\left(\frac{\mathrm{T}}{T_c}\right) \quad (3.14)$$

Where ρ_k, J_c, T_c, J_{co}, J_{c77}, E are the normal resistivity, the critical current density, the critical temperature, the critical current density at 0K, the critical current density at 77K and the electric field intensity respectively. The parameters $J_c = J$ (E_c=1μV/cm), E_o, ρ, α, β, γ at 77K depend on material operating conditions and varies within the ranges shown in Table 3.1 [172].

Table 3.1 – Parameters of Bi-2212 conductors

Parameter	Value
J_c	1000 to 10000 A/cm^2
E_o	0.1 to 10 mV/cm
ρ	100 to 2000 μΩ.cm
α	5 to 15
β	2 to 4
γ	1.4 to 1.8

The temperature rise in the superconducting film period can be calculated by Equation (3.15).

$$\Delta\mathrm{T} = \frac{\mathbf{R_{sc}}\mathbf{i}_{sc}^2 - P_{LN}}{\mathbf{C}\ell_{sc}\mathbf{A_{sc}}}\Delta\mathrm{t} \quad (3.15)$$

where i_{sc}, ΔT, C, and P_{LN} are The limited fault current, the increment in the superconducting temperature after an increment of time during the limiting period Δt, the specific heat capacity in J/m^3.K of the superconducting material, and the power losses in the liquid nitrogen, respectively. However, because the superconducting film is deposited on a substrate and surrounded by liquid nitrogen, some of the energy dissipated in the film transfers to both the liquid nitrogen and the substrate.

3.3.3. Simulation of the Resistive SFCL

The simulations throughout the work reported in this thesis were done using MATLAB and SIMULINK. The superconducting film is modeled as a "subsystem" block. A feature of the SIMULINK environment is that "subsystem" blocks can be nested, thus the overall

superconducting film block contains numerous blocks deeper within the model. The flow chart, which describes the modeling of the superconducting film, is shown in Fig. 3.7. The whole RSFCL model is shown in Appendix A. This model embodies a number of "subsystem" blocks and a large number of blocks, which make the solution difficult. There are a number of algebraic loops, which need to converge to a solution for every time step. At each time step ΔT_{sc} is calculated and added to the old T_{sc} to constitute the new T_{sc} which becomes the old T_{sc} in the next time step. R_{sc} and i_{sc} are also calculated at each time step. Results are displayed on the screen via "scope" blocks and can then be used for plotting or further processing.

The specific heat capacity of the superconducting material is not constant and varies with the material temperature during the limiting period. The variation in the specific heat capacity with temperature for Bi-2212 is shown in Fig. 3.8. This specific heat capacity versus temperature can be represented, in the developed routine for Simulink, by an n^{th} order polynomial or by a "Look up table" icon. In this work, a "Look up table" icon was used to represent the variation of heat capacity with temperature.

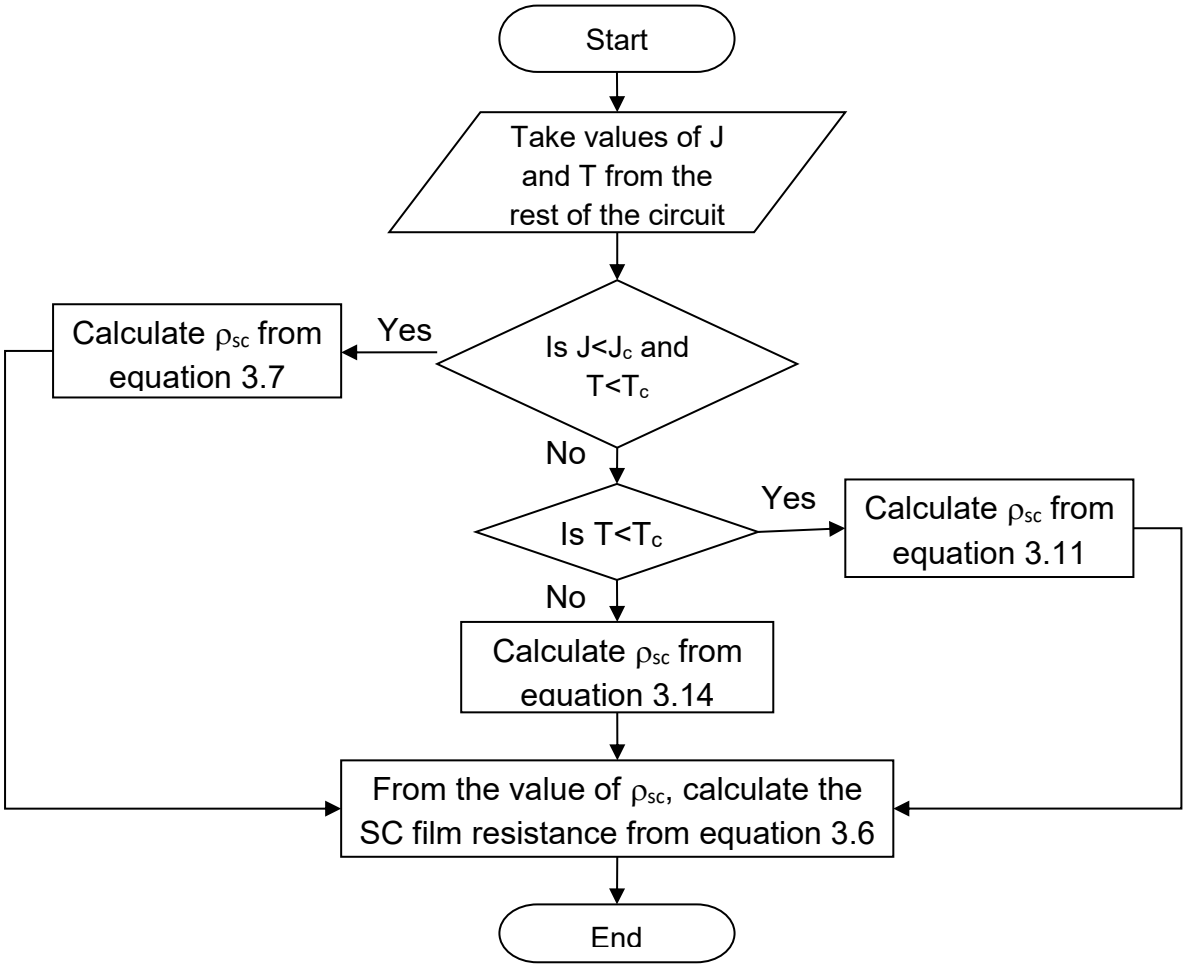

Fig. 3.7 Flowchart for the modeling of the superconducting film

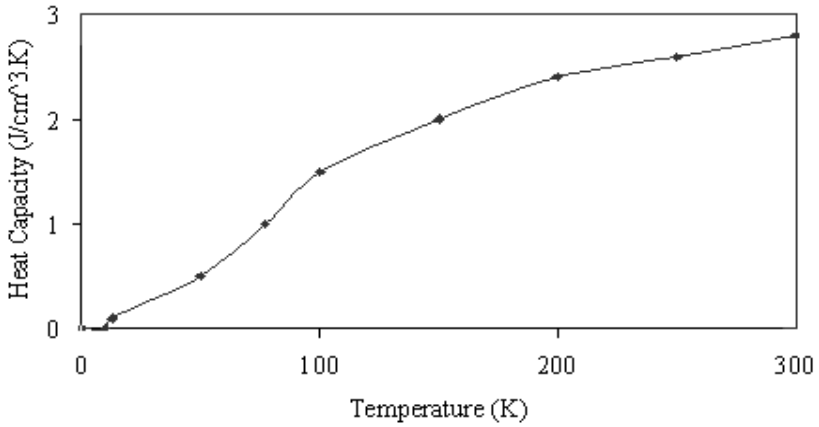

Fig. 3.8 Specific heat capacity of Bi-2212 as a function of temperature

To reduce the energy dissipated in the superconducting material during the fault period, a shunt resistance is connected across the superconducting material. The superconducting material, in this concept, is essentially a switch that commutates the fault current to the shunt resistance. The shunt resistance changes during the fault period by the effect of its temperature increment. Variation of the shunt resistance with temperature is shown in (3.16).

$$R_T = R_0\left[1+\alpha\left(T-T_0\right)\right] \tag{3.16}$$

The temperature rise in the shunt resistance during the fault period can be calculated by (3.17)

$$\Delta T = \frac{\rho\, i_{sh}^2}{\mathbf{P}CA^2}\Delta t \tag{3.17}$$

Where i_{sh}, ΔT and C are the shunt resistor current, the increment in the temperature of shunt resistor after an increment of time during the limiting period Δt and the specific heat capacity in J/kg.K of the shunt resistance, respectively. ρ and P are the resistivity and density of the shunt resistance material. In this work, aluminum shunt resistance with the specifications shown in Table 3.2 is used. The whole RSFCL model with shunt resistance is shown in Appendix A.

Table 3.2 – specifications of the shunt resistor

Material	Aluminum
Resistivity at 293 K	$2.586\text{x}10^{-8}$
Specific heat (J/kg.K)	897
Density (Kg/m^3)	$2.698\text{x}10^{3}$
Temperature coefficient (per degree K)	0.00403

3.4 Optimization of RSFCL

The design of RSFCL takes into consideration the optimal operation to damp the abrupt increase in the kinetic energy in the rotor of DFIG during the fault period and also minimizing

the energy loss of the RSFCL. Hence, the FRT capability of the wind turbine can be expected with the fault current limitation.

The first objective function is to minimize the kinetic energy stored in the rotor when the fault occurred. As a result, the first deviations of rotor angle and speed will be minimized [173].

The stored kinetic energy in the rotor of DFIG during fault can be expressed as:

$$E_k = \frac{M\delta^2}{2}(t_f - t_i)^2 \tag{3.18}$$

Where M is the inertia constant of DFIG rotor, t_i is the time of the fault occurrence; t_f is the fault clearing time, δ is the acceleration of the rotor during faults. In addition, the energy loss of RSFCL is the second function to be minimized and can be calculated as:

$$E_{SFCL} = \int i^2(t) R_{sc} dt \tag{3.19}$$

Where R_{sc} is the maximum superconducting resistance and $i(t)$ is the current flow through RSFCL.

Objective Function= $min\ (E_k + E_{SFCL})$ is Subjected to:

$(R_{sc\ min} \leq Rsc \leq R_{sc\ max})$, $(V_{min} \leq V_{PCC} \leq V_{max})$

3.5 Investigated System

Fig.3.9 shows a single line diagram of the studied system, which consists of the DFIG-based wind turbine (6*1.5 MW). It is connected to a 25kV power distribution system connected to an infinity bus with a voltage of 120 kV and a frequency of 60 Hz. During normal operation, the active power is generated depends on the characteristics of the wind turbine and the reactive power is set to zero. The location of the Outer Crowbar or the RSFCL is installed between the transformer (T1) and Bus2. Data of the DFIG and system parameters are shown in appendix A.

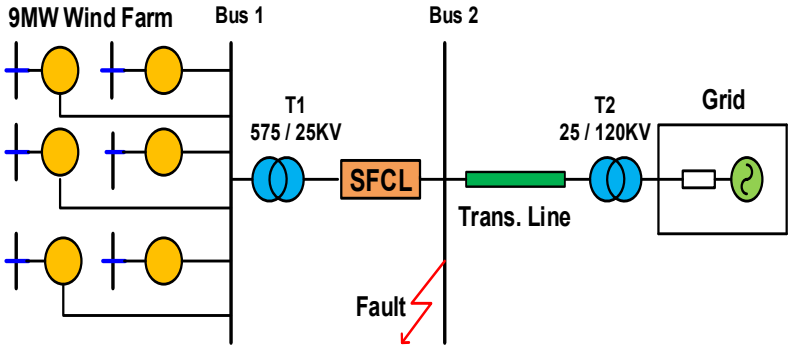

Fig. 3.9 Single machine infinite bus system with a DFIG-based wind turbine

In this case study, the RSFCL is compared with crowbar system. The crowbar system is the most well-known method that is being used to solve the problem of FRT. It is used to short the rotor windings of the DFIG through external resistances and the RSC will be disconnected from rotor windings by cutting off the pulses of the power switches in the RSC [173]. During activation of the Crowbar, the DFIG loses its controllability and will act like a squirrel cage induction generator which absorbs more reactive power from the grid leading further voltage dip on the system. In contrast, the Outer Crowbar, which consists of three resistances in parallel with bi-directional static switches connected in series with the DFIG as shown in Fig.3.10. At steady state, the switches will remain closed and the stator current will not pass through Crowbar resistances.

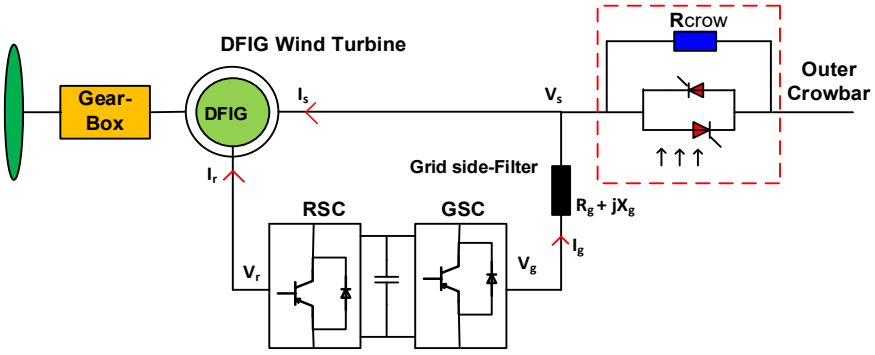

Fig. 3.10 Schematic diagram of the Outer Crowbar

When a short circuit occurred, the switches will be turned off. In this state, the output current will pass through Crowbar resistance and the Crowbar resistances will be in series with the DFIG. The static switches will be turned on or turned off according to the value of the DC-link voltage or the rotor current during the grid fault.

3.6 Results and Discussion

3.6.1. Current limiting capability

To illustrate the different effect of the Outer Crowbar and the RSFCL on the performance of the DFIG wind turbine during the fault conditions, a 3-ϕ fault was considered at the DFIG terminals. The fault is applied at 1 sec and cleared after 0.15 sec by using the usual protective devices. All results are taken at a wind turbine speed of 10 m/s. Fig. 3.11 shows the current limiting capability. In the steady state operation and without any protection as shown in Fig. 3.11(a), the stator current is 0.5 pu and during the grid fault, the first peak of the current increases to about 5 pu and became unsymmetrical. The performance of the DFIG under grid fault is studied with different values of Outer Crowbar resistances (R_{crow}). These values are multiplications of stator resistance (R_s) like (R_{crow}= R_s, $5R_s$, $20R_s$, $50R_s$, $100R_s$). From the

results, the optimum value is (R_{crow}= 5R_s) because it could limit the rotor and stator currents to the minimum permissible values during and after the fault compared with other cases. Fig. 3.11(b) shows this optimum case when the stator current first peak decreases to about 4 pu and continues in decreasing. It is noted that the Outer Crowbar action is not effective on the first peak of the fault current. This is because there is a little delay in the insertion of it depending on the triggering time of the power switches. After deactivation of the Crowbar resistance, there is a deviation in the current when the fault is cleared, that leads to the presence of transient components as it happens at the beginning of the fault but with less severity then it returns to steady state after deactivation of the Crowbar resistance.

When inserting RSFCL in the system as shown in Fig. 3.11(c), the peak value of the three-phase fault current is limited to about 2.8 pu. In contrast with the Outer Crowbar, RSFCL limits the fault current from the first peak without any control action. Also, the transient peak is reduced after fault clearance for all three phases. Therefore, the RSFCL gave a better effect on the overall dynamic performance of DFIG than the Outer Crowbar. Fig. 3.11(d) summarizes the different limiting effect of Outer Crowbar and RSFCL on the three-phase stator currents.

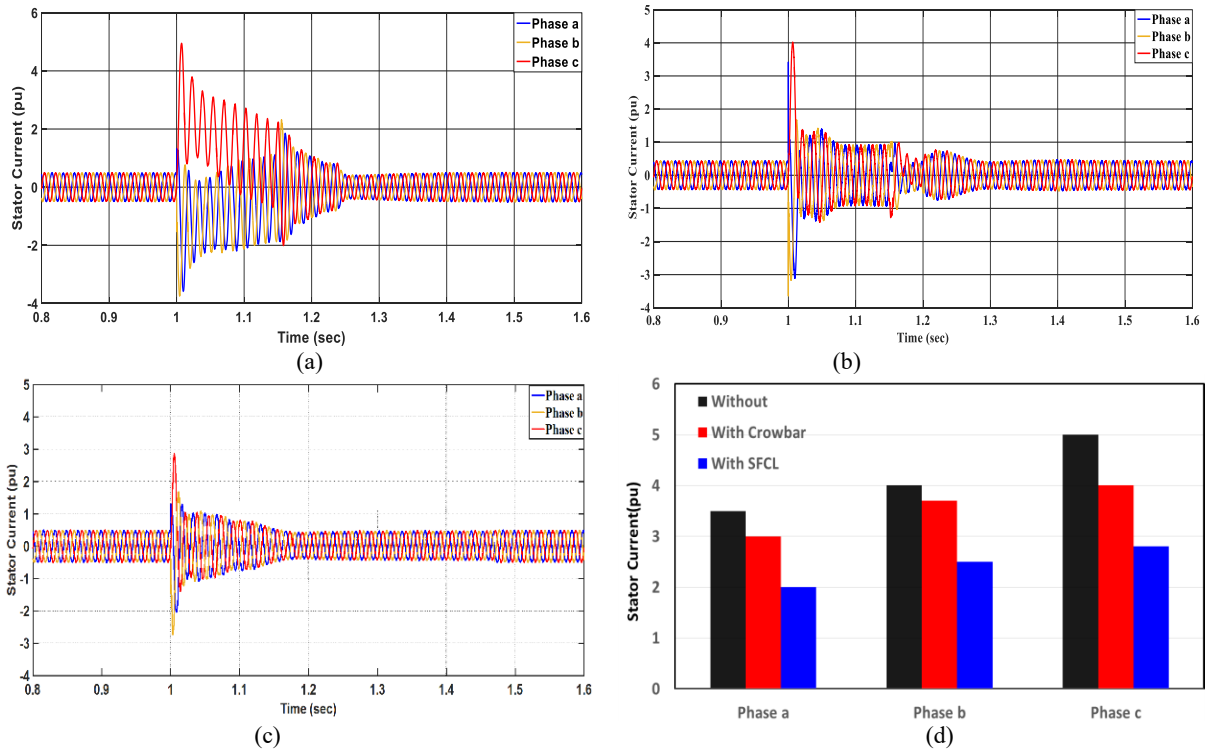

Fig. 3.11. DFIG Stator Current (a) Without; (b) With Outer Crowbar; (c) With RSFCL; (d) First Peak of Stator Current

3.6.2. Voltage Characteristics

This part explains the Characteristics of the voltage dip at the terminals of the DFIG. Without using any protection method, it is shown that the voltage is decreased to less than 0.1 pu during

fault as shown in Fig. 3.12, hence the wind turbine will automatically be disconnected. After using the Outer Crowbar, the voltage reaches to about 0.17 pu which is better than the minimum value level of 0.15 pu respected to the grid code requirements issued by AESO (Alberta Electric System Operator) [174]. However, there is a deviation in the voltage at the time of fault clearance. On the other hand, when connecting the RSFCL to the system, the rms voltage of wind turbine is decreased and reaches about 0.4 pu and the voltage deviation is reduced at the instant of fault clearance but still exist as the RSFCL cannot recover to its superconducting state immediately after removing the fault.

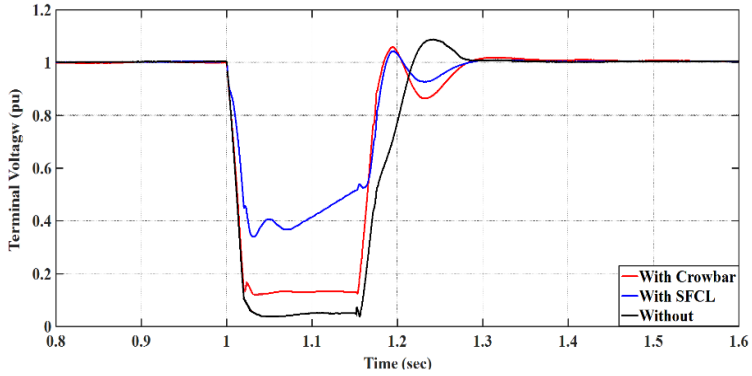

Fig. 3.12 Terminal voltage of DFIG

3.6.3. Active and Reactive Power Behavior

For more analysis of the effect of Outer Crowbar and SFCL on the performance of DFIG, active and reactive power are presented in Fig.3.13. The active power reduced to zero during the fault period without using any protection and the DFIG absorbs large reactive power from the grid. This is because the flux level needs time to readjust. Therefore, the electromagnetic torque fluctuated and reduced to zero. Hence, the rotor speed increased accordingly. But when the Outer Crowbar is used, Fig.3.13 (a) shows that the active power decreased to 2.1 MW during the grid fault. After deactivation of the Crowbar the power decreased to -4.1MW, and then it returned to the steady state. Fig.3.13 (b) shows the variations of the reactive power during the fault period. During normal operation, DFIG works at unity power factor because the reactive power is nearly zero. After fault occurrence, without Outer Crowbar or SFCL, there is a high positive deviation for about 8 MVAR then it reduced to nearly 2 MVAR during the fault period and by contrast, the DFIG absorbs large reactive power from the grid for more than 8 MVAR at the fault clearing instant. When activating the Outer Crowbar, the deviation in reactive power is reduced to about 6MVAR at fault moment and to about 4 MVAR at fault end but it Remains high to some extent.

After using the RSFCL, the active power drop is decreased to an acceptable value (4MW) which is less than the cases without and with the Outer Crowbar. In addition, the reactive power

characteristics are better than the previous cases, it has a very small deviation at the beginning and end of the fault as shown in Fig.3.13 (b). Furthermore, the RSFCL integration reduces the deviation of the torque and rotor speed as shown in Figs.3.13 (c, d). Consequently, damping the output power oscillation, and thus enhancing the stability of the wind system effectively.

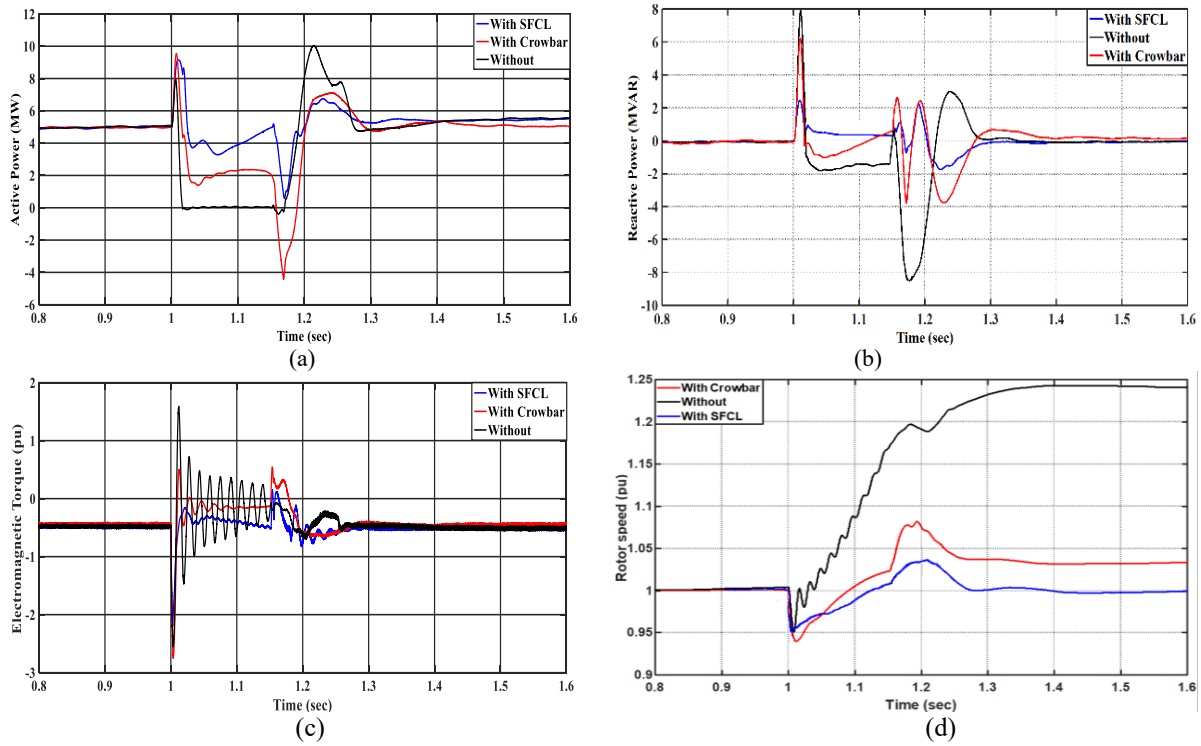

Fig. 3.13 DFIG Characteristics (a) Active Power; (b) Reactive Power; (c) Electromagnetic Torque; (d) Rotor speed

3.6.4. DC-link voltage

Fig. 3.14 shows the variation of the DC-link voltage at the converter side during the fault period. The DC-link voltage is 1200V in the steady-state operation. It increases to more than 3000V during the fault without any protection method, this value is very high and more than the allowable value. However, it reaches to about 1900V when using the Outer Crowbar. Although this value is reduced to an acceptable limit, there is some amount of energy still flowing to the DC-link. After using the RSFCL, the DC-link voltage is limited to about 1450V and returns to its steady state rapidly.

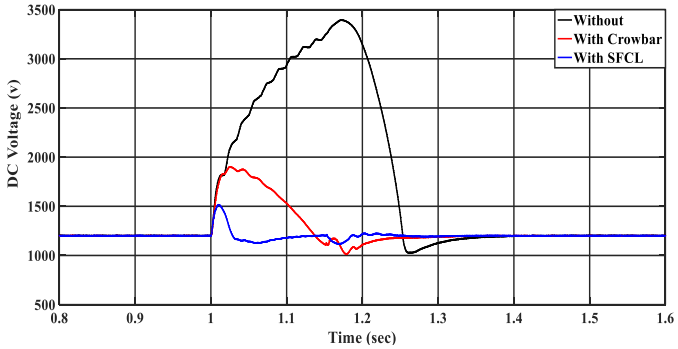

Fig. 3.14 DC-link voltage of the converter

3.6.5. Bi-2212 RSFCL characteristic

The Initial and critical temperature of the Bi-2212 RSFCL are 77 K and 87 K, respectively. Fig. 3.15(a) shows the temperature of the Bi-2212 RSFCL, it exceeds its critical value at the first cycle of the fault and continues to increase to higher values. So, the Bi-RSFCL state will change from the flux flow state to the resistive state. Hence, the resistance of the RSFCL increases continuously along with fault duration as shown in Fig. 3.15 (b) and limits the fault current. After the fault clearing, the fault current reduces and then the resistance of the RSFCL will slightly decrease. It takes some seconds to change from resistive state to its superconducting state.

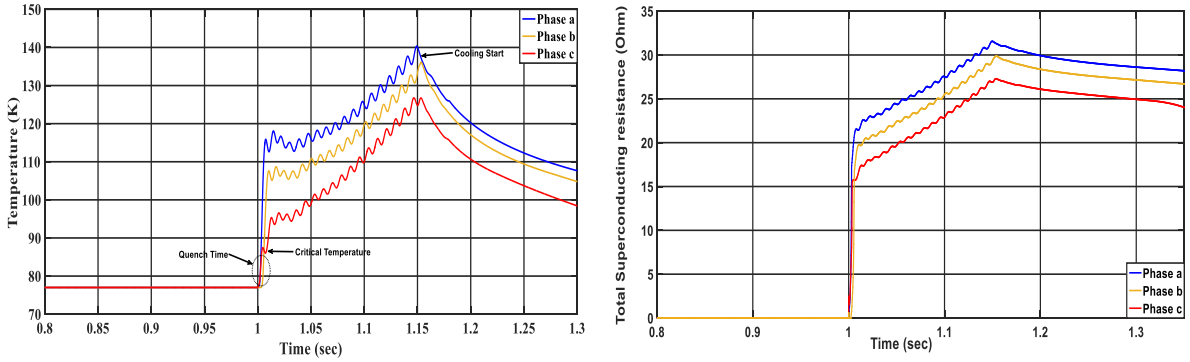

(a) (b)

Fig. 3.15 (a) Superconducting Temperature; (b) Superconducting Resistance

3.6.6. Effect of the Current Limiting Resistance

The evaluation of the current limiting resistance for both the Outer Crowbar and RSFCL has been studied with several cases of varying their resistance values. Fig. 3.16(a) shows that increasing R_{crow} value as a percentage of R_s decreases the voltage dip at the generator terminals. In contrast, the stator current dropped to values lower than the nominal current which causes a malfunctioning of the protection devices. Furthermore, there will be an undesired reactivation of the Crowbar due to the high current sensing at the end of the fault clearance. Hence, it has been found that the case of $R_{crow}=5R_s$ is the optimum value of Crowbar resistance. At this value, stator current is limited during the fault to permissible damped values as shown in the previous results. On the other hand, the voltage dip characteristics are improved for higher RSFCL resistance values as shown in Fig. 3.16 (b) with acceptable limited values of the stator current and the operation of the normal protective devices will not be affected. The minimum voltage level attained to more than 0.8 pu with higher RSFCL limiting resistance.

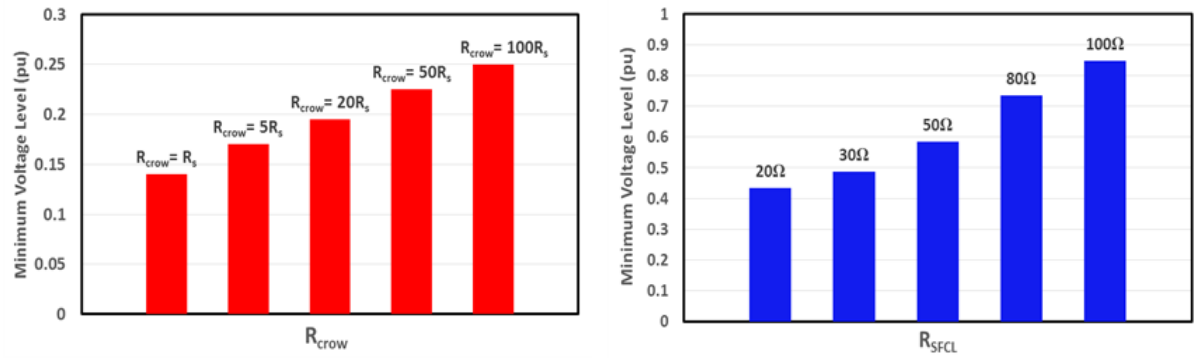

(a) (b)

Fig. 3.16 Effect of Limiting resistance on voltage dip at the generator terminal. (a) Rcrow; (b) RSFCL

3.7 Summary

In this chapter, the evaluation of the fault ride through capability enhancement of the DFIG-based wind turbine with different techniques has been proposed. In the case of using the Outer Crowbar protection, the rotor current could be already reduced. However, the voltage dip on the generator terminals still high including a high deviation in the active and reactive power at the instants of starting and ending of the fault. Also, after Crowbar deactivation, the rotor current would be very high and may lead to an undesired reactivation of the Crowbar. Furthermore, there is a little delay in the insertion of the Outer Crowbar depending on the triggering time of the power switches. Therefore, overcoming these problems needs different control strategies which are too complicated in real application.

On the other hand, RSFCL does not need any control technique to be transformed from superconducting to a normal state. So, RSFCL limits the stator current value effectively from the first peak and consequently the rotor current due to the magnetic coupling leading to an improvement of the DFIG's performance such as increasing the minimum voltage level at the generator terminals, maintaining nearly a constant rotor speed, improving the active and reactive power and FRT capability during the fault. In addition, the overall stability of the network has been enhanced.

Chapter 4

Enhancement of Microgrid Stability Using SMES Considering High Penetration of RERs

4.1 Introduction

Recently, new renewable energy resources (RERs) have become the most convenient source in replacing fossil fuels. The RERs possess several merits, such as being clean and unpolluted, renewability and they do not need for expensive maintenance. The main vastly widespread RERs sources are wind, solar photovoltaic (PV), biomass, hydropower, and geothermal energy systems. The wind energy has been given global concerns due to their high power generations up to 10 MW in a single wind turbine, low cost of generated kWh, and environmentally friendly. Therefore, wind energy systems are suitable for high penetration levels of RERs that may lead to the full replacement of conventional energy sources [175]. However, the high penetration levels of wind energy have led to frequency and voltage instabilities in the utility grid due to the fluctuating nature of wind power. In addition, the high penetration levels of large wind farms may act as adverse effects on the electrical grid under the abnormal faulty condition. Thence, voltage stability, frequency stability, and damping oscillations have been highlighted as critical challenges to the integration of wind energy with high penetration levels in the utility grid.

This chapter presents an effective solution for frequency stability problem based on optimal PID controller using moth swarm algorithm (MSA) for the superconducting magnetic energy storage (SMES) system. The proposed system can suppress frequency fluctuations due to high variations of RERs.

4.2 SMES System Model

SMES basic configuration for the power system is shown in Fig. 4.1. It consists of a three-phase transformer, voltage source converter (VSC) using an insulated-gate bipolar transistor (IGBT) triggered out with pulse width modulation (PWM), and DC-link capacitor. The heart of the SMES unit is a superconducting coil (SC), which is connected to the AC grid through a power conversion system (PCS), which includes an inverter/DC-DC chopper. The SC is

charged from the grid during the normal operation to a set value. After charging the SC, it can conduct the supporting current with the electromagnetic field. During SMES operation, the SC should be immersed in liquid Helium at 4.2 K in an insulated vacuum cryostat to maintain it in the superconducting state. Whenever there is a fluctuation in the system power during a disturbance, the discharging starts immediately through the PCS to the utility grid. The control system can restore the power system to an equilibrium condition and the SC charges again to its steady-state value. As explained in [176], neglecting the transformer and the converter losses, the SMES can be used as a linearized model to be applicable to the LFC as shown in Fig. 4.2. The RoCoF is used to calculate the SMES power change.

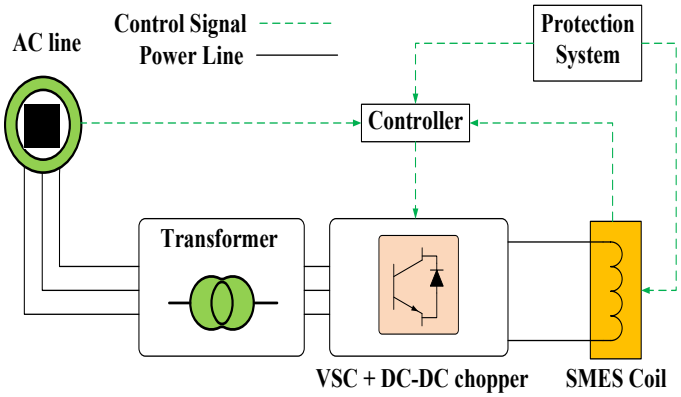

Fig. 4.1. A detailed configuration of SMES in power system

4.3 Coordination of a New Optimal LFC and SMES

This part presents an optimal LFC based Genetic Moth Swarm Algorithm (MSA). The MSA is a novel hybrid optimization algorithm. With MSA, different optimization operators are used to mimick a set of behavioral patterns of moths in nature, which allows for the flexible and powerful optimizer. Hence, a new dynamic selection strategy of crossover points is proposed based on population diversity to handle the difference vectors Lévy-mutation to force MSA to jump out of stagnation and enhance its exploration ability. In addition, a spiral motion, adaptive Gaussian walks, and a novel associative learning mechanism with immediate memory are implemented to exploit the promising areas in the search space. It was presented by Al-attar et al. [177]. It has some advantages over the other swarm algorithms such as the simplicity and flexibility as it can be applied to different problems without change the main algorithm structure, avoiding the trap in local minima, achieving fast convergence characteristics, and its lowest control parameters to adjust and easy to implement. Therefore, MSA is used in this section to find the optimal controller parameters in the LFC loops.

The main contribution of this part, a new coordinated optimal LFC using a new optimal PID controller-based MSA, with the dynamic contribution of the SMES in an islanded MG concerning high wind power integration. This coordination has been proposed to enhance the frequency stability under the impact of different load profiles, random load variation, wind power fluctuation, and system uncertainties. To facilitate and accelerate the optimization operation of LFC in the MG system, the SMES linearized model will be used as a frequency controller to be applicable to the LFC as shown in Fig. 4.2. A comparative study of different control strategies such as conventional controller, optimal PI controller, and optimal PID controller has been carried out to validate the effectiveness of the proposed coordination regarding the peak undershoot, peak overshoot, and settling time. The MG used in this study consists of domestic loads, thermal power plant, and wind farms.

4.3.1. Frequency Control Based on SMES

SMES has been used in this section as frequency stabilizer, (i.e., auxiliary secondary control) for more damping out the system frequency oscillations, which are generated from the power fluctuations of RERs, random load change, and system parameters variation. The linearized model representation of SMES such a control scheme is simulated as a first-order transfer function by a time constant T_{SMES} and SMES variable gain K_{SMES}. The criteria for selecting these two parameters are related to the stability of the system and the response required in dynamics. Moreover, it must be taken into consideration that the initial Rate of Change of Frequency (RoCoF) as well as the maximum drop of frequency (i.e., nadir frequency). In this study, the SMES parameters T_{SMES} and K_{SMES} are selected as 0.03 sec and 6, respectively, which obtained using the trial-and-error method. This selection gives a good dynamic stability during the transients even when the total system inertia is reduced to 50% of its system. The SMES as the frequency stabilizer provides the required power for any frequency deviation to the MG as shown below.

$$\Delta P_{SMES} = \frac{K_{SMES}}{T_{SMES}S+1} * \left(\frac{d(\Delta f)}{dt}\right) \tag{4.1}$$

The SMES power is obtained by estimating the Rate of Change of Frequency (RoCoF) as follow:

$$RoCoF = \frac{d(\Delta f)}{dt} \tag{4.2}$$

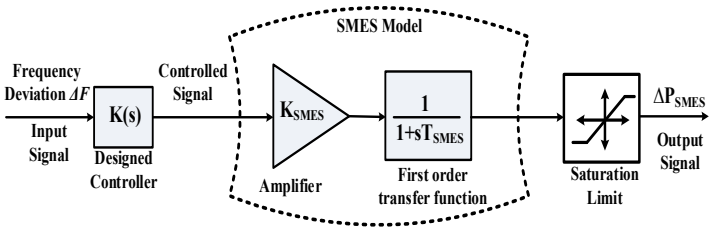

Fig. 4.2 Structure of SMES model as frequency stabilizer.

4.3.2. Control Methodology and Problem Formulation

In this research, the proposed coordinated control strategy of secondary frequency control (i.e., LFC) and SMES is based on the PID controller, which have the well-known variables such as the proportional gain k_p, the integral gain k_i, and the derivative gain k_d. The transfer function can be represented as follows:

$$G_c(s) = K_P + \frac{K_i}{S} + K_d S \tag{4.3}$$

Therefore, this research uses a novel intelligent MSA searching method to find the optimal design parameters of the PID controller, which has parameter bounds. In this study, the integral of squared-error (ISE) is used as a fitness function, which is the objective function of the optimization technique and can be formulated as follows:

$$ISE = \int_0^{t_s} (\Delta f)^2 \, dt \tag{4.4}$$

where Δf is the system frequency deviation and t_s is the simulation time. The proposed MSA is applied to minimize the objective function of the ISE subjected to the constraints of the PID controller parameters limits as shown in (4.5). Table 4.1 summarizes the MSA parameters, which are used for solving the LFC problem after making many trials and errors.

$$\begin{Bmatrix} K_{P\,\min} \le K_P \le K_{P\,max} \\ K_{i\,\min} \le K_i \le K_{i\,max} \\ K_{d\,\min} \le K_d \le K_{d\,max} \end{Bmatrix} \qquad (0 \sim 100) \tag{4.5}$$

Table 4.1 The control parameters of MSA

Parameter	Value	Parameter	Value
Maximum iteration	100	M_{urate}	0.05
Swarm size	50	K_p limits	0 - 100
Pathfinders Number	10	K_i limits	0 - 100
Trials	40	K_d limits	0 - 100

4.3.3. Overview of MSA

In this chapter, the MSA has been adapted to find the optimum parameters of the PID controller. The goal of the optimum PID controller is to reduce the frequency deviations to zero at

minimum time and minimum errors to balance the generation and load after a disturbance, and to prevent the MG from instability or system collapse. The input of the proposed MSA is the frequency deviations of the MG and then the output are an optimum PID controller parameters as shown in Fig. 4.3.

MSA is as a simple and fast searching intelligent technique. It is a global optimization algorithm based on evolutionary computation technique. It is inspired by the orientation of moths towards moonlight. The available solution of an optimization problem using MSA is performed by the light source position and its fitness is the luminescence intensity of the light source. Furthermore, the proposed method consists of three main groups, the first one is called pathfinders which are considered a small group of moths over the available space of the optimization. The main target of this group is to guide the locomotion of the main swarm by discriminating the best positions as light sources. Prospectors group is the second one which has a tendency to expatiate in a non-uniform spiral path within the section of the light sources determined by the pathfinders. The last one is the onlookers; this group of moths moves directly to the global solution which has been acquired by the prospectors. With MSA, different optimization operators are used to mimic a set of behavioral patterns of moths in nature, which allows for the flexible and powerful optimizer. Hence, a new dynamic selection strategy of crossover points is proposed based on population diversity to handle the difference vectors Lévy-mutation to force MSA to jump out of stagnation and enhance its exploration ability. In addition, a spiral motion, adaptive Gaussian walks, and a novel associative learning mechanism with immediate memory are implemented to exploit the promising areas in the search space [177].

The proposed hybrid based algorithm aims to integrate its advantages in term of sharing information and global search ability to find the optimal value of a given function using the following steps:

Step1: Initialize the moth-swarm population as shown in (4.6).

$$x_{ij} = rand[0,1] \cdot \left(x_j^{max} - x_j^{min}\right) + x_j^{min} \quad \forall\ i \in \{1,2,\dots,n\};\ j \in \{1,2,\dots,d\} \tag{4.6}$$

Where, x_j^{max} and x_j^{min} are the upper and lower limits, respectively.

Step2: Calculate the swarm finesses & identify the type of each moth.

Step3: while t < Max number of iterations (T) for each light source, identify the crossover points. $c_p \subset \{c_1, c_2, \dots, c_{n_c}\}$, Generate Lévy-flights samples $L_i \sim step \oplus Levy(\alpha) \sim 0.01 \frac{u}{|y|^{1/\alpha}}$, Create/mutate sub-trail vector $\overrightarrow{v_p^t}$, Construct the completed trail solution $\overrightarrow{V_{pi}^t}$, and Select the artificial light sources $\overrightarrow{x_i^{t+1}}$ as follows:

The full trial solution V_{pj} can be defined as:

$$V_{pj}^{t} = \begin{cases} v_{pj}^{t} & if \quad j \in c_p \\ x_{pj}^{t} & if \quad j \notin c_p \end{cases} \tag{4.7}$$

After that, the fitness value of the completed trail solution is calculated and compared with its corresponding host solution. The fitter solutions are selected for survives for the next generation, which may be outlined for minimization problems as follows:

$$\overrightarrow{x_i^{t+1}} = \begin{cases} \overrightarrow{x_p^t} & if \quad f\left(\overrightarrow{V_p^t}\right) \geq f\left(\overrightarrow{x_p^t}\right) \\ \overrightarrow{v_p^t} & if \quad f\left(\overrightarrow{V_p^t}\right) < f\left(\overrightarrow{x_p^t}\right) \end{cases} \tag{4.8}$$

Step4: End for reconnaissance.

Step5: Calculate the probability values P_p, which is estimated proportional to luminescence intensity fit_p, as follows:

$$P_p = \frac{fit_p}{\sum_{p=1}^{n_p} fit_p} \tag{4.9}$$

Each prospector moth x_i is soared into the logarithmic spiral path as shown in Appendix (B) to make a deep search around the artificial light source x_p, which is chosen based on the probability P_p using Eq. (4.9).

Step6: for each prospector moth (best group)x_i: Update the position of prospector moth.

$$x_i^{t+1} = \left|x_i^t - x_p^t\right| \cdot e^{\theta} \cdot cos\, 2\pi\theta + x_p^t \quad \forall\ p \in \{1,2,\dots,n_p\};\ i \in \{n_p+1, n_p+2, \dots, n_f\} \tag{4.10}$$

Where, $\theta \in [r,1]$ is a random number to define the spiral shape and $r = -1 - t/T$.

Step7: Calculate the fitness of prospector.

Step8: End for Transverse orientation & define the new light sources and moonlight.

Step9: For each onlooker moth: Update the position according to its type.

Step10: Step12: If (i ϵ n_g), Generate Gaussian walk steps ε_1,ε_2, and ε_3

$$x_i^{t+1} = x_i^t + \varepsilon_1 + \left[\varepsilon_2 \times best_g^t - \varepsilon_3 \times x_i^t\right] \forall\ i \in \{1,2,\dots,n_G\} \tag{4.11}$$

$$\varepsilon_1 \sim random(size(d)) \oplus N\left(best_g^t,\ \frac{\log t}{t} \times \left(x_i^t - best_g^t\right)\right) \tag{4.12}$$

Where, ε_1, is a random sample drawn from Gaussian stochastic distribution scaled to the size of this group$best_g$, is the global best solution obtained by the transverse orientation phase (both prospectors and pathfinders), ε_2 and ε_3 are random numbers distributed uniformly within the interval [0,1].

Step11: Move the onlooker position with Gaussian walks x_i^{t+1}

$$x_i^{t+1} = x_i^t + 0.001 \cdot G\left[x_i^t - x_i^{min}, x_i^{max} - x_i^t\right] + (1 - g/G) \cdot r_1 \cdot \left(best_p^t - x_i^t\right) + 2g/G \cdot r_2 \cdot \left(best_g^t - x_i^t\right) \quad (4.13)$$

Where, $i \in \{1,2,\dots,n_A\}$, $2g/G$ is the social factor, $1 - g/G$ is the cognitive factor, and r_1 and r_2 are random number within the interval [0, 1]. Similar to transverse orientation phase, $best_p$ is a light source randomly chosen from the new pathfinders group based on the probability value of its corresponding solution.

Step12: ***Else,*** drift the onlooker moth using the associative learning operators and immediate memory.

Step13: End if.

Step14: Calculate the fitness of onlooker moth.

Step15: End for Celestial navigation.

Step16: Identify the new light sources, moonlight, and type of each moth.

Step17: End while.

Step18: Print global best solution (moonlight).

The flowchart of MSA optimization technique is seen in Appendix (B).

The obtained optimal values of the PI and PID gains controllers based on MSA technique are given in Table 4.2.

Table 4.2. PID controller's parameters for MG.

Parameter	K_p	K_i	K_d
PID	9.682	0.807	*18.73*
PI	0.569	0.266	-

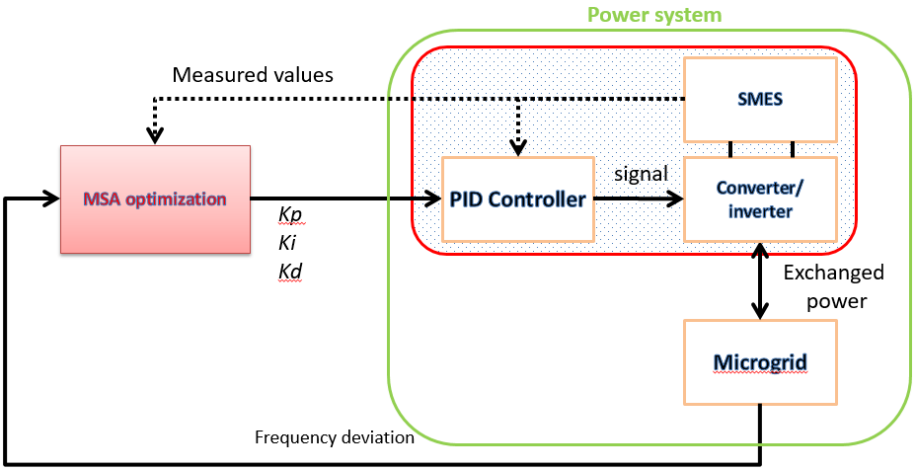

Fig. 4.3 The MSA structure for optimal PID controller

4.4 System Configuration

This research focuses on the islanded MG (base: 20 MW). It includes 15 MW of domestic loads, 20 MW of thermal power plant, and 2.5 MW of a wind farms (wind farm1 with a peak power of 6.5 MW and wind farm 2 with a peak power 6.5 MW) as shown in the single line diagram of the tested MG of Fig. 4.4.

In this study, the effects of the physical constraints such as Generation Rate Constraints (GRC) of power plant and speed governor dead band (backlash) are taken into consideration for modeling the actual islanded MG. Whereas, blackash is defined as the total magnitude of sustained speed change. All speed governors have a blackash, which is important for primary frequency control in the presence of disturbances. The GRC limits the generation rate of output power which is given as 0.2 pu MW/min for the non-reheat power plant. The V_U and V_L are the maximum and minimum limits that restrict the rate of the valve-gate closing or opening speed. In this research, the power variation of renewable energy sources such as; the wind power variation (ΔP_{Wind}), and the load power variation (ΔP_L) are considered as disturbance signals for islanded MG. The dynamic model of the studied MG system is as shown in Fig. 4.5. The MG nominal parameters values are shown in Table 4.3.

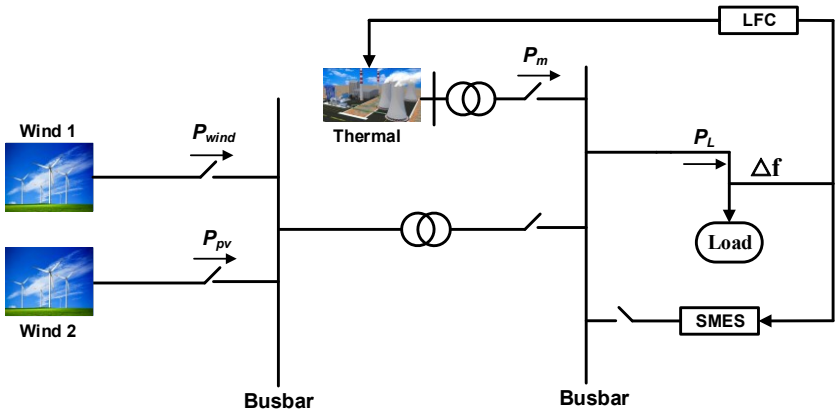

Fig. 4.4 Single-line diagram of the MG case study

Table 4.3 Islanded microgrid parameters

Parameter	Value	Parameter	Value
D	0.015	R	204
H	0.083	GRC	20%
T_g	0.1	V_U	0.3
T_t	0.4	V_L	-0.3
T_{WT}	1.5	f	50
β	1	K_{SMES}	6
ΔP_{SMES}	0.15 p.u	T_{SMES}	0.03

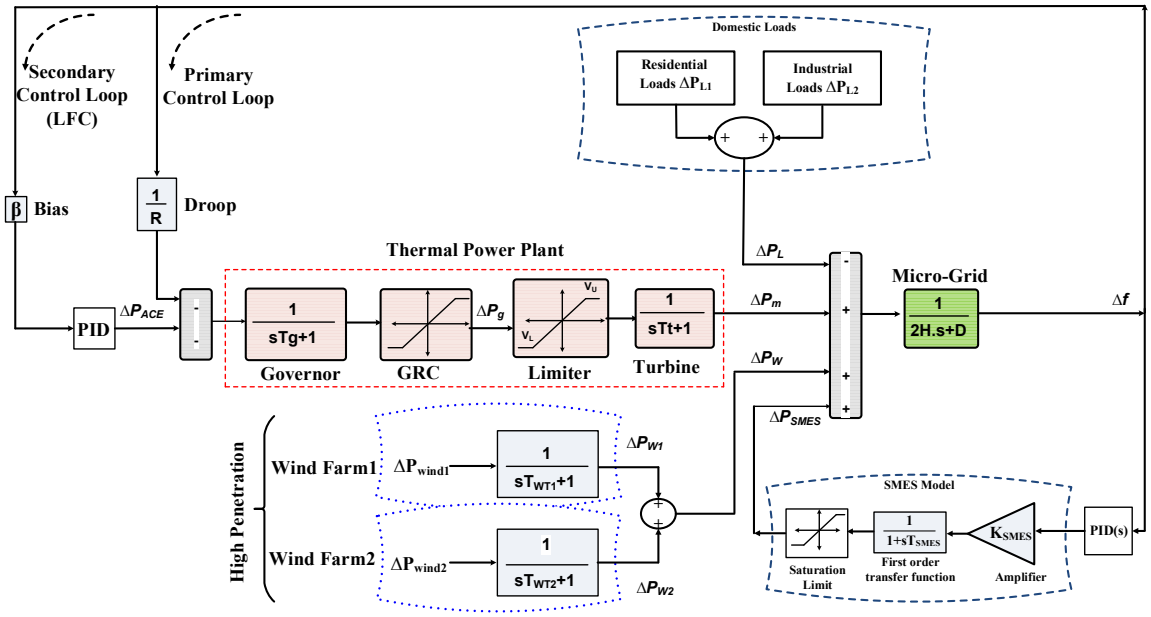

Fig. 4.5. Dynamic model of the islanded microgrid considering high penetration of RERs.

4.4.1. State-Space of MG Dynamic Modeling

The frequency deviation of the studied MG system considering the effect of the primary control loop (i.e., governor action), a secondary control loop (i.e., LFC), and SMES controller (i.e., an auxiliary LFC) can be obtained as:

$$\Delta f = \frac{1}{2Hs+D}(\Delta P_m + \Delta P_w \pm \Delta P_{SMES} - \Delta P_L) \tag{4.14}$$

Fig. 4.5 shows a block diagram of transfer functions describing the different subsystems of the studied MG system. Where the blocks are:

I. Thermal power plant

A thermal turbine acts as the prime mover for the generator, which converts the stored energy from high pressure and temperature into rotating energy, which in turn converted to electrical energy by moving the generator. These turbines may be either reheat or non-reheat type. The governor is modeled by a first-order function of a unity gain and time constant (T_g) as in (4.15).

$$TF_g = \frac{1}{1+sT_g} \tag{4.15}$$

Where the governor with speed-droop (1/R) represents the primary frequency control of governor action. The turbine model considered in this study is a steam turbine, which represents a first-order transfer function as this relation:

$$TF_t = \frac{1}{1+sT_t} \tag{4.16}$$

II. Rotating mass and load

The machine mechanically dynamic loop is modeled by a first-order transfer function of a system inertia constant (H) and damping coefficient (D) as seen in (4.17).

$$TF_r = \frac{1}{2Hs+D} \tag{4.17}$$

The generated thermal power deviation can be calculated from the next equation:

$$\Delta P_m = \frac{1}{1+sT_t}\Delta P_g \tag{4.18}$$

$$\Delta P_g = \frac{1}{1+sT_g}(\Delta P_{ACE} - \frac{1}{R}\Delta f) \tag{4.19}$$

$$\Delta P_{ACE} = \frac{ACE}{s} = \left[K_P + \frac{K_i}{s} + K_d s\right][\beta.\Delta f] = K_{pid}[\beta.\Delta f] \tag{4.20}$$

III. Wind power system

This study uses an aggregated model to form the wind farm as a large capacity induction generator. The generator is modeled by a given by a first-order lag transfer function with a unity gain and time constant (T_{WT}), neglecting all nonlinearities, as given below:

$$TF_{WTG} = \frac{\Delta P_w}{\Delta P_{wind}} = \frac{1}{1+sT_{WT}} \tag{4.21}$$

IV. SMES model

$$\Delta P_{SMES} = \frac{K_{SMES}}{T_{SMES}S+1} * \left(\frac{d(\Delta f)}{dt}\right) \tag{4.22}$$

The state space model of the islanded MG is given in (4.23) and (4.24).

$$\dot{X} = AX + B_1 w + B_2\ u \tag{4.23}$$

$$y = Cx \tag{4.24}$$

Where,

$$x^T = \left[\Delta f\ \Delta P_m\ \Delta P_g\ \Delta P_{ACE}\ \Delta P_W\ \Delta P_{SMES}\right] \tag{4.25}$$

$$w^T = [\Delta P_{wind}\ \ \Delta P_{SMES}\ \ \Delta P_L\ ] \tag{4.26}$$

$$y = \Delta f \tag{4.27}$$

$$\dot{X} = \begin{bmatrix} -\frac{D}{2H} & \frac{1}{2H} & \frac{1}{2H} & \frac{1}{2H} & \frac{1}{2H} & \frac{1}{2H} \\ 0 & -\frac{1}{T_t} & -\frac{1}{T_t} & 0 & 0 & 0 \\ -\frac{1}{RT_g} & 0 & -\frac{1}{T_g} & \frac{1}{T_g} & 0 & 0 \\ 0 & 0 & 0 & 0 & \frac{1}{T_{WT}} & 0 \\ 0 & 0 & 0 & 0 & 0 & -\frac{1}{T_{SMES}} \end{bmatrix} * \begin{bmatrix} \Delta f \\ \Delta P_m \\ \Delta p_g \\ \Delta p_{ACE} \\ \Delta p_W \\ \Delta P_{SMES} \end{bmatrix} + \begin{bmatrix} 0 & 0 & 0 \\ 0 & 0 & 0 \\ 0 & 0 & 0 \\ 0 & 0 & 0 \\ \frac{1}{T_{WT}} & 0 & 0 \\ 0 & \frac{1}{T_{SMES}} & 0 \end{bmatrix} * \begin{bmatrix} \Delta P_{wind} \\ \Delta P_{SMES} \\ \Delta P_L \end{bmatrix} + \begin{bmatrix} 0 \\ 0 \\ 0 \\ 0 \\ 0 \\ \frac{K_{SMES}}{T_{SMES}} \end{bmatrix} u \tag{4.28}$$

$$y = [1\ \ 0\ \ 0\ \ 0\ \ 0\ \ 0]x \tag{4.29}$$

4.4.2. Wind Power Generation System

Fig. 4.6 shows the model of Wind Power Generation System (WPGS) for frequency control. In this model, the wind speed is multiplied by the random speed fluctuation, which derived from the white noise block in MATLAB/Simulink to estimate the random wind output power fluctuation. The WPGS model described by the following equations. The output power of wind turbine is calculated as follows:

$$P_W = \frac{1}{2}\rho A_T V_W^3 C_P(\lambda, \beta) \tag{4.30}$$

Where ρ is air density (Kg/m^3), A_T is the rotor swept area (m^2), V_W is the rated wind speed (m/s), and C_P represents the power coefficient of the rotor blades. C_P is defined below in terms of turbine coefficients C_1 to C_7.

$$C_P(\lambda, \beta) = C_1 * \left(\frac{C_2}{\lambda_I} - C_3\beta - C_4\beta^2 - C_5\right) * e^{\frac{-C_6}{\lambda_I}} + C_7\lambda_T \tag{4.31}$$

Where β is the pitch angle, λ_T corresponds to the optimal tip-speed ratio (TSR) and defined by the following:

$$\lambda_T = \lambda_T^{op} = \frac{\omega_T * r_T}{V_W} \tag{4.32}$$

Variable speed wind turbines operate at an optimal TSR value during all wind speed conditions, and r_T is the rotor radius. In (4.33), λ_I is intermittent TSR and is related to λ_T and β as demonstrated below:

$$\frac{1}{\lambda_I} = \frac{1}{\lambda_T + 0.08\beta} - \frac{0.035}{\beta^3 + 1} \tag{4.33}$$

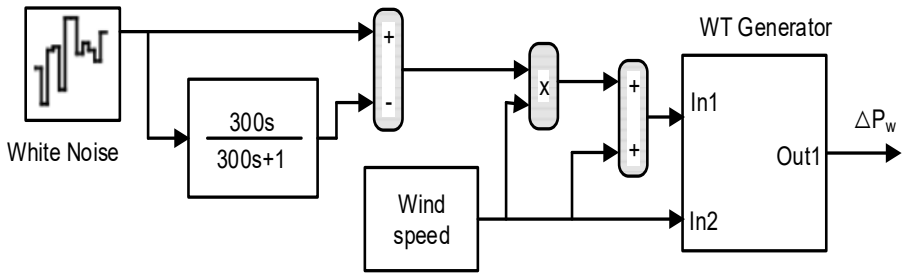

Fig. 4.6. The model of WTG

This research studies the effect of merging high wind power penetration on the system frequency response of an islanded MG system. In this paper, the MG includes aggregated wind turbines models with different power rates, which are wind turbine units of 2.5 MW (wind farm 1), and wind turbine units of 6.5 MW (wind farm 2) beside the conventional generation units. The MG is tested in the presence of low fluctuated wind power (wind farm 1) and high fluctuated wind power (wind farm 2) as shown in Fig. 4.7. The parameters values of each wind turbine model are presented in Table 4.4 and Table 4.5.

Table 4.4 Nominal wind turbine parameters of wind farm 1

Parameter	Value	Parameter	Value
$P_{W,1}$	2.5 MW	C_2	116
$V_{W,1}$	15 m/sec	C_3	0.4
ρ	1.225 $Kg.m^2$	C_4	0
A_T	1648 m^2	C_5	5
r_T	22.9 m	C_6	21
C_1	-0.6175	C_7	0.1405

Table 4.5 Nominal wind turbine parameters of wind farm 2

Parameter	Value	Parameter	Value
$P_{W,2}$	6.5 MW	C_2	116
$V_{W,2}$	12 m/sec	C_3	0.4
ρ	1.225 $Kg.m^2$	C_4	0
A_T	5905 m^2	C_5	5
r_T	43.36 m	C_6	21
C_1	0.3915	C_7	0.0192

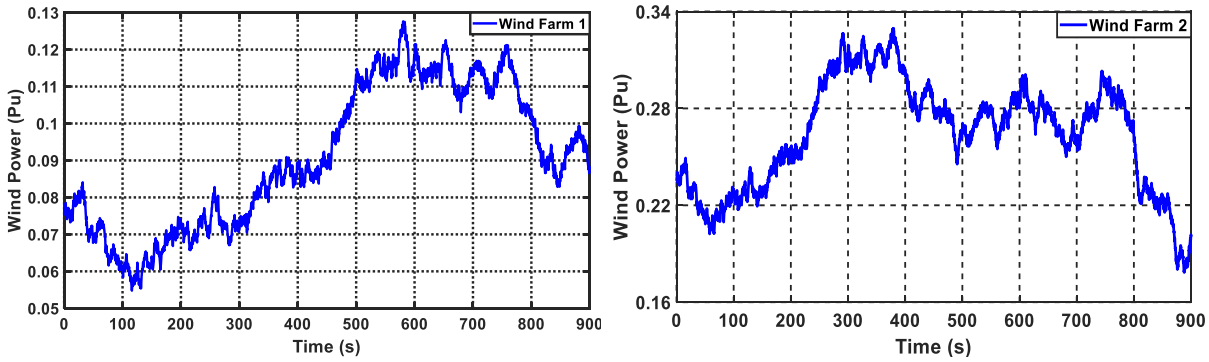

Fig. 4.7 The wind Power output profiles of the MG

4.4.3. Modeling of Power System Loads

In this research, the input power fluctuation of the MG is estimated by considering the deviation from the initial load value as shown in Fig. 4.8. The standard deviation is multiplied by the random output fluctuation derived from the white noise block in MATLAB/Simulink in order to simulate the real-time random power fluctuation on the load profile. Whereas, low random load change (residential load) and high random load change (industrial load) are tested on the MG as shown in Fig. 4.9. The load deviation is simulated close to an actual load change by the following function:

$$\Delta P_L = 0.6\sqrt{P_{Load}} \tag{4.34}$$

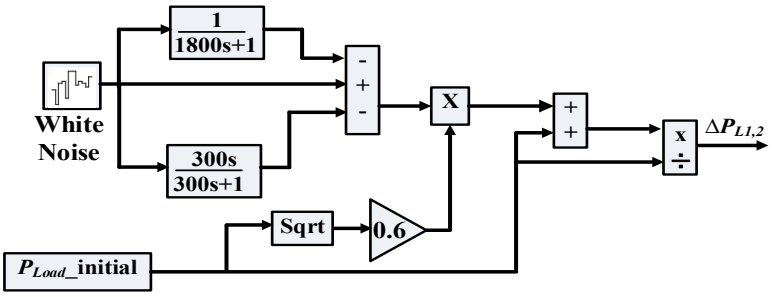

Fig. 4.8 The model of random load using MATLAB/Simulink

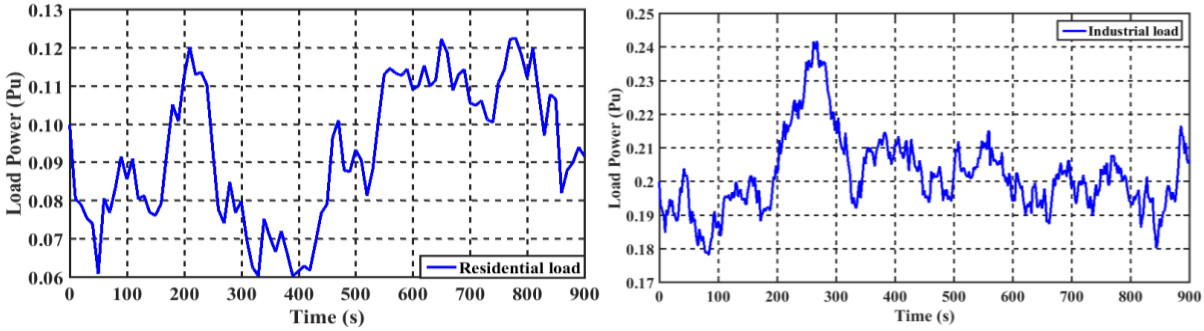

Fig. 4.9 The random load fluctuations

4.4.4. Results and discussion

The model of the targeted MG system including high wind power penetration with inherent nonlinearities is built using MATLAB/Simulink model, which takes the GRC of thermal generation source into account. The code of the MSA as an m-file is interfaced with the MG model to execute the optimization process. Analysis of different control strategies has been implemented in the MG system. Many types of research assume the load profile is a step change disturbance, which is represented by the forced outage of generation unit or sudden switch off a massive load. However, in fact, the load disturbances are complex and random nature. The actual load disturbance can be represented by several types of disturbance besides step change disturbance. Therefore, this research applied some random loads variations, which are low random load change (residential load), and high random load change (industrial load) on the MG in the presence of low and high wind power fluctuation models for wind farm1 and 2, respectively. Two scenarios are applied to the studied system and the simulation time of each one is 15 minutes as the follows:

Scenario A

In this scenario, the studied islanded MG considering high wind power penetration is considered as the test system to confirm the robustness and effectiveness of the proposed coordination. The proposed coordination of LFC using a new optimal PID controller-based MSA and modified control signal to SMES-based PID controller for compensating the MG

frequency deviation (Δf) is tested by implementing the high fluctuated wind power (wind farm 2) at 500 sec. However, the other disturbance sources, which are low fluctuated wind power (wind farm1), residential load, and the industrial load applied from initial. Fig. 4.10 shows the frequency deviation of three different control strategies for the MG considering the high wind power integration. It is clearly shown that the dynamic contribution of conventional SMES improves the frequency response and reduces the transient frequency deviation compared with the LFC of the MG system without SMES. Moreover, in case of no SMES controller, the frequency is fluctuating more with high deviation. On the other hand, the proposed control strategy with a new coordination of LFC using a new optimal PID controller-based MSA and SMES-based PID controller gives a superior performance and more reduction of the frequency excursions Δf and wind power fluctuation than other strategies. The performance specifications (maximum overshoot, maximum undershoot and maximum settling time) of the studied system with different control strategies of SMES understudy of Scenario A during the whole period of simulation (15 minutes) have been compared in Table 4.6.

Table 4.6. The performance specification of the studied system for scenario A

Scenario A	Proposed Coordination			Conventional SMES			No SMES Controller		
	Δf_{Max} *Undershoot*	Δf_{Max} *Overshoot*	*Max. Settling time (sec)*	Δf_{Max} *Undershoot*	Δf_{Max} *Overshoot*	*Max. Settling time (sec)*	Δf_{Max} *Undershoot*	Δf_{Max} *Overshoot*	*Max. Settling time (sec)*
	0.0173	0.0042	19	0.021	0.0044	38	0.0466	0.0476	90

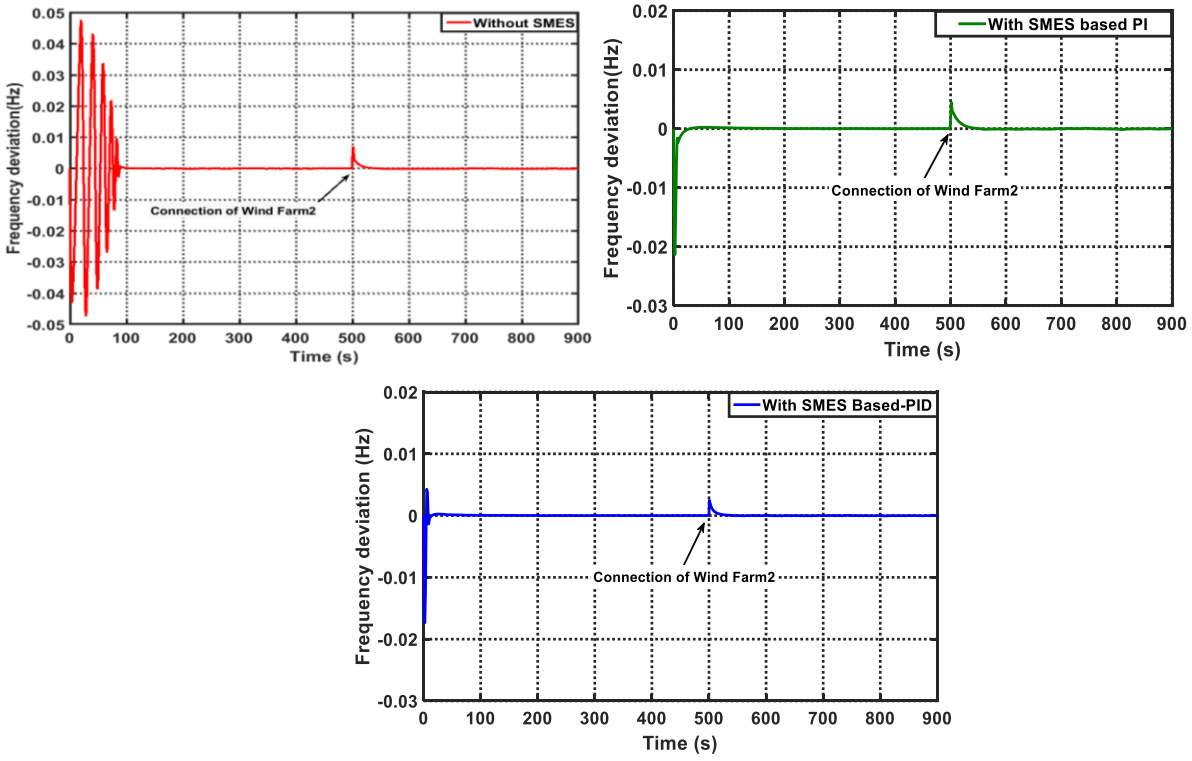

Fig. 4.10 Frequency deviation of scenario A

Scenario B

In this scenario, the effectiveness and robustness of the proposed coordination of LFC using a new optimal PID-based MSA and modified control signal to SMES-based PID controller is evaluated by implementing high and low fluctuated wind farms and different random loads (residential and industrial loads), which participate under the assumed multiple operating conditions in Table 4.7. This scenario divided into three sub-scenarios as following:

Table 4.7. Multiple operating conditions of the MG considering high wind penetration

Source	Starting time (sec)	Stopping time (sec)	Rate Power (pu)
Industrial load	300 sec	-	0.24
Residential load	initial	700 s	0.12
Wind farm 1	initial	-	0.125
Wind farm2	500 sec	-	0.325

I. Scenario B1

In this case, the MG is considered as the test system with high system inertia (100% of default system inertia) considering the multiple operating conditions of wind and load variations as shown in Table 4.7. The frequency deviation of the MG with different control strategies of SMES is illustrated in Fig. 4.11. From this figure, it has been noticed that the frequency deviation of the MG considering high wind power penetration with the proposed coordination is about ±0 .005 Hz while the MG with/without the dynamic contribution of convention SMES is ± 0.012Hz, ±0.025 Hz, respectively. Therefore, the proposed coordination gives a fast response for damping the frequency fluctuation during the multiple operating conditions of the MG compared to others control strategies.

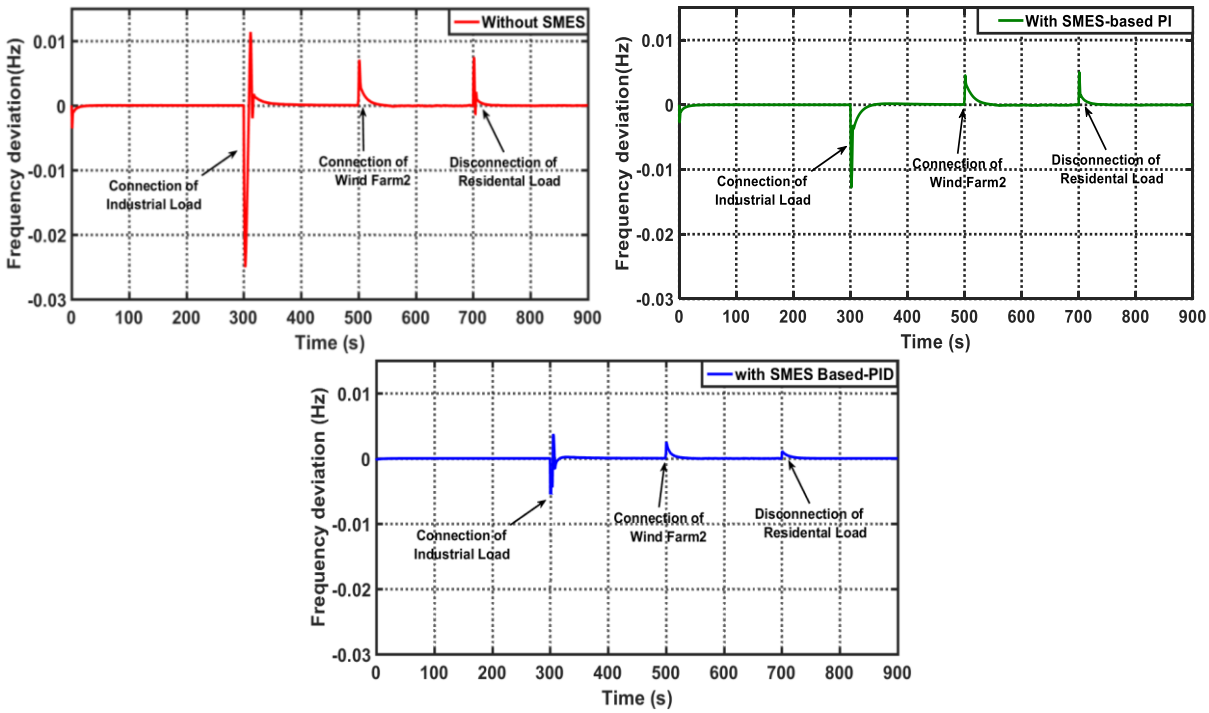

Fig. 4.11 Frequency deviation of scenario B1

II. Scenario B2

In this case, the MG considering high wind power penetration is tested under the condition of 75% of default system inertia with multiple operating conditions of wind and load variations as shown in Table 4.7. The frequency deviation of the three control strategies for the studied system considering the low and high fluctuation of wind power and load with high penetration of RERs is investigated in Fig. 4.12. In the case of no SMES controller, the frequency deviation is about (± 0.03 Hz). While the MG with the dynamic contribution of conventional SMES gives the frequency deviation of about (± 0.014 Hz) at connecting the industrial load in the MG at 300 sec compared to the MG considering high penetration wind level with SMES controller. The proposed coordination shows a response better than other methods during all disturbance instants. Furthermore, it gives a robust stability and it has a faster settling time than others control strategies.

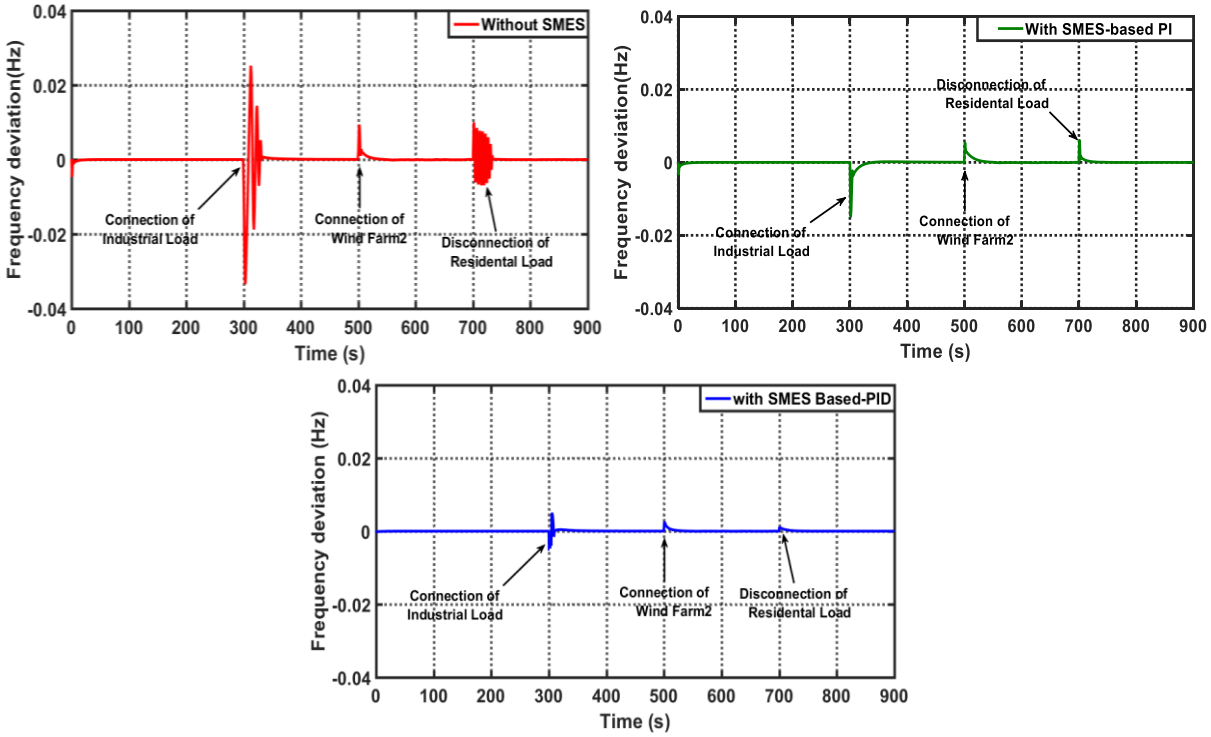

Fig. 4.12 Frequency deviation of scenario B2

III. Scenario B3

The robustness of the proposed coordination of LFC using a new optimal PID-based MSA with the dynamic contribution of SMES-based PID controller is tested in the extreme scenario. In this case, the system inertia is decreased to half of the default system inertia (50% of default system inertia). This can happen in case of integration high wind power, which the power electronic interface-based RERs will reduce the overall system inertia and cause to fluctuate the system frequency. Fig. 4.13 shows the frequency deviation of the MG considering high

RERs penetration under the condition of 50% of default system inertia with multiple operating conditions of wind and load variations as shown in Table 4.6. The simulation results concluded that the frequency is fluctuating more with high deviation, whereas the studied system with no SMES Controller oscillates to such an extent that it is not acceptable. While the MG considering the high level of wind power integration with the conventional SMES controller takes a long time to reach at steady state of system frequency compared with the proposed coordination of optimal LFC with SMES-based PID controller.

The performance specifications (maximum overshoot, maximum undershoot and maximum settling time) of the studied system with different control strategies of SMES under all studied cases of Scenario B during the whole period of simulation (15 minutes) have been compared in Fig. 4.14.

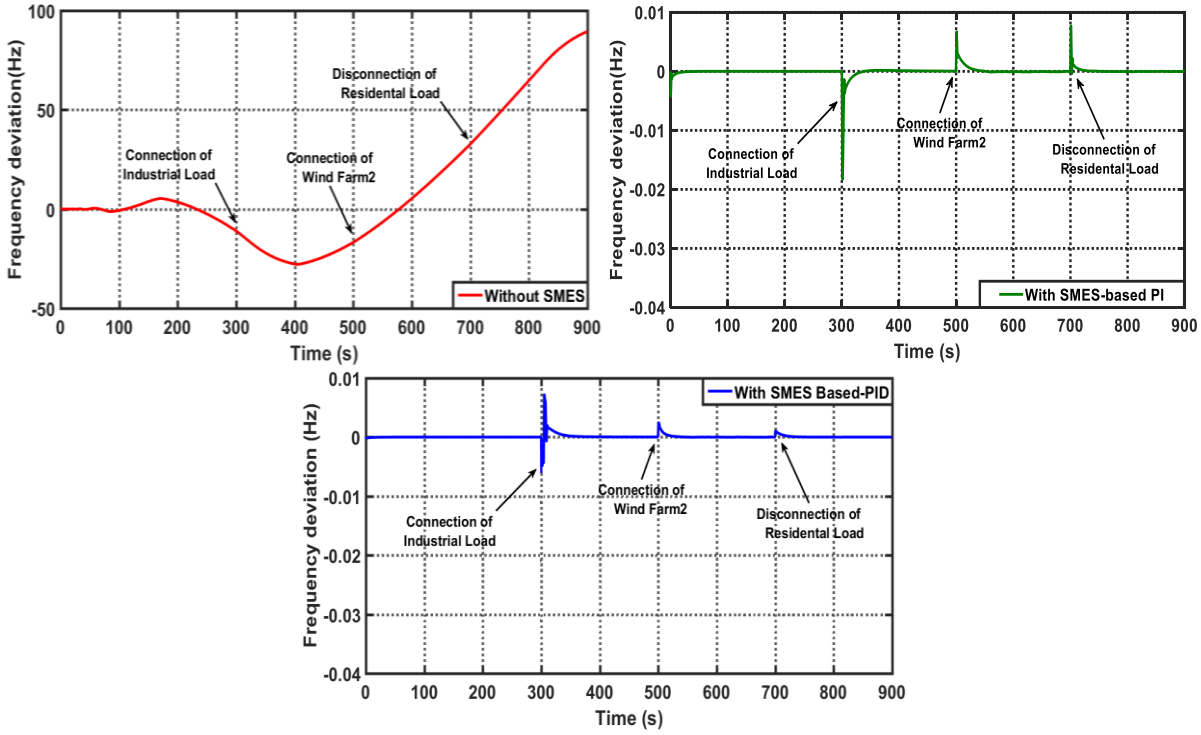

Fig. 4.13 Frequency deviation of scenario B3

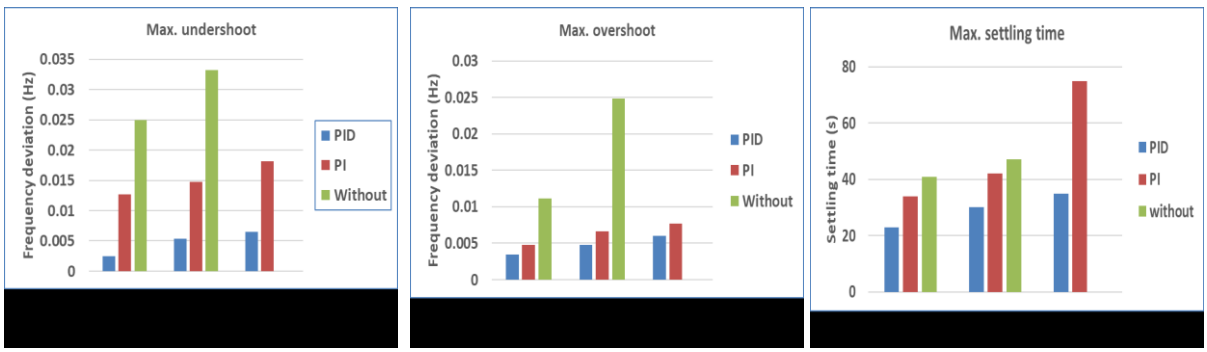

Fig. 4.14 Comparison of SMES controllers in terms of Max. Undershoot, Max. Overshoot, settling time

4.5 Summary

This chapter has proposed a new coordination of optimal LFC using a new PID controller-based MSA with the modified control signal to SMES-based PID controller to enhance the frequency stability in an islanded MG system concerning high wind power penetration. The SMES is used as a linearized model for frequency control to be applicable to the LFC. A recently developed hybrid algorithm namely MSA has been applied to optimize the PID controller parameters with the aim of both frequency regulation and enhance the input control signal to SMES. To prove the effectiveness of the proposed coordination, the MG was analyzed in the presence of high renewable energy penetration using different scenarios considering the multiple operating conditions of wind and load variations, which are high and low fluctuated wind power (wind farms1, 2), and high and low random load change (Residential and Industrial load). The results observed by simulations proved that the proposed coordination achieved a robust frequency stability in the presence of high wind power penetration and different load power fluctuations against all cases of studied scenarios in terms of peaks overshoot, peaks undershoot and settling time. Whereas, the studied MG system with the dynamic contribution of conventional SMES as a frequency stabilizer model gave a satisfactory performance but needs a little long time to suppress the frequency deviations compared with the proposed coordination.

Chapter 5

Enhancement of Microgrid Security Using a Coordination of SMES and Digital Protection Considering High Penetration of RERs

5.1 Introduction

Due to the cases of a large generation loss disturbance or high integration levels of RERs, the conventional power reserve may not be enough to return the stable condition of the system frequency, the emergency control and protection schemes plan may be followed, such as over/under frequency load shedding must be used to restore the system frequency. Hence, this chapter presents an intelligent coordination of optimal load frequency control (LFC) based-new optimal PID controller and digital over/under frequency relay (OUFR). This relay operates for both conditions of over and under frequencies to trip necessary generations or loads after the failure of the combined response of the primary and secondary controls to avoid market failure and to stop further frequency decline. Then, the effect of SMES device integration on this coordination will be presented to improve the dynamic security of the MG system. The dynamic security of MG is the ability of the electric grid to maintain the system synchronism when subjected to various transient disturbances. Fig. 5.1 shows the dynamic security issues of MG. One of these issues is the lack of system inertia due to the high integration of RERs. Consequently, increase the voltage and frequency fluctuations, loss of generation source, forced load shedding, and short circuit faults. Furthermore, RERs exchange electrical power to MGs through power electronic inverters, which cause higher power fluctuations than the traditional synchronous generators. Hence, if the RERs penetration becomes larger, the islanded MGs might become insecure as the stabilizing in system frequency and voltage is difficult in that situation. Moreover, there will be unbalanced between the generation and load due to the variable nature of RERs. These changes lead to the appearance of challenges for the MG dynamic security such as nature of transient variations in MG.

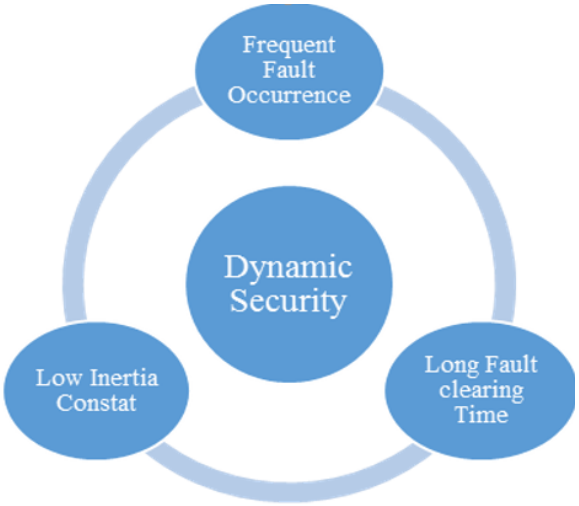

Fig. 5.1. The dynamic security issues

Recently, the frequency control and protection of MGs are the main issues that face the challenges of the RERs integration, especially of islanded MG mode. They have changed significantly from the bygone decade and will change continuously because of the advancement of technology. Therefore, the power systems designers have sought to apply digital devices to handle the increase in power system complexity. The digital technology has appeared in the protection system of microprocessor relays since 1980 and developing to those with communications interfaces in the 1990s [178]. Today, digital relays have featured with high-speed communication, which helped in replacing wires for safety interlocking, control and circuit breakers tripping action. Furthermore, there are many applications of digital relays in transmission and generation system protection due to their flexibility, high-performance level, and capability of operating under different temperatures compared to the classical electromechanical relays. On the other side, the discrete-time controllers become more appealing to replace analog controllers in different power systems. Using digital control systems reduces the implementation cost and increase the reliability of the control system [179]. Therefore, many digital devices have been used in electrical power systems such as digital Proportional- Integration-Derivative (PID) controller, digital Power System Stabilizer (PSS), Digital Automatic Voltage Regulator (AVR), and digital protection devices i.e. digital OUFR . There are two approaches to designing digital control systems [180]. The first one is the direct digital design approach, which converts the analog plant to discrete and then defines a digital controller for the discretized plant. The second approach is the digital redesigns approach [181], which designs a good analog controller for the analog plant and then carry out the digital redesign for the good designed analog controller.

5.2 The proposed coordination strategy

This part presents a coordination strategy of load frequency control (LFC) and digital OUFR protection without and with SMES for an isolated MG considering high penetration of RERs.

5.2.1. Control scheme

The power system frequency may have high variations if there is no longer a balance between the generation and load demand. The normal frequency deviations can affect the power systems efficiency and reliability, while large deviations can destroy the equipment, overload transmission lines and cause interference with the system protection. Therefore, the frequency control is divided into three main operations based on the size of the frequency deviations. The frequency deviation ranges and their control actions are shown in Table 5.1. The normal frequency deviations up to Δf_1, the power requirement is balanced by attenuating these deviations by the governor natural autonomous, which named primary control. If the frequency deviations more than Δf_1 up to Δf_2, the secondary control (i.e. LFC) must recover the system frequency to its steady-state condition within the limits of standard time deviations. The tertiary control should take an action if the frequency deviation increased in the range between Δf_2 up to Δf_3. However, in case of large frequency deviations such as Δf_4 and over, which lead to imbalances in active power during the fault periods, the LFC cannot maintain the system frequency. In that situation, the protection devices (i.e. frequency relays) may be activated and trip generators. This action will interrupt power system supply. Hence, there must be an accurate coordination of LFC or emergency control and protection scheme.

Table 5.1 Frequency operation and control/protection actions

Frequency deviation	Condition	Action
Δf_1 (0.3 Hz)	No contingency or load event	*Primary Control*
Δf_2 (1 Hz)	Generation /Load event	*Secondary Control*
Δf_3 (2 Hz)	Contingency/ Separation event	Tertiary operation
Δf_4 (5 Hz)	Multiple contingency events	*Protection operation*

In this study, a new optimal PID controller-based MSA has presented as LFC for regulation the islanded MG frequency. The design parameters of the optimal PID controller in presence of PV power and wind power are given in Table 5.2.

Table 5.2 PID controller's parameters for the microgrid

PID Parameters		
K_p	K_I	K_d
9.682	0.807	*18.73*

5.2.2. Digital Protection Scheme

5.2.2.1. Modeling of digital frequency relay

The digital OUFR measures the digital value of the system frequency using Frequency Measuring Unit (FMU). The FMU unit implemented on Simulink is shown in Fig. 5.2 (a). The block of 'Hit Crossing' is used to detect the zero crossing instant and passes the signal to the 'if' block, which in turn sending ramp signal to the output. The time duration of the ramp signal is measured and saved to 'A'. This variable is memorized in another variable B by the block 'Transport Delay' Subtracting B from A will give half the time period. This value is held using the block 'Sample and Hold', until the next zero crossing. After doing some calculations, the frequency is measured. Then the FMU sends to the frequency detection element (FDE) to take an action based on OUFR limit for necessary tripping action. The output from frequency is logically AND. The output of FDE under normal case is 1, otherwise, 0 (for tripping) as shown in Fig. 5.2 (b). According to the modeling for the OUFR, it can be implemented by an intelligent electronic device (IED) using microprocessor-based technology. The design block offers flexibility in terms of further research and improvement. Fig. 5.3 shows the logic diagram for the OUFR block.

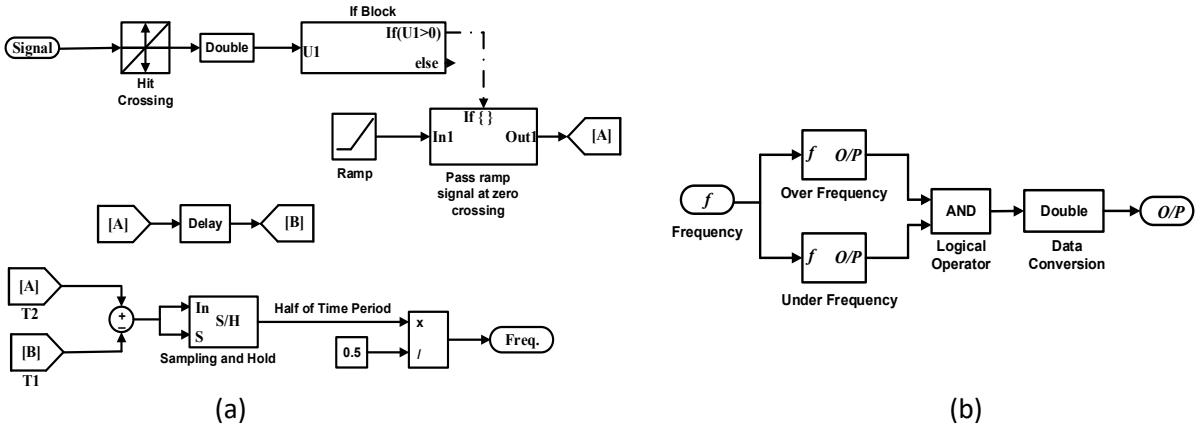

Fig. 5.2 OUFR (a) Frequency Measurement Unit, (b) Frequency Detection Element

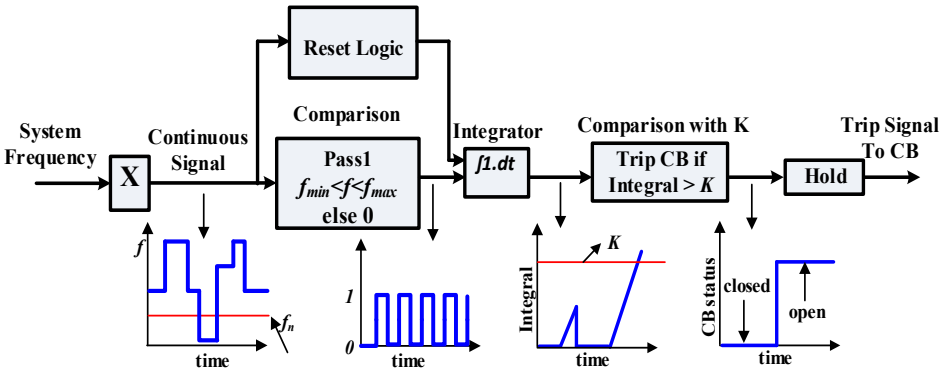

Fig. 5.3 Logic diagram of the OUFR block

5.2.2.2. Principal operation of OUFR

The digital OUFR model implemented in this study is presented in Fig. 5.4. The system frequency *f* is measured and then compared with over/under frequency limit ($f_{min}<f<f_{max}$). If the frequency is over or under the setting of the relay and the magnitude of the integrator output is larger than the minimum integrator setting (*K*=5sec), then the OUFR sends a trip signal to the generator circuit breaker. In contrast, if the integrator value doesn't exceed the magnitude *K,* the relay will not trip. The relay setting is given in Table 5.3 according to the European grid code of islanded mode [183]. In the case of normal condition, if the measured frequency is within the controlled frequency limits (±0.1Hz), the digital LFC will readjust the frequency to its stable value (*f*=50Hz). The limits of the digital frequency relay are depended on the European codes and could be set to other values based on country standards. The frequency system measurement can be derived from the swing equation, whereas the mechanical power P_G of DG is balanced with the load power P_d and electrical power generated or consumed by the grid. Hence the angle δ and rotor speed ω of DG are constant. When a disturbance occurs causing power imbalance, the system frequency starts to deviate due to the transients of DG. The swing equation is given as follows:

$$\begin{cases} \frac{2H}{\omega_o}\frac{d\omega}{dt} = P_G - P_d = \Delta P_{sys} \\ \frac{d\delta}{dt} = \omega - \omega_o \end{cases} \quad (5.1)$$

where,

$$\Delta P_G = \Delta P_m + \Delta P_W + \Delta P_{PV} \quad (5.2)$$

Where, ΔP_m *is the* Generated thermal power deviation, ΔP_W is the wind power variation, and ΔP_{PV} is the solar power variation.

The rotor speed (ω) can be calculate from (5.2) as:

$$\omega = \frac{\omega_o \Delta P}{2H} t + \omega_o \quad (5.3)$$

By substituting the system angular speed ($\omega=\omega o+\Delta\omega$) in (5.2):

$$\omega_o + \Delta\omega = \frac{\omega_o \Delta P}{2H} t + \omega_o \rightarrow \Delta\omega = \frac{\omega_o \Delta P}{2H} t \quad (5.4)$$

where $\omega_o=2\pi f_o$ and $\Delta\omega=2\pi\Delta f$. Hence, equation (5.5) represents the relationship between the frequency deviations (Δf) for relay setting, the power change (ΔP) and the detection time (t).

$$\Delta f = \frac{f_o \Delta P}{2H} t \quad (5.5)$$

The digital OUFR can be adjusted with the integrator (time-delay settings). In this condition, the deviations of system frequency must persist during a pre-defined time interval for energizing the relay. Hence, the delay time setting can be presented as:

$$t = \frac{2H\,\Delta f}{f_o\,\Delta P} + K \tag{5.6}$$

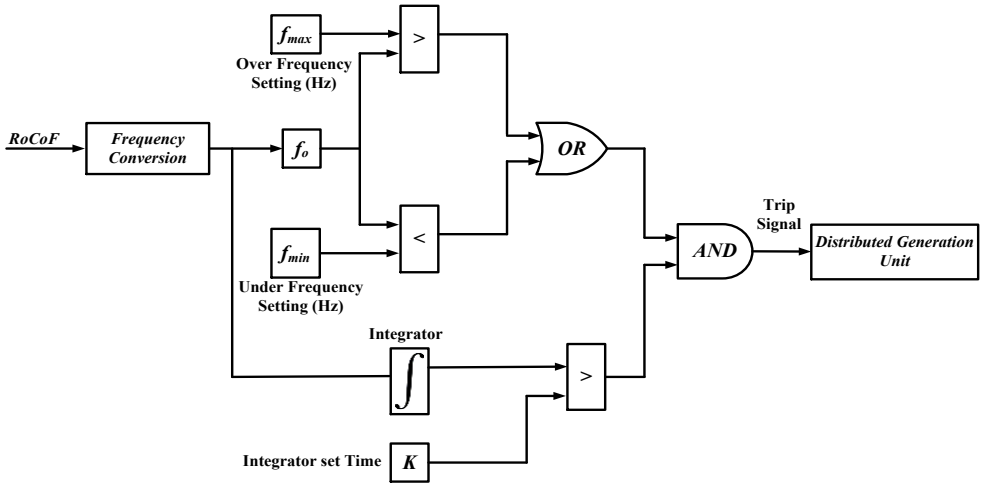

Fig. 5.4 Over/Under Digital Frequency Relay Computational Model

Table 5.3. FREQUENCY RELAY SETTINGS

Nominal Frequency (f)	*Frequency Relay*	*Limit*	*Threshold Time*
50	Over Under	f_{max} =51 Hz f_{min} =49 Hz	K=5 sec

The operation of the digital OUFR coordinated with optimal LFC and SMES is represented in the flowchart of Fig. 5.5.

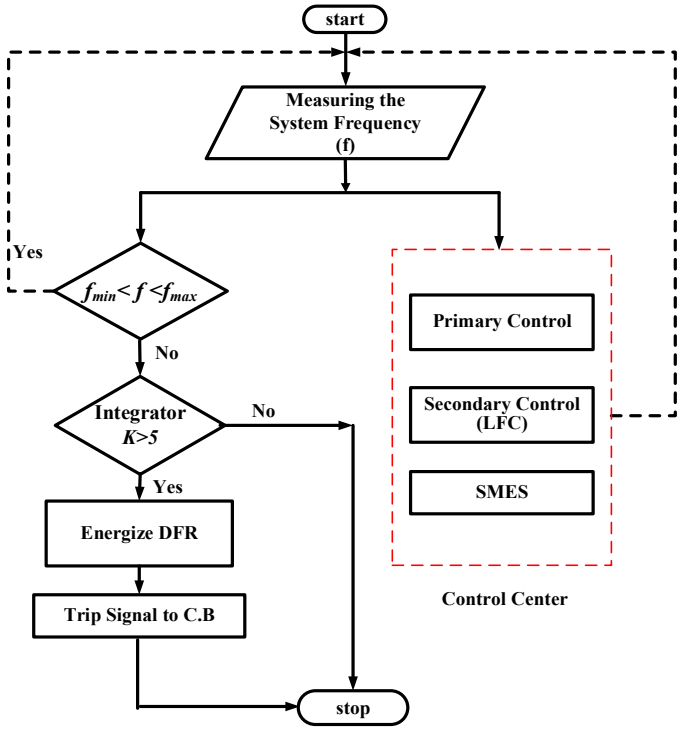

Fig. 5.5 Flowchart of the proposed coordination

5.3 Coordination of SMES and OUFR for MG Security Enhancement

This part discusses the effect of SMES integration on the performance of the OUFR for MG protection. Whereas the SMES installation in power system change the voltage and frequency values, consequently, the operation of the protective devices may be affected. The proposed coordination of optimal LFC and the OUFR in presence of SMES is validated using the same studied islanded MG in the MATLAB/Simulink considering high integration of the RERs and system uncertainties. A comparative study of optimal PID controller, conventional SMES, and SMES based on optimal PID has been carried out to determine the superior coordination with the digital OUFR for best MG performance.

5.4 Investigated System

Fig. 5.6 shows a single line diagram model of the tested islanded MG. The MW base of this MG is 20 MW. It consists of 15 MW of domestic loads, 20 MW of thermal power plant, and 5 MW of a wind farm, and 3 MW of solar power plant. The Generation Rate Constraints (GRC) limit is 0.2 pu MW/min. Table 5.4 summarized all rest of the MG parameters. The disturbance sources for the tested MG are the fluctuations of the PV solar power (ΔP_{PV}), the wind power (ΔP_{Wind}) and the load power change (ΔP_L). While the damping (D) and the inertia (H) act as the MG uncertainty parameters. Fig. 5.7 shows the dynamic modeling of the MG case study.

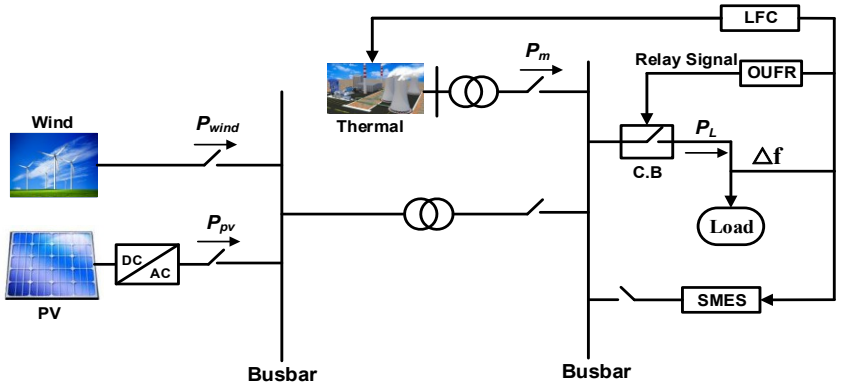

Fig. 5.6 Single line diagram of the islanded microgrid system

Table 5.4 Islanded microgrid parameters

Parameter	Value	Parameter	Value
D	0.015	T_{PV}	1.8
H	0.083	R	204
T_g	0.1	GRC	20%
T_t	0.4	V_U	0.3
T_{WT}	1.5	V_L	-0.3
f	50	K_{SMES}	6
ΔP_{SMES}	0.15	T_{SMES}	0.03

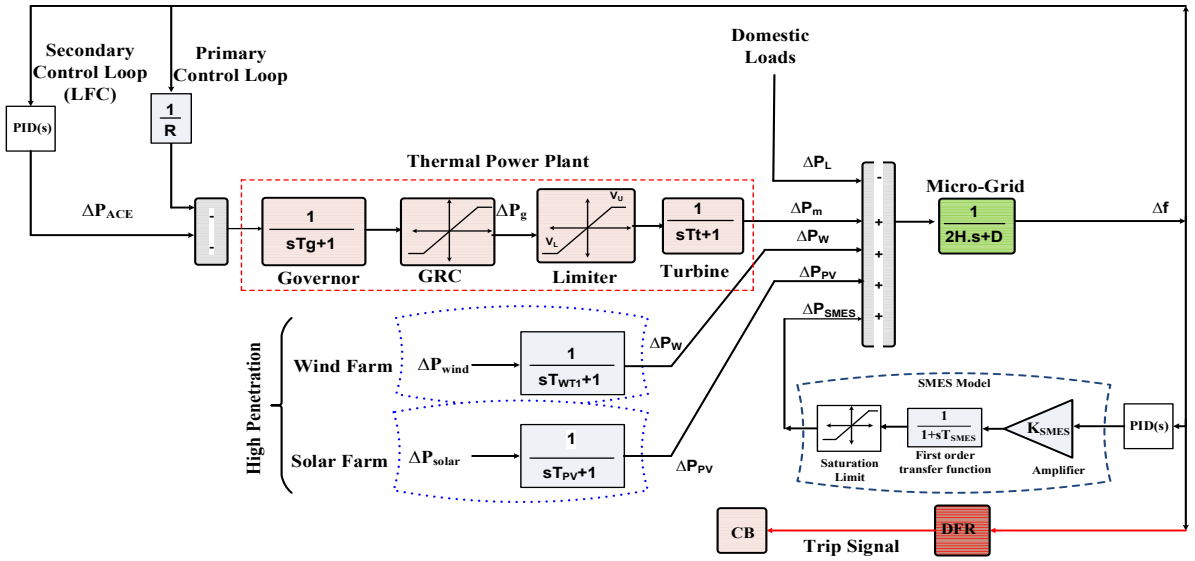

Fig. 5.7 The studied model of the MG including SMES and OUFR

The frequency deviation (Δf) of the islanded MG considering this case can be obtained as:

$$\Delta f = \frac{1}{2Hs + D}(\Delta P_m + \Delta P_W + \Delta P_{PV} + \Delta P_{SMES} - \Delta P_L) \tag{5. 7}$$

The state space model of the islanded MG is given in (5.18) and (5.19).

$$\dot{x} = Ax + B_1 w + B_2 u \tag{5. 8}$$

$$y = Cx \tag{5. 9}$$

where,

$$\dot{x} = \begin{bmatrix} -\frac{D}{2H} & \frac{1}{2H} & \frac{1}{2H} & \frac{1}{2H} & \frac{1}{2H} & \frac{1}{2H} & \frac{1}{2H} \\ 0 & -\frac{1}{T_t} & \frac{1}{T_t} & 0 & 0 & 0 & 0 \\ -\frac{1}{RT_g} & 0 & -\frac{1}{T_g} & \frac{1}{T_g} & 0 & 0 & 0 \\ \beta.K_{pid} & 0 & 0 & 0 & 0 & 0 & 0 \\ 0 & 0 & 0 & 0 & -\frac{1}{T_{SMES}} & 0 & 0 \\ 0 & 0 & 0 & 0 & 0 & \frac{1}{T_{WT}} & 0 \\ 0 & 0 & 0 & 0 & 0 & 0 & -\frac{1}{T_{PV}} \end{bmatrix} \begin{bmatrix} \Delta f \\ \Delta P_m \\ \Delta P_g \\ \Delta P_{ACE} \\ \Delta P_{SMES} \\ \Delta P_W \\ \Delta P_{PV} \end{bmatrix} + \begin{bmatrix} 0 & 0 & -\frac{1}{2H} \\ 0 & 0 & 0 \\ 0 & 0 & 0 \\ 0 & 0 & 0 \\ 0 & 0 & 0 \\ \frac{1}{T_{WT}} & 0 & 0 \\ 0 & \frac{1}{T_{PV}} & 0 \end{bmatrix} \begin{bmatrix} \Delta P_{wind} \\ \Delta P_{solar} \\ \Delta P_L \end{bmatrix} + \begin{bmatrix} 0 \\ 0 \\ 0 \\ 0 \\ \frac{K_{SMES}}{T_{SMES}} \\ 0 \\ 0 \end{bmatrix} u \tag{5.10}$$

$$y = \begin{bmatrix} 1 & 0 & 0 & 0 & 0 & 0 & 0 \end{bmatrix} x \tag{5.11}$$

5.5 Results and discussion

The proposed coordination of optimal LFC using a new optimal PID controller-based MSA, with the dynamic contribution of the SMES for an islanded MG has been tested under the nature variety RERs, random load variation, and system parameters variations, which are known the important characteristics of an actual MG. The simulation results and analysis of the islanded MG frequency during multiple changes in wind power generation (WPG), solar

power, domestic loads (i.e. disturbances), system inertia and parameters (i.e. uncertainties) are carried out using MATLAB/Simulink. The wind power of a 25% (5 MW) from the system base is integrated to the islanded MG at 500sec, while the PV solar power of 15% (3 MW) from the system base is connected from the initial time. The islanded MG is tested in the presence of high fluctuated wind power and low fluctuated solar power shown in Fig. 5.8 for a simulation time of 15 minutes. To investigate the dynamic performance of the islanded MG by using the proposed coordination of LFC and SMES and their impacts on the design and operation of the OUFR, four scenarios are applied on the MG as follows:

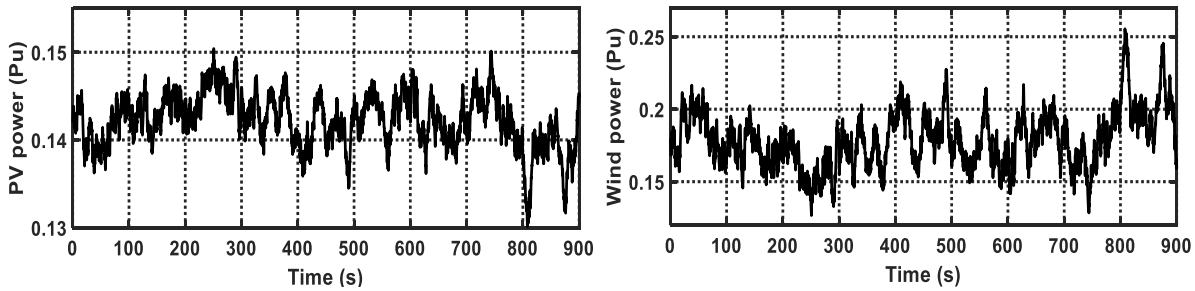

Fig. 5.8. PV and wind power variation profiles

Scenario A

In this scenario, the effectiveness of the proposed coordination performance for the islanded MG is tested by implementing the random load variations as shown in Fig. 5.9(a). In addition to, connecting the wind power and solar power generations. In this case, the variation of the system frequency is within the second type of frequency deviations (Δf_2) and within the limits of the digital relay. Fig. 5.9(c) shows the frequency response of the studied islanded MG. Although the system frequency fluctuated out of the given protection range at 600 secs due to the shedding of a large load, the OUFR does not trip as seen in Fig. 5.9(b). This is because the integrator output value does not exceed the set value.

Scenario B

In this scenario, the MG system is subjected to the power change under different load disturbance profile as shown in Fig. 5.10(a) beside the power fluctuations from wind and PV sources. The LFC can handle the frequency deviations and succeed to maintain the dynamic security of the MG frequency during the first load change at 300 sec as seen in Fig. 5.10(c). Hence, there is no need for relay action. On the other hand, the LFC was unable to control the frequency at the instant of wind farm connection at 500 sec as the system frequency fluctuated out of the given digital relay setting limits. In addition to, the integrator output exceeds the integrator set time *K*. Therefore, the digital relay is energized and sending a trip signal to the

circuit breaker in this case as shown in Fig. 5.10(b). This case has been made without using SMES.

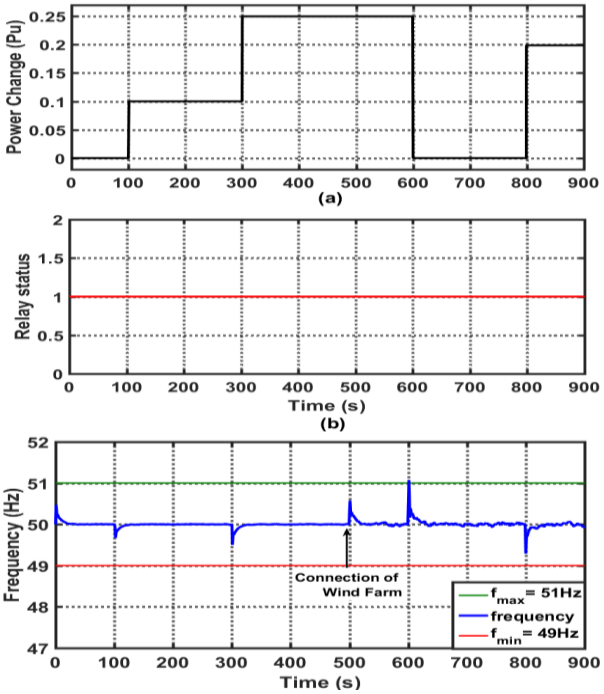

Fig. 5.9. Case A without SMES (a) power change, (b) Relay status, (c) MG Frequency

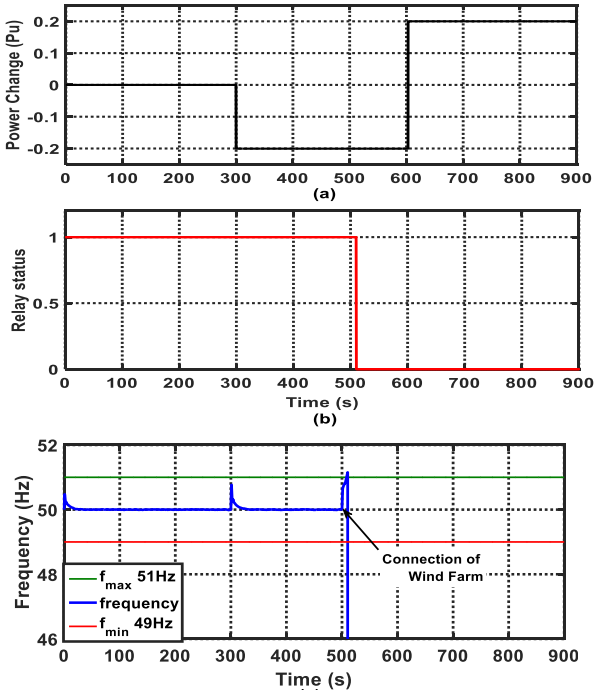

Fig. 5.10. Case B without SMES (a) power change, (b) Relay status, (c) MG Frequency

Therefore, the LFC using only the PID controller succeeded to readjust the frequency to its normal value in that case. This case proves the effectiveness of the LFC as it can adjust the frequency to its normal value in all five stages of this scenario without needs to protection action.

Fig. 5.11 shows the impact of using SMES on the system performance under the same conditions of load profile and RERs. The conventional SMES-based PI controller can restore the system frequency at different disturbance instants, such as at 300 sec and 500 sec. It also stabilized the frequency at 600 sec despite the frequency deviation exceeded the limits as shown in Fig. 5.11(c). This is because the integrator value does not reach its set value. Therefore, this case required readjusting the relay settings and this is not practical. Hence, the modified SMES-based optimal PID controller using the same signal from the optimal PID as an input; succeeded to solve this problem eventually as seen in Fig. 5.11(d).

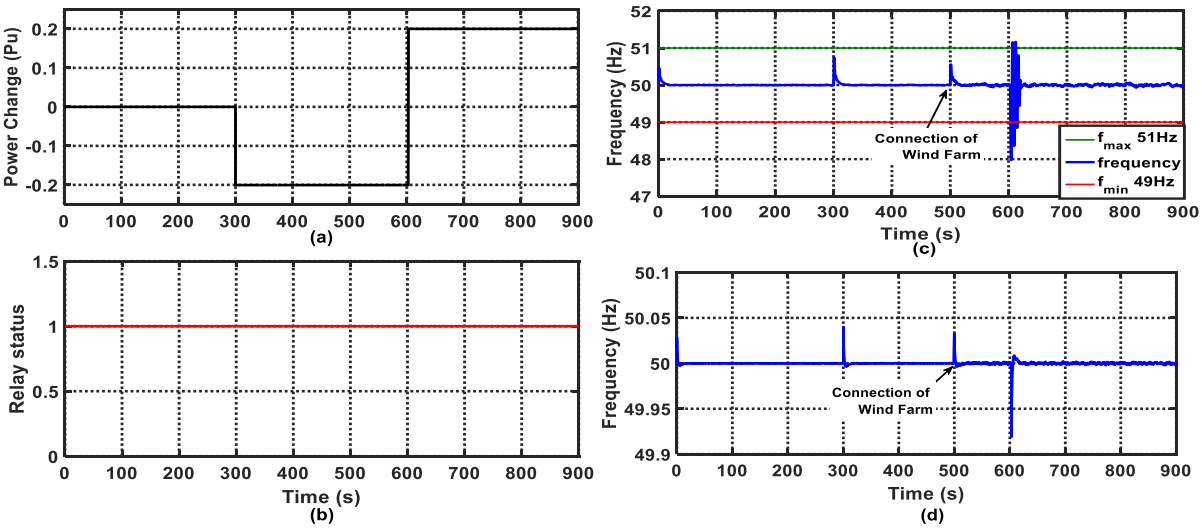

Fig. 5.11. Case B (a) power change, (b) Relay action, (c) with conventional SMES, (d) with Modified SMES

Scenario C

In this case, the same profile of power change as the previous scenario is applied as seen in Fig. 5.12(a) and increasing the wind penetration to 35%. It is connected to the MG at instant 500 sec. The LFC can control and stabilize the frequency deviations at the first at power change at 300 sec, while it cannot withstand the large frequency fluctuation caused by connected wind generation at 500 sec as noted in Fig. 5.12(c). Therefore, the digital OUFR is activated, and then send a trip signal to the CB in this case as shown in Fig. 5.12(b) as the integrator exceeds the value of *K*. This case proved the effectiveness of the presented coordination of control and protection scheme.

On the other side, the modified SMES has the ability to readjust the frequency variation to its normal value at three times of load disturbances without the need for a protection action. While the conventional SMES still need to improve the OUFR settings especially with sudden large load change as shown in Figs. 5.13(c, d).

Scenario D

This case checked the MG system uncertainty by reducing the system inertia (50% of default system inertia) with the same conditions and operations of wind power, PV solar power variations and power change profile as depicted in Fig. 5.14(a). The LFC has the ability to return the frequency variations to its normal value at 100 sec as shown in Fig. 5.14(c). However, it cannot solve it at the second step with more load change at 300 sec. This is due to occurring of two conditions for activating the OUFR; the system frequency is out of the limits and the integrator output exceeded (*K*). Hence, the OUFR sent a trip signal quickly to

disconnect the generations in this scenario to protect the equipment from failure as shown in Fig. 5.14(b).

Fig. 5.15(c) shows the effect of the conventional SMES on the system performance, whereas the SMES can maintain the system frequency at al disturbance steps and under the low inertia effect. But the DFR sent a trip signal to the circuit breaker as seen in Fig 5.16(b, c). This is due to the integrator, which exceeded the threshold value of 5sec in this case. Hence, the relay has a mal-operation in that case and need to readjust the relay settings or use the modified SMES as depicted in Fig. 5.16. The modified SMES type succeeded to solve the mal-operation of the OUFR in that case as shown in Fig. 5.15(c). Therefore, the modified SMES using the optimal PID controller is considered the best compared to conventional PID controller and conventional SMES. This is not only for the good results regarding the maximum overshoot, maximum undershoot, and maximum settling time but also it can solve the mal-operation of the presented OUFR in the MGs.

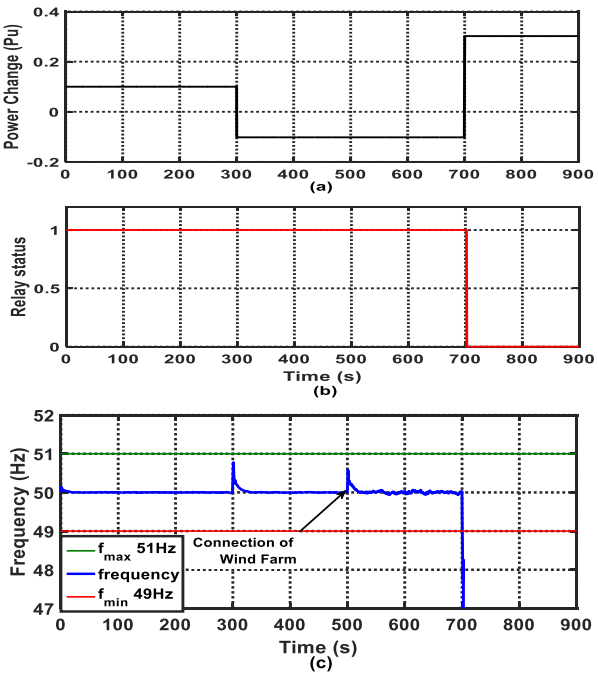

Fig. 5.12. Case C without SMES (a) power change, (b) Relay status, (c) MG Frequency

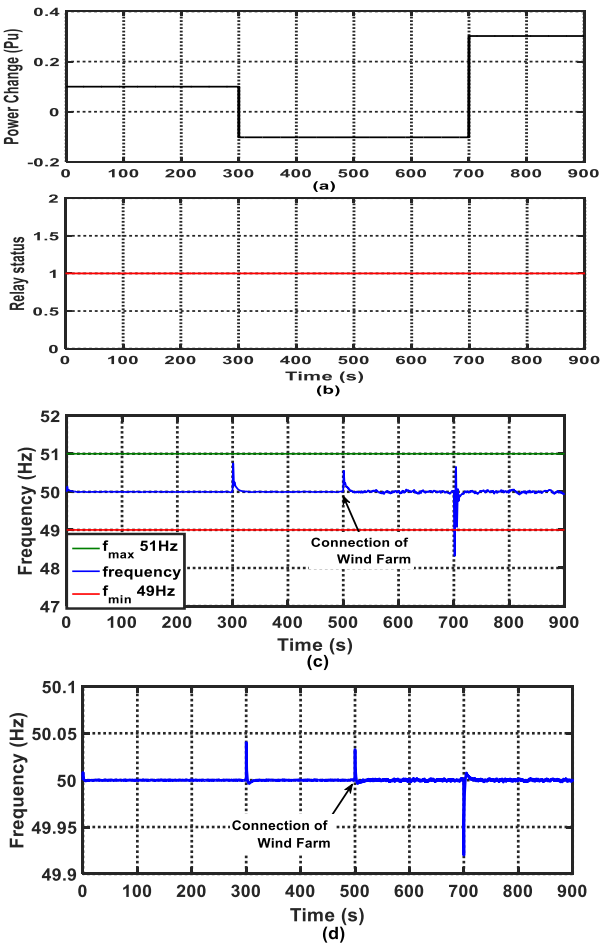

Fig. 5.13. Case C (a) power change, (b) Relay action, (c) with conventional SMES, (d) with Modified SMES

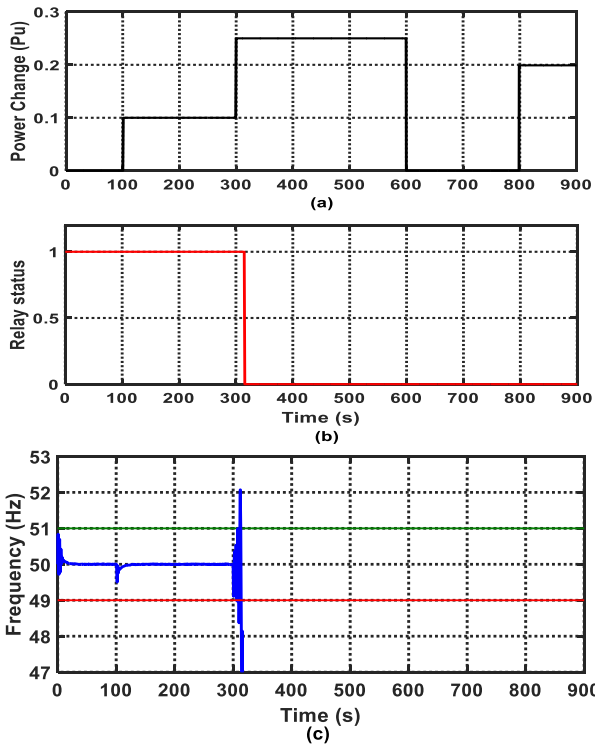

Fig. 5.14. Case D without SMES (a) power change, (b) Relay status, (c) MG Frequency

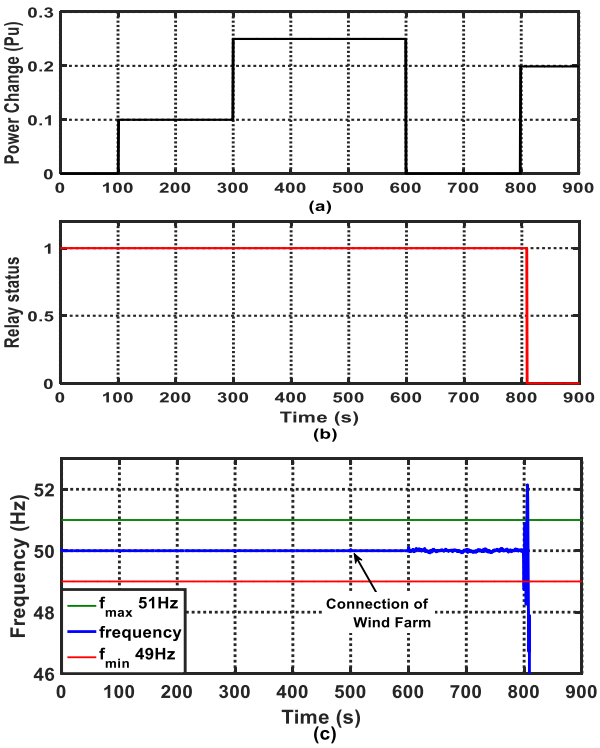

Fig. 5.15. Case D with conventional SMES (a) power change, (b) Relay status, (c) MG Frequency

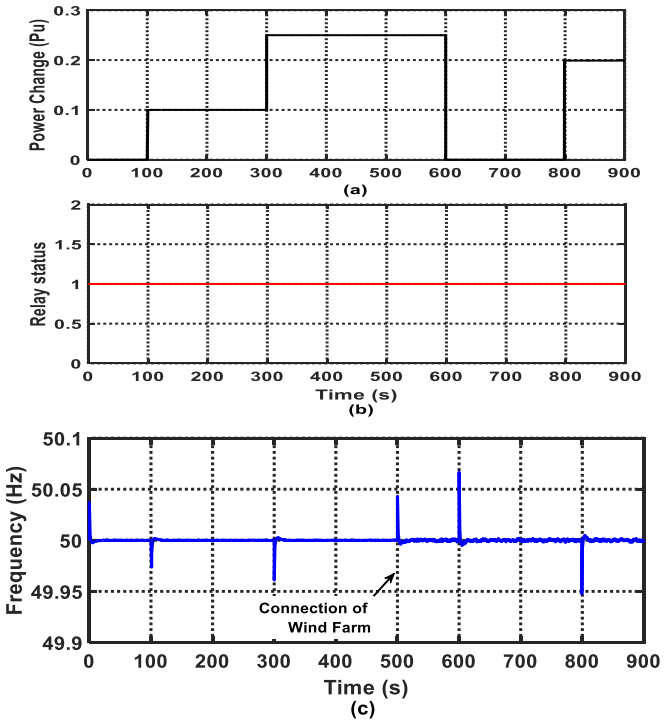

Fig. 5.16. Case D with modified SMES (a) power change, (b) Relay action, (c) MG Frequency

5.6 Summary

This chapter has presented a new coordination of optimal LFC using a new PID controller-based MSA combined with the modified application of SMES-based PID controller and the operation of the digital OUFR to enhance the frequency stability and dynamic security of the islanded MG system with the integration of renewable energy sources. The new optimal PID and SMES coordination achieved a robust frequency stability in the presence high wind/PV power penetration and different load power fluctuations against all cases of studied scenarios in terms of peaks overshoot, peaks undershoot and settling time. These results have been compared with conventional PID controller and conventional SMES, which needs a little long time to suppress the frequency deviations compared with the proposed coordination. Furthermore, the modified SMES solve the interference problem between the frequency control and protection by damping the frequency fluctuations quickly. While the PID and conventional SMES need to readjust the setting of the OUFR to avoid the mal-operation.

Chapter 6

Stability and Protection Enhancement of Egypt Power System using SMES and Digital Protection Considering high Penetration of RERs

6.1 Introduction

To verify the effectiveness and feasibility of the new optimal LFC based-MSA with coordination of SMES as a frequency stabilizer and their impacts on the frequency protection relays, a large-scale power system such as the Egyptian power system (EPS) is tested under the same disturbance cases of different load profiles, random load variation, wind/PV power fluctuations, and system uncertainties. The EPS consists of three dynamics subsystems; hydro, reheat and non-reheat power plants. In addition, the Egyptian Electricity Holding Company (EEHC) aims to cover 20% of the electric energy demand from RERs by the year 2020. About 12% of the 20% target is anticipated from wind power and the remaining 8% from others RERs; such as solar energy, and Concentrated Solar Power Plant (CSP) [183]. However, the RERs can bring significant impacts to the inertia of the system when increasing their penetration level in the EPS. Hence, the system inertia constant will be reduced along with increasing the penetration level of RERs, which leads to increase the system frequency deviation. Therefore, the frequency control may be difficult in case of any mismatch between electric power generation and load demand, particularly with penetration growing of RERs (e.g., wind and solar energy), which integrated into the power system.

6.2 EPS Configuration and Modeling

6.2.1. Dynamic Model of the EPS

The real EPS is divided into seven strongly tied zones, which are Cairo, Middle Egypt, Upper Egypt, East El-Delta, El-Canal, West El-Delta and Alexandria as shown in Fig. 6.1. Each zone comprises several power plants (non-reheat, reheat, and hydropower plants or a combination of each). The EPS has more than 180 power plants, moreover it is classified into three categories: a) Non-reheat power plants represented by gas turbine power plants and a few numbers of steam power plants. b) Reheat power plants mainly represented by thermal power

plants or combined cycle power plants. c) Hydropower plants such as High Dam in Aswan city. Furthermore, the EPS includes RERs, (i.e., wind turbines and solar power plants), which contribute almost 3% of the installed capacity. On the other hand, by the year 2020, the Egyptian Electricity Holding Company (EEHC) aims to cover 20% of the electric energy demand from RERs. About 12% of the 20% target is anticipated from wind power and the remaining 8% from others RERs; such as PV power plant, and Concentrated Solar Power Plant (CSP). The total generation capacity and peak loads are 38 ,000 MW and 29 ,000 MW respectively according to the annual report of the EEHC in 2016 [183]. The base of the system frequency is 50 Hz, while the power base is 38,000MW. Therefore, this chapter study the EPS considering the effect of high wind power penetration (HWPP) as a future planning of EPS, which including the proposed coordination of LFC and modified control signal to SMES using a new optimal PID controller-based MSA technique as shown in Fig. 6.2.

The National Energy Control Center (NECC) in Egypt has advanced dynamic model of Egyptian LFC [184]. Moreover, this model was rebuild using MATLAB/Simulink with some manipulation, which including the effect of HWPP, and the dynamic contribution of SMES as an auxiliary LFC technique coordinated with optimal LFC as shown in Fig. 6.3. The NECC in Egypt estimates the system parameters values, which used in the nonlinear model of the EPS and independent from the system operation as in Table 6.1 [185]. However, the other parameters vary with time are depending on the operating conditions. The nominal parameters values are summarized in Table 6.2.

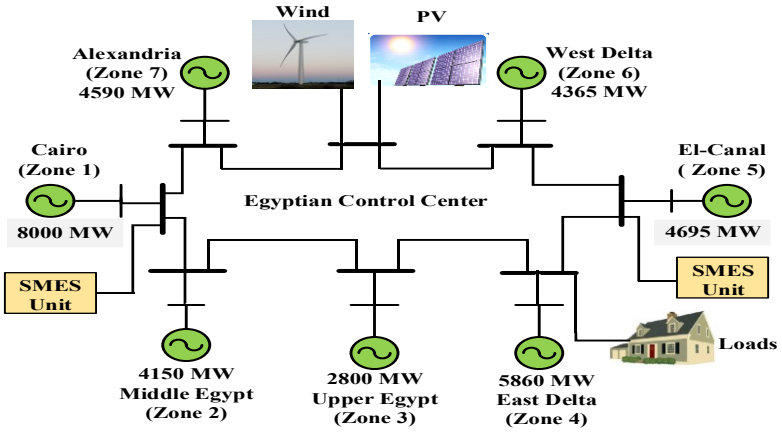

Fig. 6.1. Typical single line diagram of the EPS

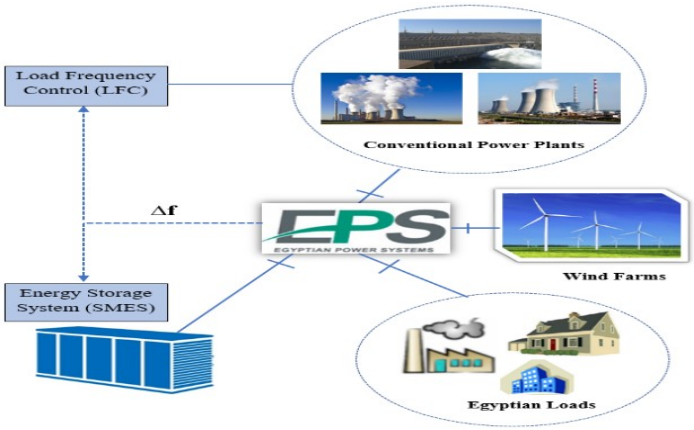

Fig. 6.2. A simplified model of the EPS considering HWPP

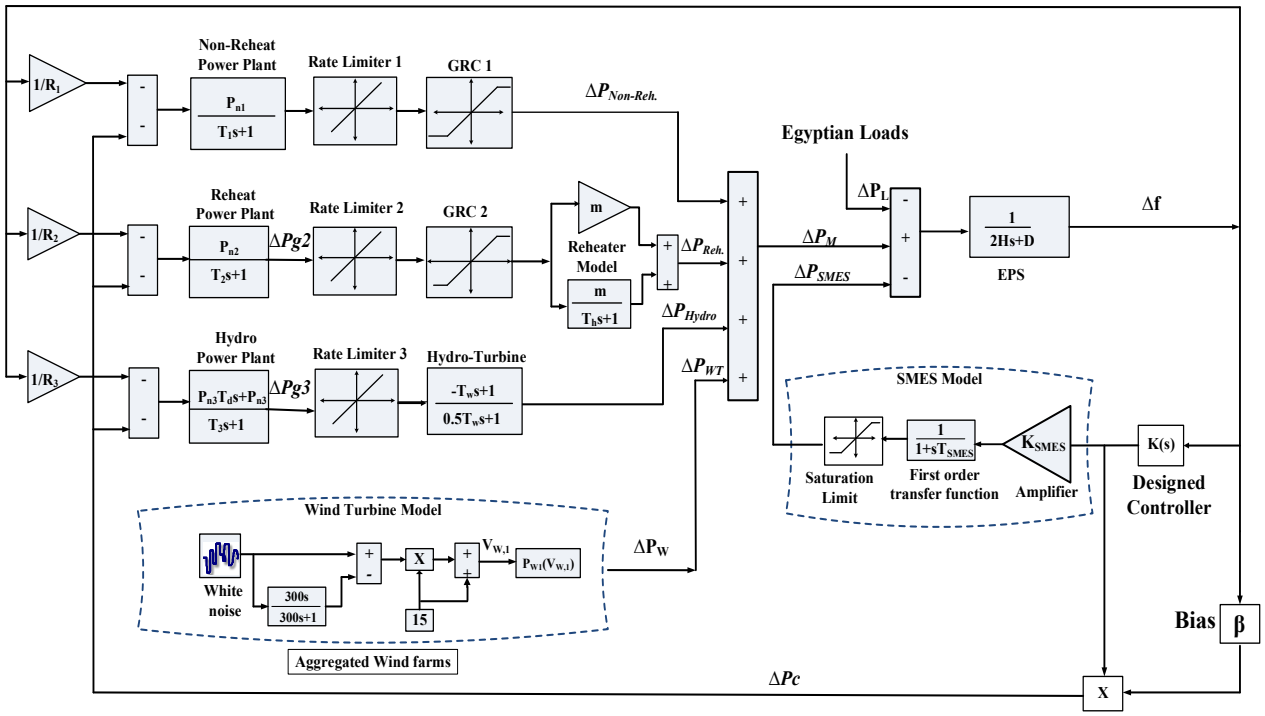

Fig. 6.3. A nonlinear model of the EPS for seven strongly tied zones considering HWPP

Table 6.1 Nominal parameters of the EPS

Parameter	Value	Parameter	Value
D	0.028	T_w	1.0
T_1	0.4	m	0.5
T_2	0.4	R_1	2.5
T_3	90	R_2	2.5
T_d	5	R_3	1.0
T_h	6	β	1.0
f	50	K_{SMES}	5
ΔP_{SMES}	0.1 p.u	T_{SMES}	0.025

Table 6.2 Dynamic parameters of the EPS

Parameter	H	P_{n1}	P_{n2}	P_{n3}
Value	5.7096	0.2529	0.6107	0.1364

6.2.2. A mathematical model of the EPS

The real hybrid EPS considered in this study is the eighth order linearized multi-source power system considering HWPP and the SMES technology. The frequency deviation of the studied power system considering the effect of the primary control loop (i.e., governor action), a secondary control loop (i.e., LFC), and SMES controller (i.e., an auxiliary LFC) can be obtained as:

$$\Delta f = \frac{1}{2Hs+D}(\Delta P_{Non-Reh.} + \Delta P_{Reh.} + \Delta P_{Hydro.} + \Delta P_{WT} \pm \Delta P_{SMES} - \Delta P_L) \quad (6.1)$$

Fig. 6.3 shows the block diagram of the transfer functions, which describe the different subsystems of the studied nonlinear power system.

I. The non-reheat power plants

$$\Delta P_{Non-Reh} = \frac{P_{n1}}{T_1 S+1} * \left(\frac{-1}{R_1} * \Delta f - \Delta P_c\right) \quad (6.2)$$

II. The reheat power plant

$$\Delta P_{g2} = \frac{P_{n2}}{T_2 S+1} * \left(\frac{-1}{R_2} * \Delta f - \Delta P_c\right) \quad (6.3)$$

$$\Delta P_{Reh.} = \left(m + \frac{m}{T_h S+1}\right) * \Delta P_{g2} \quad (6.4)$$

III. The Hydropower plants

$$\Delta \mathrm{P_{g3}} = \frac{\mathrm{P_{n3}T_d S+P_{n3}}}{\mathrm{T_3 S+1}} * \left(\frac{-1}{\mathrm{R_3}} * \Delta \mathrm{f} - \Delta \mathrm{P_c}\right) \quad (6.5)$$

$$\Delta P_{Hydro.} = \left(\frac{-T_w S+1}{0.5*T_w S+1}\right) * \Delta P_{g3} \quad (6.6)$$

IV. Wind turbines model

$$\Delta P_{WT} = \frac{1}{T_{WT} S+1} * (\Delta P_{Wind}) \quad (6.7)$$

V. The SMES model

The complete model of SMES with its parameters is explained in chapter four, subsection 4.3.1.

$$\Delta P_{SMES} = \frac{K_{SMES}}{T_{SMES} S+1} * \left(\frac{d(\Delta f)}{dt}\right) \quad (6.8)$$

where wind power variation (ΔP_{WT}), and load power variation (ΔP_L) are considered as power system disturbance signals. Whereas, wind power farms are modelled as high and low fluctuated wind power as well as load Model.

Using Eqs. (6.1) - (6.8), the dynamic equations of the studied hybrid power system of Fig. 6.3 can be derived and written in the state variable form as follows:

$$\dot{X} = AX + BU + EW \quad (6.9)$$

$$Y = CX + DU + FW \quad (6.10)$$

where,

$$X^T = [\Delta f \quad \Delta P_{Non-Reh.} \quad \Delta p_{Reh.} \quad \Delta p_{g2} \quad \Delta P_{Hydro.} \quad \Delta P_{g3} \quad \Delta P_{WT} \quad \Delta P_{SMES}] \tag{6.11}$$

$$U^T = [\Delta P_{Wind} \quad \Delta P_L],\ W = [\Delta P_C] \tag{6.12}$$

$$\dot{X} = \begin{bmatrix} -\frac{D}{2H} & \frac{1}{2H} & \frac{1}{2H} & 0 & \frac{1}{2H} & 0 & \frac{1}{2H} & \frac{1}{2H} \\ -a_1 & -\frac{1}{T_1} & 0 & 0 & 0 & 0 & 0 & 0 \\ -ma_2 & 0 & -\frac{1}{T_h} & b_1 & 0 & 0 & 0 & 0 \\ -a_2 & 0 & 0 & -\frac{1}{T_2} & 0 & 0 & 0 & 0 \\ (-2b_2D + 2a_3) & 2b_2 & 2b_2 & 0 & (2b_2 - \frac{2}{T_w}) & (\frac{2}{T_w} + \frac{2}{T_3}) & 0 & 0 \\ (b_2D - a_3) & -b_2 & -b_2 & 0 & -b_2 & -\frac{1}{T_3} & 0 & 0 \\ 0 & 0 & 0 & 0 & 0 & 0 & -\frac{1}{T_{WT}} & 0 \\ -b_3 & b_3 & b_3 & 0 & b_3 & 0 & b_3 & (b_3 - \frac{1}{T_{SMES}}) \end{bmatrix} \begin{bmatrix} \Delta f \\ \Delta P_{Non-Reh} \\ \Delta p_{Reh.} \\ \Delta p_{g2} \\ \Delta P_{Hydro.} \\ \Delta P_{g3} \\ \Delta P_{WT} \\ \Delta P_{SMES} \end{bmatrix} +$$

$$\begin{bmatrix} 0 & -\frac{1}{2H} \\ 0 & 0 \\ 0 & 0 \\ 0 & 0 \\ 0 & -2b_2 \\ 0 & b_2 \\ -\frac{1}{T_{WT}} & 0 \\ 0 & -b_3 \end{bmatrix} \begin{bmatrix} \Delta P_{Wind} \\ \Delta P_L \end{bmatrix} + \begin{bmatrix} 0 \\ -\frac{P_{n1}}{T_1} \\ -\frac{m*P_{n2}}{T_2} \\ -\frac{P_{n2}}{T_2} \\ \frac{2*P_{n3}}{T_3} \\ -\frac{P_{n3}}{T_3} \\ 0 \\ 0 \end{bmatrix} [\Delta P_c] \tag{6.13}$$

$$Y = [\beta \quad 0 \quad 0 \quad 0 \quad 0 \quad 0 \quad 0 \quad 0] \begin{bmatrix} \Delta f \\ \Delta P_{Non-Reh} \\ \Delta p_{Reh.} \\ \Delta p_{g2} \\ \Delta P_{Hydro.} \\ \Delta P_{g3} \\ \Delta P_{WT} \\ \Delta P_{SMES} \end{bmatrix} + [0 \quad 0] \begin{bmatrix} \Delta P_{Wind} \\ \Delta P_L \end{bmatrix} + [0][\Delta P_c] \tag{6.14}$$

The state variables of matrices are:

$$a_1 = \frac{P_{n1}}{T_1 R_1},\ \ a_2 = \frac{P_{n2}}{T_2 R_2},\ \ a_3 = \frac{P_{n3}}{P_{n3}},\ \ a_4 = \frac{T_d}{2H},\ \ b_1 = \frac{2m}{T_h} - \frac{m}{T_2},\ \ b_2 = a_3 a_4,\ \ b_3 = \frac{K_{SMES}}{T_{SMES}S+1}$$

6.2.3. Wind power generation system

The full model of Wind Power Generation System is described in details in chapter four, subsection 4.4.2. This section studies the effect of merging HWPP on the system frequency response of a real hybrid EPS. The EPS includes aggregated wind turbines models, which are 1000 wind turbine units of 750-KW for each unit beside the conventional generation units. The EPS is tested in the presence of fluctuated wind power as shown in Fig. 6.4. The parameters of the wind turbine model are presented in Table 6.3.

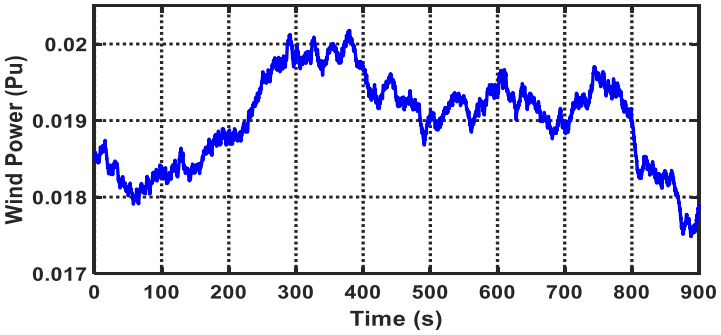

Fig. 6.4. The wind Power output profiles of the EPS

Table 6.3 Nominal wind turbine parameters of wind farm

Parameter	Value	Parameter	Value
$P_{W,1}$	750 KW	C_2	116
$V_{W,1}$	15 m/sec	C_3	0.4
ρ	1.225 Kg.m^2	C_4	0
A_T	1648 m^2	C_5	5
r_T	22.9 m	C_6	21
n_T	22.5 rpm	C_7	0.1405
C_1	-0.6175		

6.2.4. Control Methodology and Problem Formulation

In this case study, the proposed coordinated control strategy of secondary frequency control (i.e., LFC) and SMES (i.e. auxiliary LFC) based on the optimum PID controller is applied. This work uses a novel intelligent searching method (i.e., The MSA), which is described in details in chapter four, section 4.3.3 to find the optimal design parameters of the PID controller, which has parameter bounds.

In this study, the integral of squared-error (ISE) is used as a fitness function, which is the objective function of the optimization technique and can be formulated as follows:

$$ISE = \int_0^{t_s} (\Delta f)^2 \, dt \tag{6.15}$$

where (Δf) is the frequency deviation of the EPS and t_s is the simulation time. The proposed MSA technique is applied in the EPS to obtain the minimum value of objective function through getting on the optimal parameters of the PID controller. The simulation results show that the best solution of optimal PID parameters values is shown in Table 6.4. All MSA parameters, which are used for solving the LFC problem after making several trials and errors are summarized in Table 6.5.

Table 6.4 PID Controller's Parameters for the EPS

Parameter	K_p	K_i	K_d
Value	71.25	5.91	6.11

Table 6.5 The control parameters of MSA

Parameter	Value	Parameter	Value
Maximum iteration	100	M_{urate}	0.05
Swarm size	50	K_p limits	0 - 100
Pathfinders Number	20	K_i limits	0 - 100
Trials	40	K_d limits	0 - 100

6.3 Simulation study

The proposed coordination performance of LFC and SMES using a new optimal PID controller-based MSA is compared with both; the optimal LFC-based MSA with/without the effect of conventional SMES without modifying the input control signal for the realistic hybrid EPS in the presence of HWPP considering the effect of nonlinearity. The EPS comprises steam power plants (reheat and non-reheat turbine), gas power stations (non-reheat turbine), hydro-power plants, wind power plants, and SMES technology. Three subsystems (non-reheat, reheat, and hydropower plants) are given for the EPS with inherent nonlinearities, which are speed governor backlash and GRCs of power plants. Backlash is defined as the total magnitude of sustained speed change. All speed governors have a backlash, which is important for LFC in the presence of disturbances. The GRCs limit the generation rate of the output power which is given as 0.2 pu MW/min and 0.1 pu MW/min for non-reheat and reheat turbines, respectively. Moreover, the actual GRC of a hydropower plant is about 0.5 pu MW/min, which is higher than the generation rate corresponding to any practical disturbance and hence it will be neglected.

6.4 RESULTS AND DISCUSSION

The Simulation results and analysis are carried out using MATLAB/Simulink® software, which takes the GRCs of different generation sources of the EPS into account. Analysis of different control strategies has been implemented on the EPS concerning wind farms. Many types of research assume the load disturbance is a step change disturbance, which is represented by the forced outage of generation unit or sudden switch off a massive load. However, in fact, the load disturbances are complex and random nature. Therefore, three scenarios of different load profiles are applied to examine the performance of the implemented control strategies, which the simulation time of each one is 15 minutes. Moreover, the EPS is tested in the presence of the fluctuated wind power, which is connected to the EPS at 400 s for all scenarios.

Scenario A

The simulation result for this scenario is shown in Fig. 6.5, where a step load disturbance (ΔP_L=5%) during a period from 200 to 600 sec in addition to connecting the wind farms at 400 sec are implemented. Fig. 6.5 shows the frequency response of the EPS concerning wind farms for three different control strategies. It is clear that the performance of the LFC using a new optimized PID controller-based MSA with the SMES is more robust and faster frequency response than the optimal LFC without SMES. On the other hand, the proposed coordination between the LFC and the controlled SMES using the optimal PID controller-based MSA achieved a superior performance and more reduction of the frequency excursions (Δf) and the wind power fluctuations than other strategies.

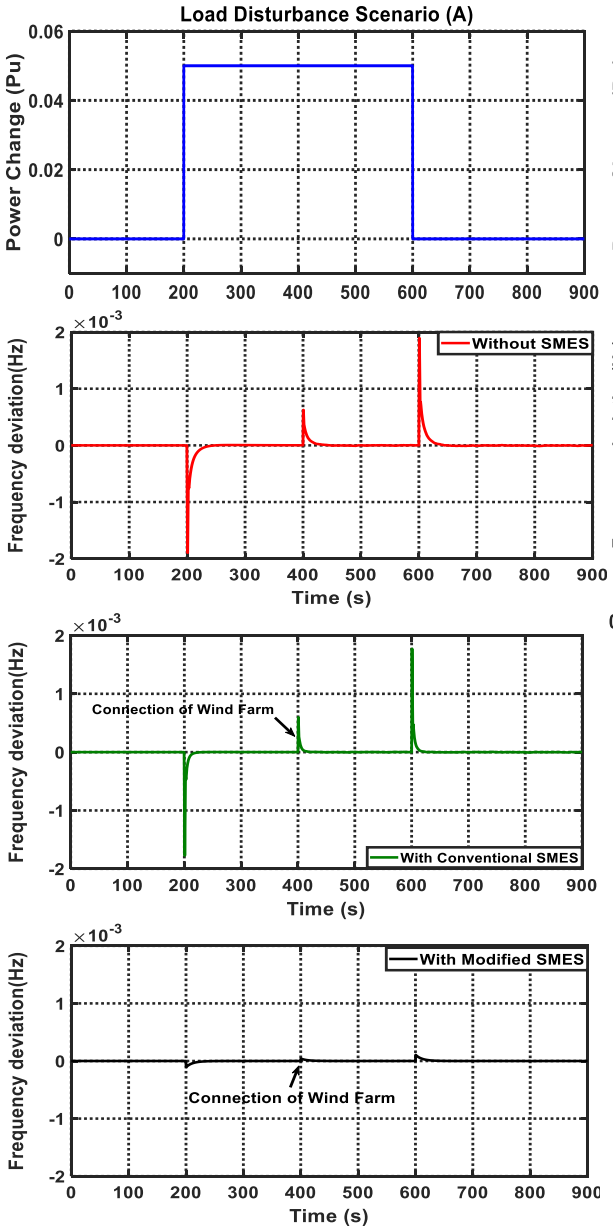

Fig. 6.5. The frequency deviation of scenario A

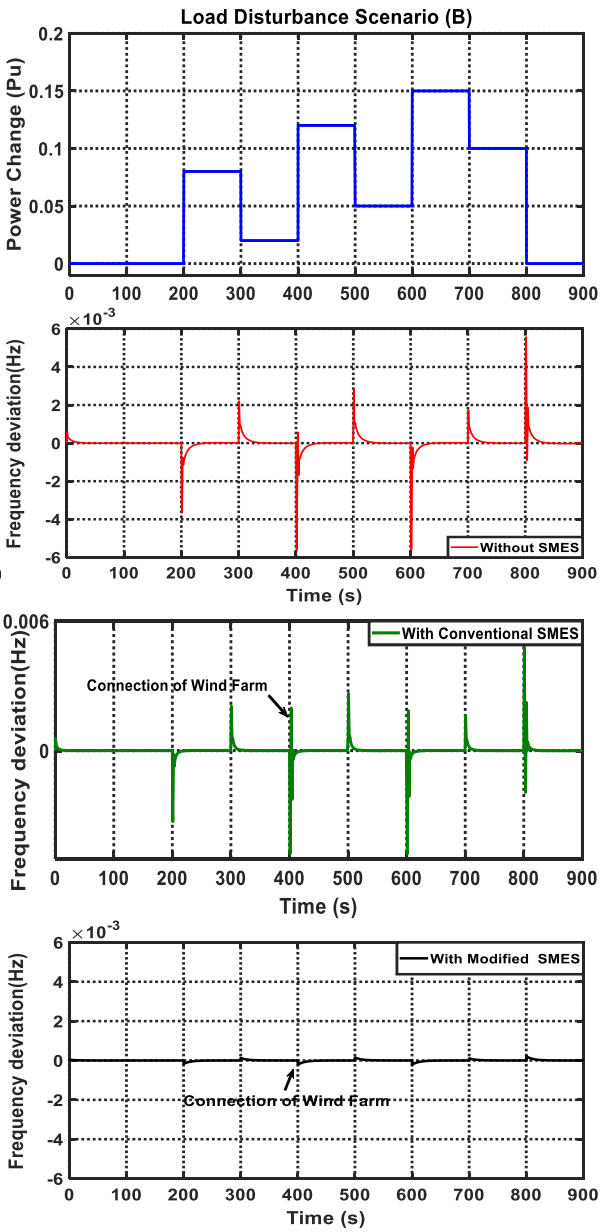

Fig. 6.6. The frequency deviation of scenario B

Scenario B

The effectiveness and robustness of the proposed coordination against system parameters variation (i.e., system uncertainty) have been validated under the different operating condition of the EPS as tabulated in Table 6.6. Therefore, this scenario applies a series of load disturbance with random magnitudes during the period from 200 sec to 800 sec in addition connection wind power fluctuations at 400 sec as depicted in Fig. 6.6. It is clearly seen that the proposed coordinated control strategy achieved a robust stability against changing the system parameters and operating load condition. Moreover, there is no need of re-tuning the controller parameters when the system is subjected to either variation in loading condition or system parameters. While, the performance of the other control strategies, takes a long time to reach a steady-state of system frequency compared with the proposed control strategy.

Table 6.6. Two Operation Conditions of the EPS

Parameter	H	P_{n1}	P_{n2}	P_{n3}
Scenario B	6.1452	0.3335	0.5455	0.1210
Base Case	5.7096	0.2529	0.6107	0.1364

Scenario C

The EPS integrated with wind energy is subjected to a random load variation as a load disturbance. The proposed control strategy based on the coordination between the LFC and the controlled SMES can suppress the system frequency deviation nearly to zero value as seen in Fig. 6.7, while the other control strategies gave large overshoot and oscillated to such an extent that it is not satisfying. A comparison graph for this scenario is shown in Fig. 6.7, which proves the effectiveness and robustness of the suggested coordinated control strategy. Hence, it presents a very powerful control strategy to solve the frequency instability problem and may become a very promising tool for solving more complex power system problems particularly, with increasing the penetration of the RERs.

The previous simulations results showed that the proposed control strategy of a new coordination between the secondary control (i.e., LFC) and the controlled SMES using a new optimal PID controller-based MSA succeeded for frequency stability improvement of large-scale power system such as the EPS. It has achieved a robust stability in terms of peaks overshoot, peaks undershoot and settling time. Whereas, the optimal LFC system with/without the SMES model (i.e., uncontrollable SMES) gave a satisfactory performance but needs a very

long time to suppress the frequency deviations with high peaks overshoot/undershoot particularly, in case of large disturbances.

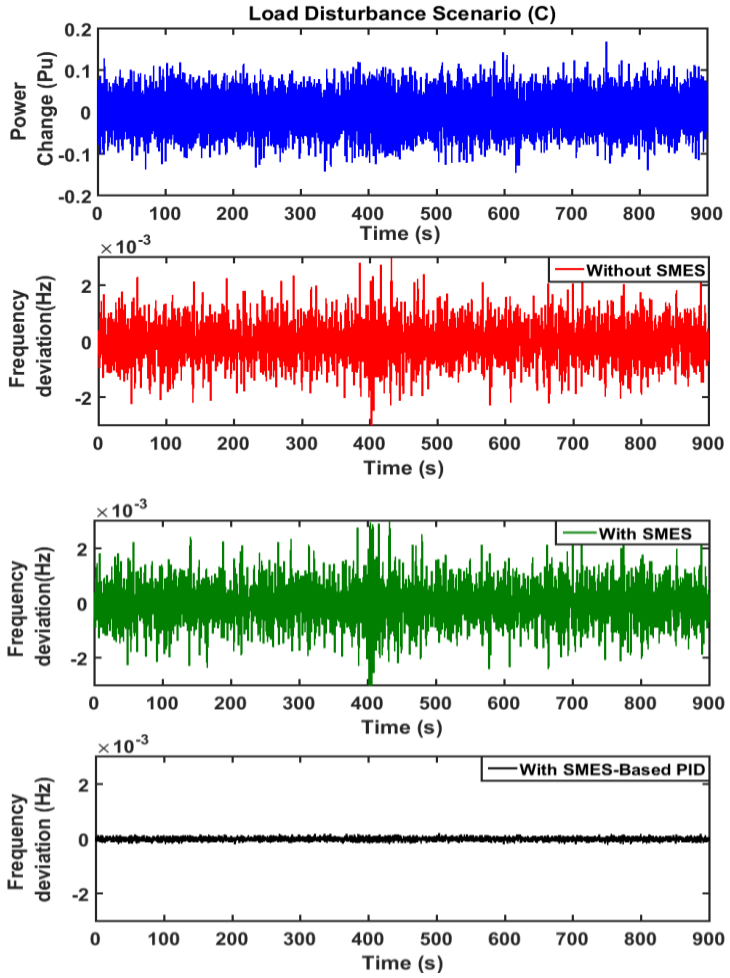

Fig. 6.7 The frequency deviation of scenario C

6.5 Coordination of OUFR and LFC for EPS Protection

This section discusses the application of the coordination of the OUFR and LFC on a large power system scale such as the EPS. The EPS suffers from many issues due to the increase of interconnection of different power plants. These issues such as, the frequency stability, which is a basic principle in the power system operation. Many reasons such as, load shedding, load restoring, and short circuits cause large frequency fluctuations, which threaten the system security and could lead to complete blackouts as well as damages to the system equipment. For example, a large blackout happened in Egypt in September 2014 [186]. This event affected more than 20 million people, as they were not accessible to electricity for hours. Therefore, this part proposes the coordination of Load Frequency Control (LFC), which uses an optimized PID controller-based new Moth Swarm algorithm (MSA) and digital OUFR for a realistic

multi-source EPS considering different cases study of load disturbances. This new coordination has been described in details in chapter five, section 5.2 for MG stability and protection. Furthermore, the complete design and modeling of the digital frequency relay are explained in chapter five subsection 5.2.2.

The MSA method has been used to tune the PID parameters gains (K_p, K_i, and K_d) for the model of EPS. The obtained values of the PID gains controller based on MSA are summarized in Table 6.4. The Simulation results and analysis are carried out on the EPS model with the effect of system nonlinearity as shown in Fig. 6.8. The GRC limits of the generation rate output power, which is given as 0.2 pu MW/min and 0.1 pu MW/min for non-reheat and reheat turbines, respectively. However, the actual GRC of a hydropower plant is about 0.5 pu MW/min, which is higher than the generation rate corresponding to any practical disturbance and hence it neglected. The proposed coordination is tested under different cases of load shedding and restoring. Each case has some different scenarios and the simulation time of each one is 5 minutes. The studied scenarios on the EPS are as the follows:

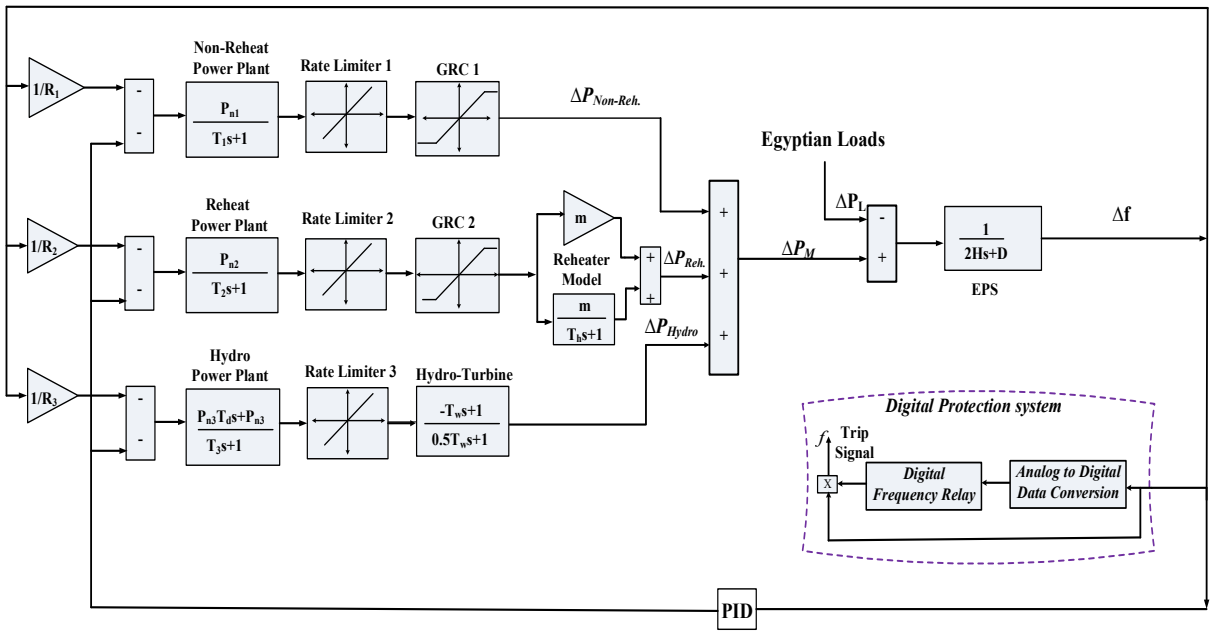

Fig. 6.8 The dynamic model of the EPS for seven strongly tied zones including OUFR

Scenario A

In the first scenario, 12% of the load is added at 50 sec; then it is shed at 100 sec, later on, further 20% of the load is applied at 150 sec as shown in Fig. 6.9. In this case, although, the system frequency exceeds the allowable limits of under frequency. the digital frequency relay does not trip as seen in Fig. 6.9 due to the value of the integrator output does not exceed the set value.

Therefore, LFC succeeded to readjust the frequency to its normal value as shown in Fig. 6.10. This case proves the effectiveness of the proposed optimal LFC, which used PID controller-based MSA as it can adjust the frequency to its normal value in all three stages of this scenario without needs to protection action.

Scenario B

In this scenario, the load disturbance is greater than the previous one, whereas a 20% of the load is added at 100 sec then it followed by adding another 25% of the load at 200 sec in addition to the base load and the relay is observed. Fig. 6.11 represents the power change and relay status under different load conditions. In the first load change (added 20% of the load), the frequency fluctuations are not within the allowable frequency limits. However, the value of the integrator output does not exceed the set value.

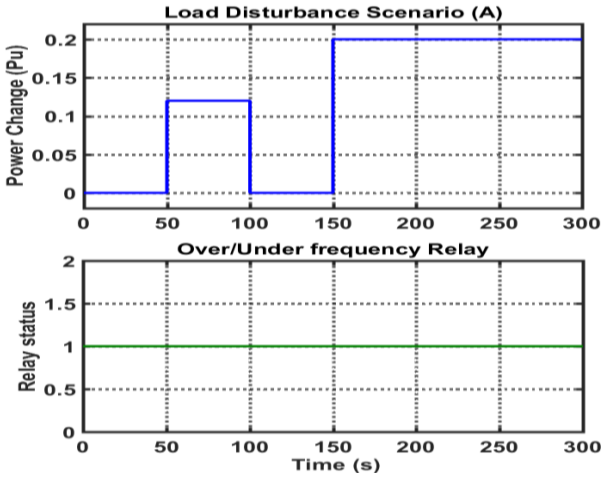

Fig. 6.9. Load Disturbance and Relay Status of Case A.

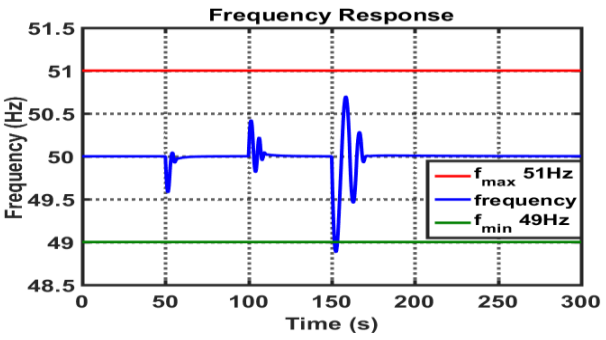

Fig. 6.10. The frequency response of EPS for Case A.

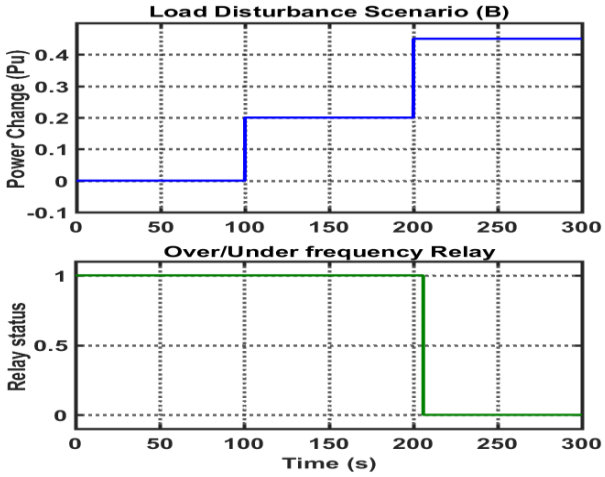

Fig. 6.11. Load Disturbance and Relay Status of Case B.

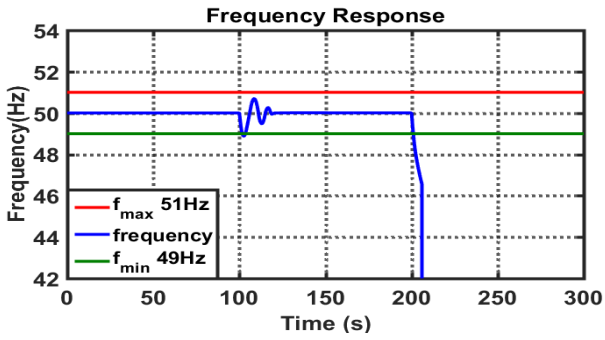

Fig. 6.12. The frequency response of EPS for Case B.

Hence, the control action returned the frequency to the stable case without any action from the protection side. On the other hand, when a heavy load applied on the EPS, the digital frequency relay tripped the system. Fig. 6.12 shows the performance of the frequency in the two stages of scenario B.

Scenario C

In the third scenario, the behavior of the proposed optimal LFC and digital protection coordination is tested under shedding loads conditions. Fig. 6.13 shows that 20% of the load is switched off at 100 sec, followed by another 20% of the load shedding at 200 sec. The control action of optimal LFC overcome the first change in frequency at 100 sec instant. However, it cannot handle the change of system frequency when a huge load applied at 200 sec. therefore, the digital frequency relay (as an over frequency relay in this case) trips the system at that time as shown in Fig. 6.13 whereas the integrator output exceeds the threshold value of 5. Hence, the effectiveness of the proposed coordination is proved; the frequency behavior is depicted in Fig. 6.14.

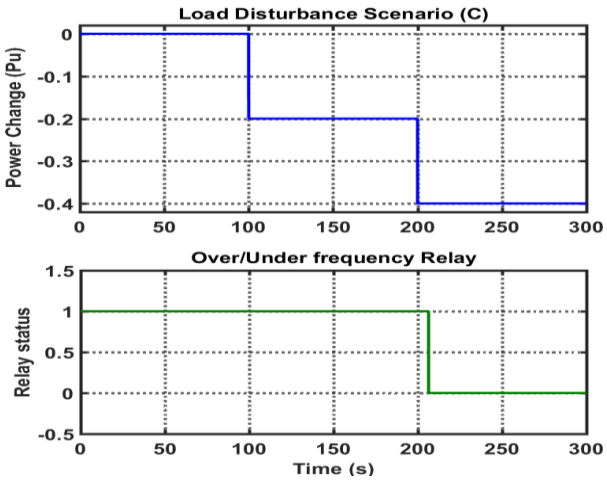

Fig. 6.13. Load Disturbance and Relay Status of Case C.

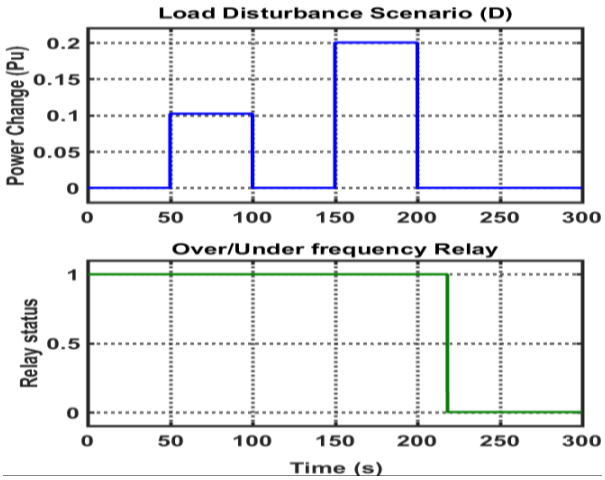

Fig. 6.15. Load Disturbance and Relay Status of Case D.

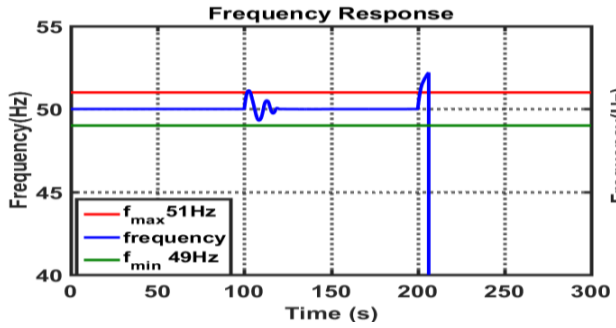

Fig. 6.14. The frequency response of EPS for Case C.

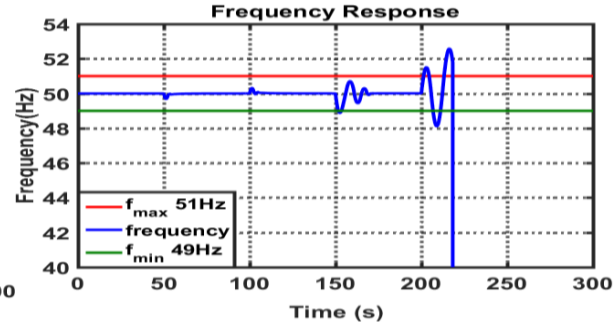

Fig. 6.16. The frequency response of EPS for Case D.

Scenario D

In this case, the optimal LFC has the ability to readjust the frequency variation to its normal value at three times of load disturbances, firstly 10% of the load is added at 50 sec then it is shed at 100 sec followed by adding 20% of the load from 150 to 200 sec as shown in Fig. 6.15. However, the load shedding at 200 sec leads to obtaining large frequency fluctuations and the controller could not reset the frequency to the normal value. Moreover, the integrator reached

quickly and exceeded the threshold value of 5sec. Therefore, the digital frequency relay trips the system as seen in Fig. 6.15. In the last case of a load change, the frequency exceeded the allowable limits which are used for designing the digital relay. The change in the system frequency under the load shedding and restoring can be observed in Fig. 6.16.

Scenario E

In the last scenario, the robustness of the proposed coordination technique against series changes in loads has been tested as depicted in Fig. 6.17. It is clearly shown in Fig. 6.18 that the optimal LFC can maintain the frequency stability of the EPS under different cases of transient and permanent conditions from 50 sec to 200 sec. However, at 230 sec, the load disturbance is huge and permanent results that the frequency value was not within the control limits. Hence, the digital frequency relay action became necessary to protect the electrical system. Fig. 6.17 shows the action of the under-frequency relay, which trips after the integrator exceeded its threshold value. Results proved that a high-performance of coordination of protection and control unit for application in the EPS was developed. The proposed coordination succeeded in maintain the protection and control functions by eliminating the power-system faults or prevent the spreading.

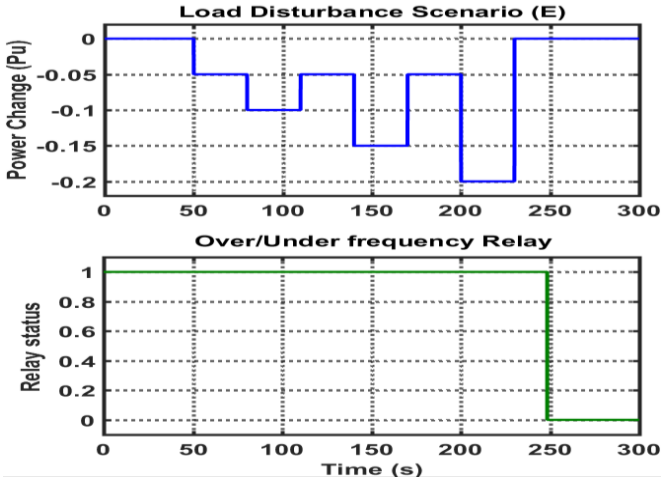

Fig. 6.17. Load Disturbance and Relay Status of Case E.

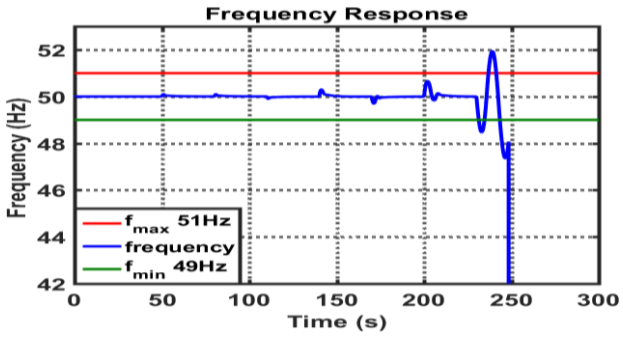

Fig. 6.18. The frequency response of EPS for Case E.

6.6 Dynamic Security Enhancement of EPS Using Coordination of SMES and OUFR

This section presents a control strategy between the robust superconducting magnetic energy storage (SMES)-based a new optimal PID controller-based Genetic Moth Swarm Algorithm (GMSA) and the load frequency control (LFC) to emulate virtual inertia into the control loop of the EPS, thus stabilizing the EPS frequency during contingencies. Moreover, the proposed control strategy is coordinated with digital over/under frequency relay (OUFR) for enhancement the frequency stability and preservation EPS dynamic security because of the high penetration level of the RERs. To prove the effectiveness of the proposed coordination strategy, it has been tested considering different load and RERs disturbances under varying the inertia level of EPS. The operation of the digital OUFR coordinated with LFC and SMES is represented in the flowchart of Fig. 6.19.

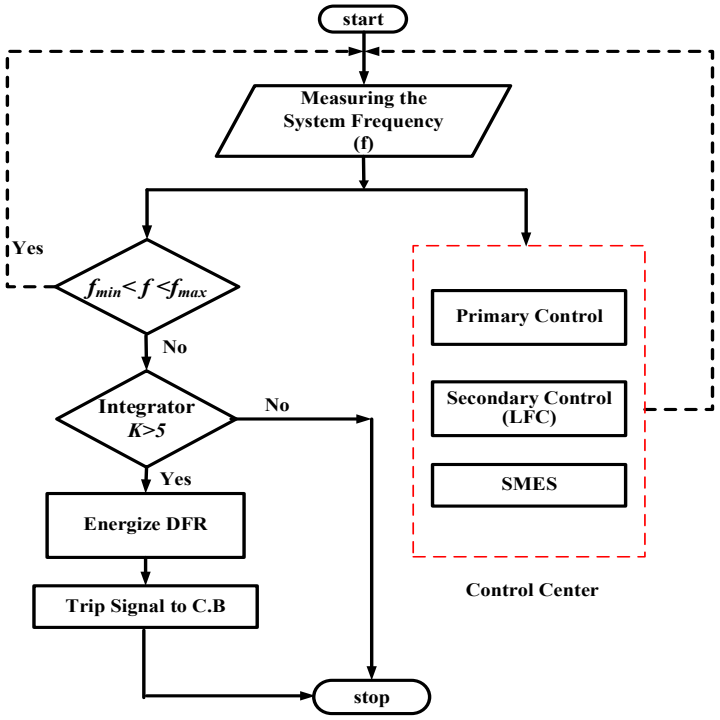

Fig. 6.19. Flowchart of the OUFR/SMES control coordination

The EPS total generation capacity is 38,000 MW, base peak loads of 29,000 MW, and system frequency is 50 Hz based on the annual report of the Egyptian Electricity Holding Company (EEHC). Fig. 6.20 shows the EPS dynamic model, which is presented by the National Energy Control Centre (NECC) in Egypt. It has been rebuilt using MATLAB software with some manipulation to include the new penetration of RERs and the coordination of SMES and OUFR. NECC estimated the nominal parameters of the EPS dynamic model in Table 6.7. This study takes into consideration the effects of the physical constraints such as Generation Rate

Constraints (GRC) of power plant and speed governor dead band (backlash) for modelling the actual EPS. Whereas, backlash is defined as the total magnitude of sustained speed change. All speed governors have a backlash, which is important for primary frequency control in the presence of disturbances. The GRC limits the generation rate of output power, which is given as 0.2 pu MW/min. In this research, the power variation of renewable energy sources such as; the wind power variation (ΔP_{Wind}) and the PV solar power variation (ΔP_{PV}), and the load power variation (ΔP_L) are considered as disturbance signals for the EPS.

Table 6.7 EPS parameters

Parameter	Value	Parameter	Value
D	0.028	T_{PV}	1.2
H	5.7096	T_{WT}	1.0
T_1	0.4	m	0.5
T_2	0.4	R_1	2.5
T_3	90	R_2	2.5
T_d	5	R_3	1
T_h	6	P_{n2}	0.6107
P_{n1}	0.2529	P_{n3}	0.1364
f	50	K_{SMES}	5
ΔP_{SMES}	0.15 p.u	T_{SMES}	0.025

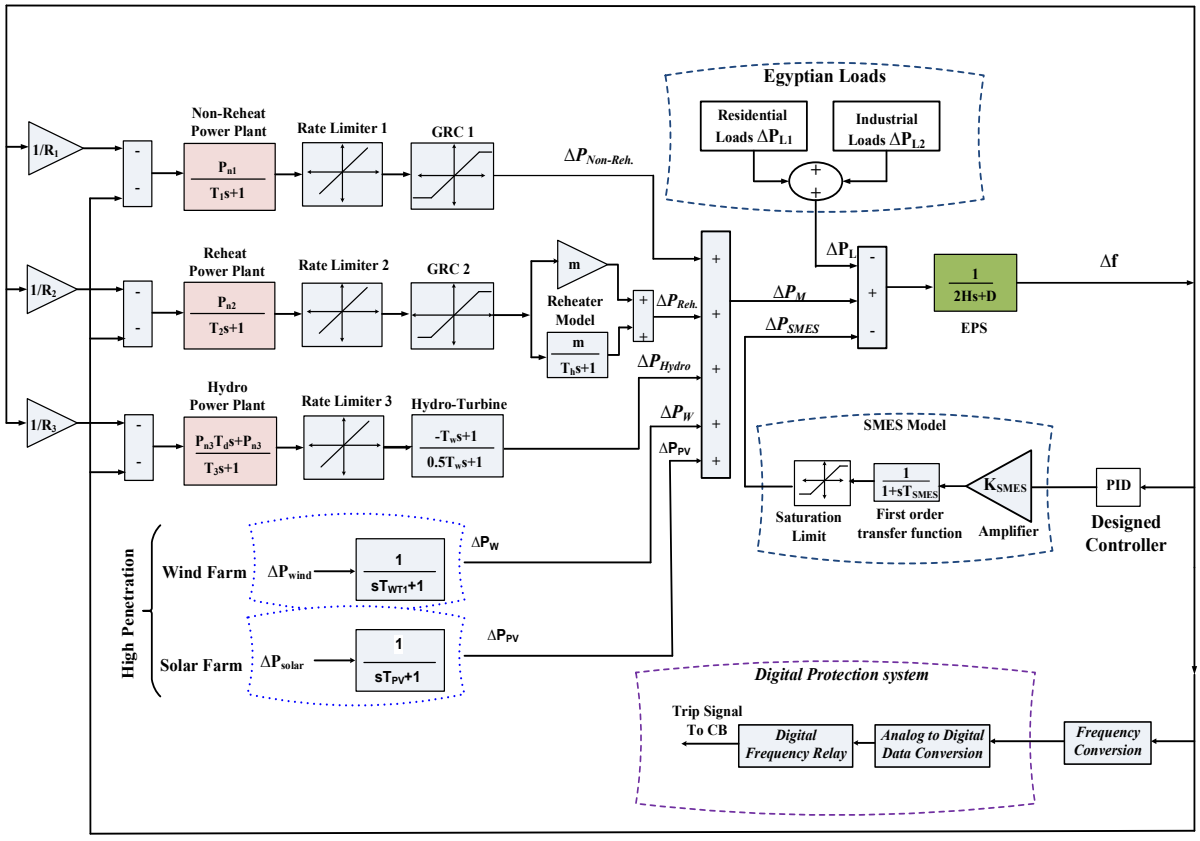

Fig. 6.20 The dynamic model of the EPS including RERs.

6.7 Results and discussion

The proposed coordination of SMES and OUFR protection is tested on the EPS single line diagram in Fig. 6.21 under the intermittent sources, load variation, and system inertia variations (i.e., system uncertainties). The simulation results of the EPS frequency during multiple changes in wind power generation, solar power, domestic loads (i.e. disturbances), system inertia and parameters (i.e. uncertainties) are carried out using MATLAB/Simulink. The EPS is tested in the presence of high-fluctuated wind power of about 8750 MW and solar power of 5700 MW as shown in Fig. 6.22, in addition to load variations as shown in Fig. 6.23 for a simulation time of 10 minutes. To investigate the dynamic security of the EPS by using the proposed coordination of control and OUFR, three scenarios are applied to the EPS as follows:

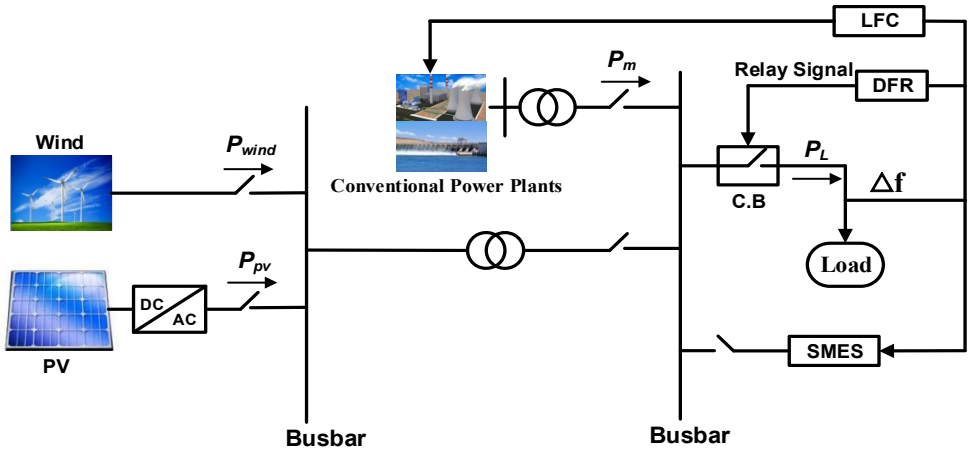

Fig. 6.21. Single-line diagram of the EPS case study

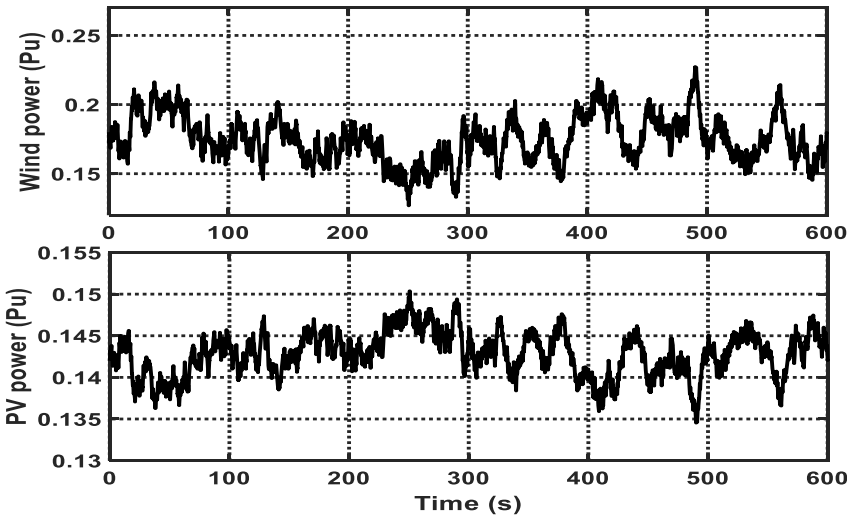

Fig. 6.22. Power variations of wind/ solar generations

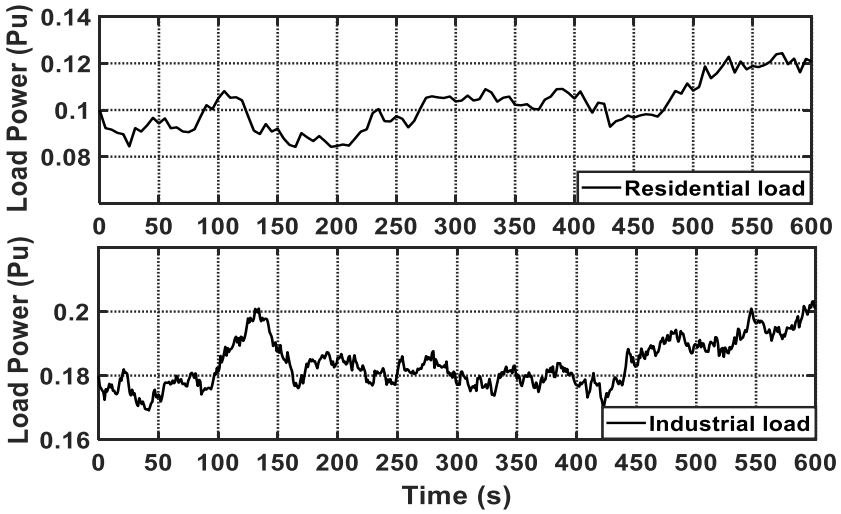

Fig. 6.23. Random Load deviation

The main objective of this section is to investigate the EPS performance with the proposed coordinated strategy of LFC, SMES, and OUFR by implementing high-fluctuated wind and PV variation, in addition to load variations during three different levels of system inertia. Table 6.8 summarizes the different disturbance condition during the simulation.

Table 6.8 Multiple operating conditions of the EPS

Source	Starting	Stopping	Size (pu)
Industrial load	150 sec	-	0.22
Residential load	initial	400 s	0.12
Wind power	300 s	-	0.23
PV	initial	-	0.15

Scenario A

Fig. 6.24 shows the frequency response of the EPS under the sequence of operating conditions as shown in Table 6.8 without change the system inertia level (100% of default system inertia). The EPS cannot withstand the first step of a disturbance at 150 sec at the instant of connecting the industrial load, as the frequency deviation exceeds the allowable limits. Hence, the OUFR energized in that case and sent a trip signal to the circuit breaker. While the conventional SMES can damp the frequency oscillations under the acceptable limits but the EPS suffered at the instant of wind farm connection at 300 sec as it takes long settling time to return to its stable case with frequency change of ±0.72Hz. When using the proposed modified SMES based on the optimal PID controller, the frequency change is only ±0.2Hz and returns the frequency stability case in 5 secs only without need of OUFR action. Fig.6.25 shows the fase charge/discharge process of SMES based on the optimal PID controller. Hence, the proposed coordination is effective in that case for maintaining the EPS dynamic security compared to the case of with/without the conventional SMES.

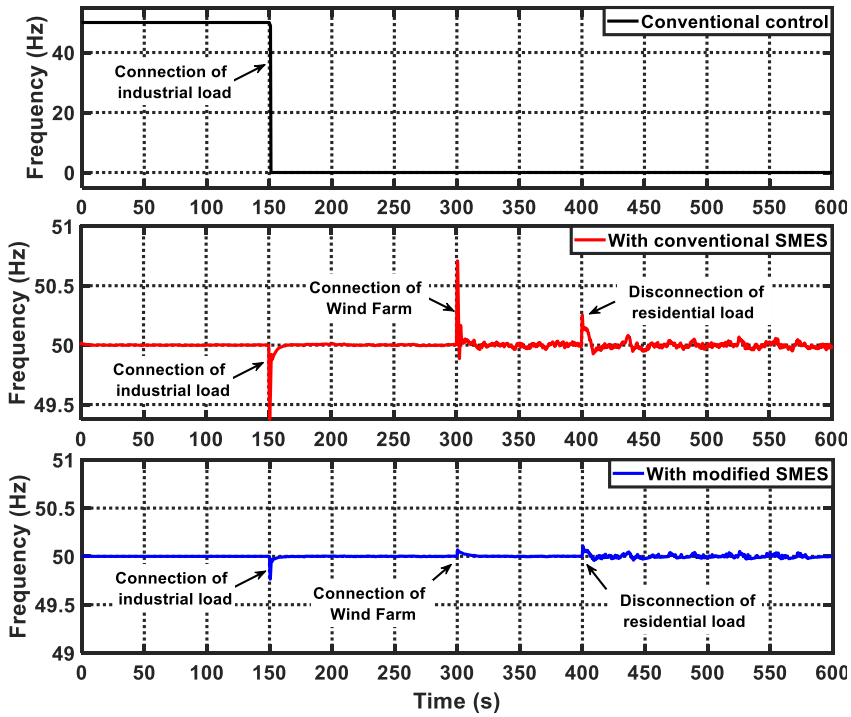

Fig. 6.24 The frequency response of the EPS for scenario A (100% of default system inertia)

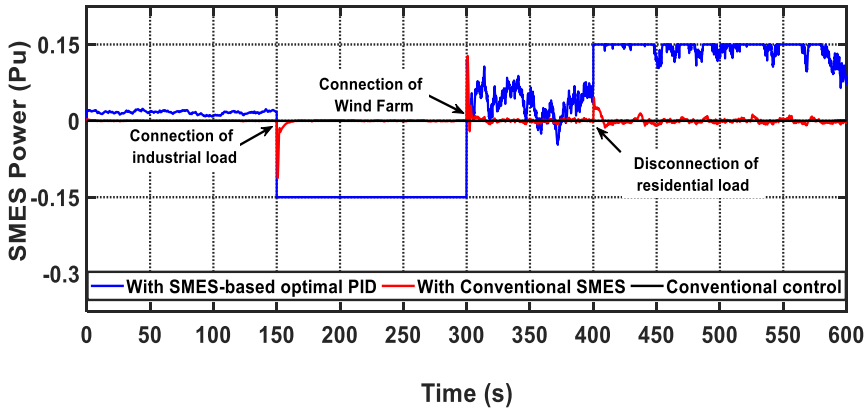

Fig. 6.25 The response of SMES

Scenario B

In this scenario, the EPS system is subjected to the same operating conditions of Table 6.8, in addition to reducing the system inertia to 55% of the default system inertia level. The EPS in that case with only conventional controller failed to restore the system frequency, where the frequency deviation increased over than the allowable limits. Hence, the OUFR energizes and sends a trip signal to the circuit breaker because the integrator value (K) exceeds its threshold value at the 150 sec when the industrial load connected as shown in Fig. 6.26. While, the impact of conventional SMES on the system performance under the same conditions can restore the system frequency at different disturbance instants, such as at 150 sec and 400 sec. It also stabilized the frequency at 300 sec despite the frequency deviation exceeded the allowable limits by nearly ±1.1Hz as shown in Fig. 6.26. This is because the integrator value does not

reach its set value (5 sec). Therefore, this case required readjusting the OUFR settings. However, the utilization of modified SMES-based the optimal PID as an input signal; succeeded to solve this problem eventually with frequency change of ±0.25Hz. Hence, the proposed coordination solved the mal-operation problem of the OUFR in that case without the need to readjust the integrator setting of the digital frequency relay.

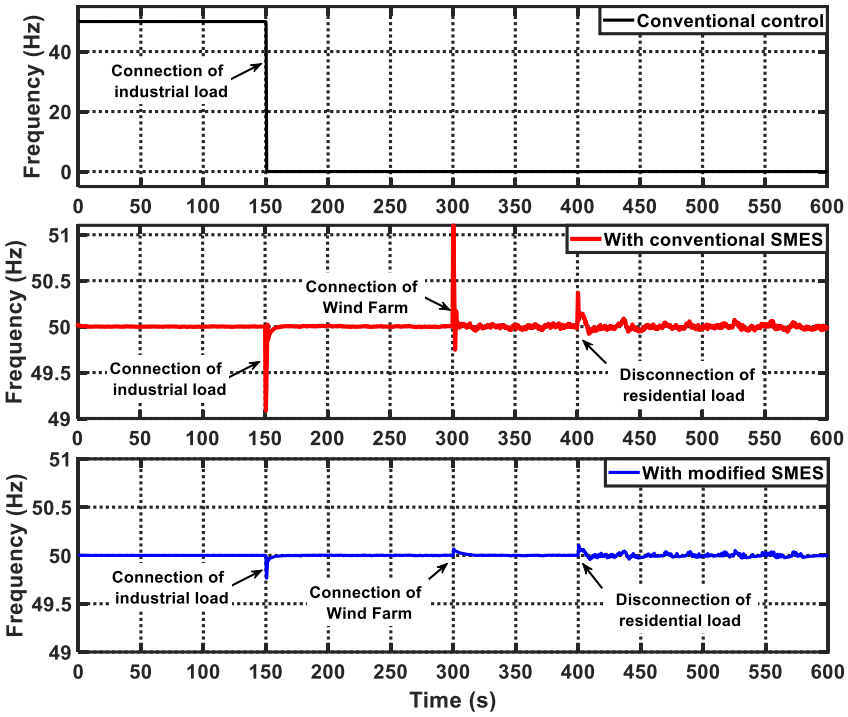

Fig. 6.26. The frequency response of the EPS for scenario B (55% of default system inertia)

Scenario C

The effectiveness of the proposed control/protection coordination is approved in this extreme scenario. Whereas, the EPS is estimated under the situation of very low system inertia (35% of default system inertia) with the default parameters and multiple operation conditions of wind power, PV solar power variations and load disturbance profile as summarized in Table 6.8. Fig. 6.27 shows that the EPS cannot withstand this critical case of inertia reduction with the conventional controller only and the frequency deviation exceed the allowable limits. Hence, the OUFR keeps the system security with immediately sending a signal to the circuit breakers to trip the generation units at the first disturbance operation at 150 sec. While the utilization of conventional SMES can return the frequency variations to their normal value at 150 sec as shown in Fig. 6.27. However, it cannot solve it at the moment of wind connection at 300 sec. This is due to occurring of two conditions for activating the OUFR; the system frequency is out of the limits and the integrator output exceeded (K). Therefore, the OUFR sends a trip signal with quick responding to protect the equipment from failure. On the other hand, the

modified SMES has the ability to readjust the frequency variation to its normal value at three times of load and wind power disturbances and under the extreme low inertia effect without the need for a protection action. Therefore, the modified SMES-based optimal PID controller is considered the best compared to with/without conventional SMES.

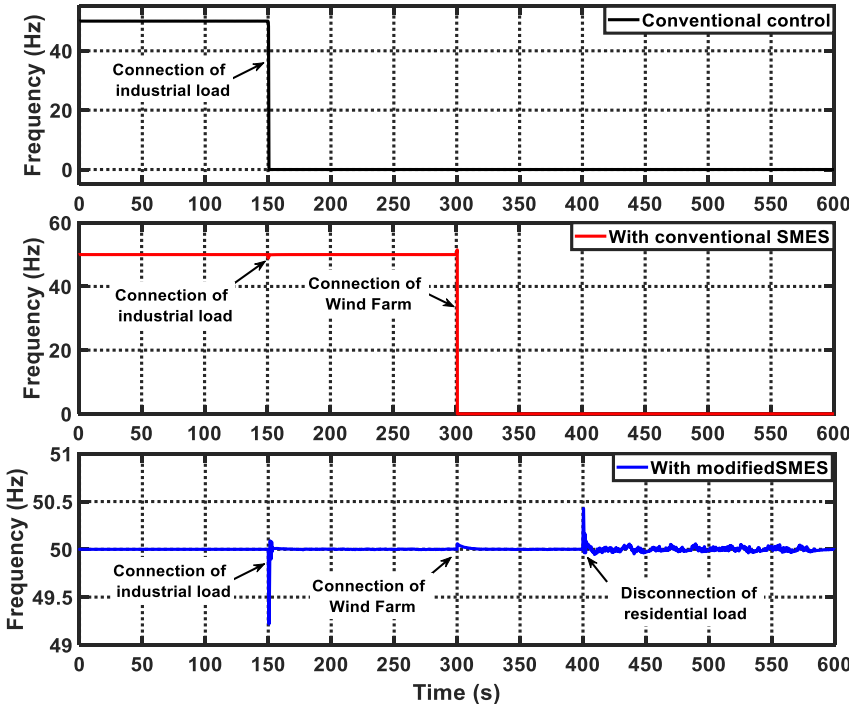

Fig. 6.27. The frequency response of the EPS for scenario C (35% of default system inertia)

6.8 Summary

The novel coordination of optimal LFC using PID controller-based MSA and the contribution of SMES technology (i.e. auxiliary LFC) proved a robust performance in the large-scale power system such as the EPS in this chapter as well as the MG systems in chapters four and five. This coordination enhanced the frequency stability of the realistic hybrid EPS concerning high RERs penetration as a future planning for Egypt electrical network. The EPS is decomposed into three subsystems; non-reheat, reheat and hydropower plants with inherent nonlinearities considering RERs. Furthermore, the frequency control based on the new optimal LFC using the new swarm intelligence technique with coordination of the digital protection scheme achieved an effective performance for maintaining the EPS frequency and enhanced its dynamic security due to the superiority of the digital OUFR in terms of accuracy and sensitivity and wide range controlling. Finally, the utilizing of SMES based-optimal PID controller solved the interference problem between the frequency control and the OUFR protection scheme by damping the frequency fluctuations quickly. While the LFC and conventional SMES need to readjust the setting of the OUFR in some cases to avoid the mal-operation.

Chapter 7

Conclusion and Future Work

7.1 Conclusions

The integration of renewable energy resources (RERs) with increased penetration has been of extreme interest to the engineers and power system operators for a while now. However, the grid integration of large RERs and the continuous load disturbances in power system especially in islanded MGs can pose the adverse impacts on several significant ways, such as changing the fault current levels and directions, transient voltage and frequency stability, the protection coordination, power leveling, and energy balancing. Furthermore, the system inertia might not stable and cannot maintain the frequency deviations within the acceptable limits, leading to weakening of the MG, which threaten the system security. To protect the network from threats related to these issues, this dissertation has proposed firstly the utilization of RSFCL in MG system with RERs integration, aimed to mitigate the effects of RERs penetration by reducing the fault current value during fault periods. Consequently, enhancement of the LVRT capability of RERs. Secondly, this thesis has developed an intelligent control technique, which is based on new swarm intelligence called moth swarm algorithm (MSA). This is to determine the optimal LFC coordinated with the SMES technology (i.e. auxiliary LFC) based- a new optimal PID to enhance the frequency stability of small and large scale of power systems concerning high RERs penetration, violence load variations, and system uncertainties. The modified SMES based on optimal PID controller has compared with the optimal LFC with/without the effect of conventional SMES.

Finally, a new coordination of optimal LFC based-new optimal PID controller and digital protection scheme in the presence of SMES has been developed to improve the MG dynamic security particularly, in the cases of a large generation loss disturbance, high integration levels of RERs or natural disasters. In these cases, the conventional power reserve may not be enough to return the stable condition of the system frequency, the emergency control and protection schemes plan should be followed, such as over/under frequency load shedding must be used to restore the system frequency. This part utilizes the digital OUFR, which operates for both conditions of over and under frequencies to trip necessary generations or loads after the failure of the combined response of the primary and secondary controls to avoid market failure and to

stop further frequency decline. Then, the effect of SMES device integration on this coordination has been presented to improve the dynamic security of the MG system.

In this thesis, different aspects related to the design, optimization, implementation, protection, and energy management of MGs with RERs are presented. The research performed in this thesis work includes the followings:

I) An introduction to the essential needs and benefits of the RERs is presented. Moreover, the weaknesses and threats regarding the penetration of RERs into MGs including instability, protection coordination, energy balancing, malfunction operation of LVRT, reduction of network inertia are highlighted. In addition, problem definition, research motivations, and thesis outlines are introduced as well (Chapter 1).

II) A deep literature review of the RERs impacts and problems, the role of superconducting power devices such as SFCL and SMES, LFC in power system and intelligent techniques of LFC in MG systems have been introduced (Chapter 2).

III) Presenting the application and accurate mathematical electro-thermal derivations of the optimized resistive superconducting fault current limiter (RSFCL) to limit the negative impact of RERs integration. Moreover, the RSFCL can protect the DFIG-based wind turbine from tripping during faults by enhancing the LVRT of the wind generators as it can limit the grid current during the fault and minimize the voltage reduction at the generator terminal, leading to a compliance with international grid codes. Furthermore, it decreased the activation of the conventional control scheme for the wind power generator. The performance of RSFCL is validated by comparing with a conventional method such as crowbar technique. Therefore, it has been demonstrated that the RSFCL can be a promising solution for improving the wind turbine controller performance with respect to the dc-link fluctuations and the extreme loads on the wind (Chapter 3).

IV) The fluctuation due to the high penetration of wind and PV generations is another challenge due to the integration of RERs. This problem could not be solved by the SFCL integrating. Hence, an intelligent coordination control technique based on optimal PID controller based-MSA technique to obtain a rapid response of the SMES system to stabilize the RERs fluctuations and hence smooth the output power. The SMES based-optimal PID is tested under large disturbances such as extreme wind speed variations and abrupt load change. The proposed method has been compared with the conventional PI and PID controllers. It showed better performance than the PI and PID controllers in terms of overshoot, undershoot, and response speed for charge/discharge operations of SMES (Chapter 4).

V) A robust coordination strategy of optimal LFC with a digital protection scheme in the presence of SMES has been proposed for protecting the MG during very large disturbances, which are called emergency cases. In these cases, the conventional power reserve may not be enough to return the stable condition of the system frequency. Therefore, the emergency control and protection schemes plan should be followed (Chapter 5).

VI) The intelligent optimal LFC based on new MSA technique, SMES based on the signal from the new optimal controller, and the coordination with the digital OUFR have been designed and investigated on a large power system such as the EPS for validation. The results proved that the proposed techniques show a better suitable performance than the conventional methods to manage high levels of uncertainty (Chapter 6).

It is concluded that the proposed optimized RSFCL can be a promising solution to enhance the stability of MG systems during faults. Furthermore, the application of the RSFCL, in providing an additional LVRT support to the DFIG-based wind turbine. On the other side, the SMES linearized model as a frequency controller based on the optimal PID controller as the main MG system controller succeeded to enhance the MG performance without the need to design a special controller for SMES. According to the general scheme of MG with the LFC model, both violence load change and output power of RERs are considered as ΔP. Therefore, the proposed coordination can be used in different configurations of MG systems, including different loads, RERs and grid topologies. This has shown the credibility to implement the proposed coordination in real the power system.

7.2 Future Scopes

The following investigations are recommended for future research based on the results presented in this thesis work: -

- This thesis suggests to determine the recovery period of the RSFCL and take it into consideration for the potential applications, particularly in RERs integrations.
- Study the coordination between the optimized RSFCL and existing protection schemes as an extension for this thesis.
- Testing the RSFCL for power system application utilizing the recently discovered second generation superconducting materials such as Magnesium diboride (MgB2) for reducing the cost.

- In this thesis, the islanded MG is based on two RERs, i.e. wind energy source, and Solar PV energy source. In the power industry, many other types of renewable energies, for example, Tide power is also receiving increasing interest, so in the future may be to integrate more renewable energy sources and design the corresponding solution.
- Comparing the proposed coordination strategy with other intelligent control techniques such as the adaptive neuro-fuzzy interference system (ANFIS) and Model predictive control (MPC) in different scale power systems to see the best control type of SMES for improving the power system stability and reliability.
- Performing a detailed comparison between SMES and other types of ESSs on different power systems to see the merits and demerits of each type.
- Design a multistage digital OUFR for multi-operations in islanded MG for more security improvement such as load shedding and tripping generation units.
- Enhancement the MG dynamic security utilizing an adaptive protection system based on other digital protection relays such as a digital differential relay, digital overcurrent relay, digital negative sequence relay, digital reverse power relay, and digital distance relay with the coordination of LFC techniques.
- Integrating the digital OUFR with other intelligent electronic devices (IEDs) into all-digital substation system.
- This research work can also be extended in the future by incorporating advanced hybrid intelligent algorithms to achieve more robustness for LFC in MG systems.

APPENDIX (A): RSFCL Modeling

A.1 DEVELOPED ROUTINES FOR SIMULINK

The block diagram by which the entire RSFCL with a shunt resistance was modelled is shown in Fig. A.1. The model is connected to the system as a controlled voltage source, where its value depending on the total resistance (the parallel connection of the SC film and the shunt resistance) and the current value.

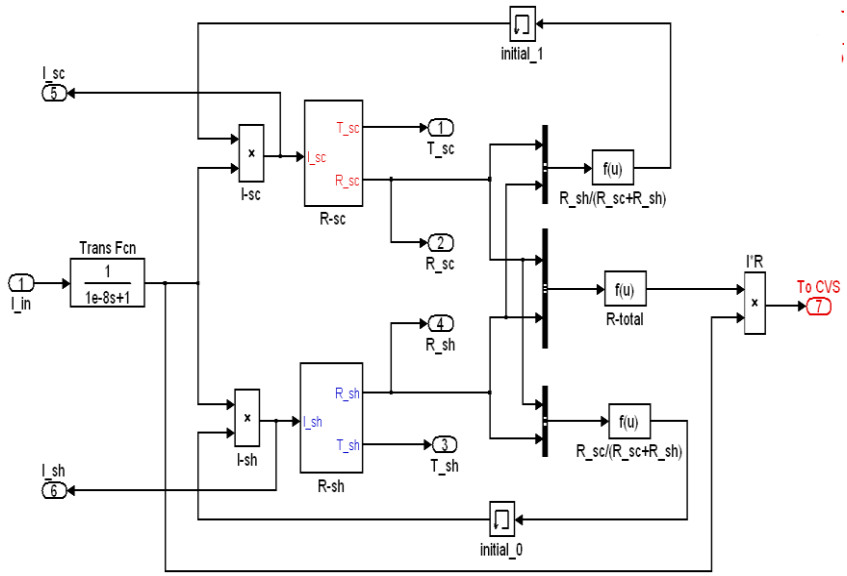

Fig. A.1 – Modeling of the RSFCL with shunt resistance

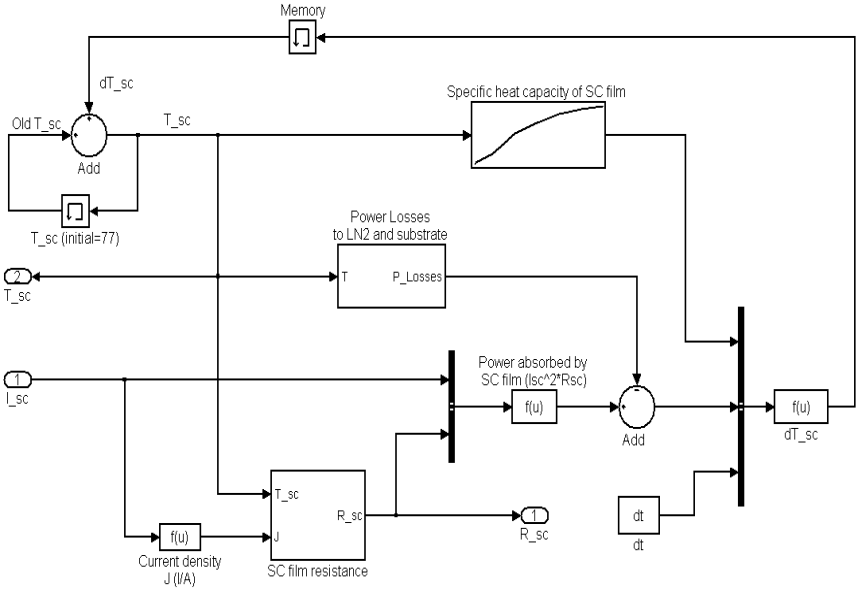

Fig. A.2 – Modeling of the R_{sc} block

Modeling of the "R_{sc}" block is shown in Fig. A.2. Figs. A.3 – A.8 show the details of the "R_{sc}" block. Fig. A.9 shows the "R_{sh}" block model. In three phase systems, a RSFCL is connected to each phase as shown in Fig. A.10.

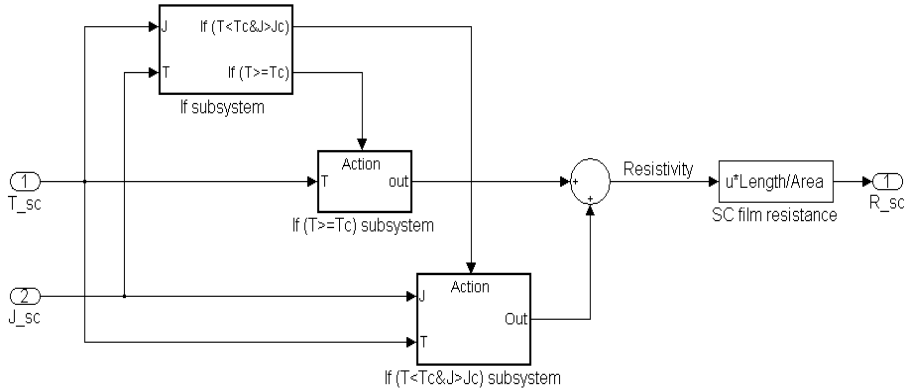

Fig. A.3 – Modeling of the "SC film resistance" block shown in Fig. A.2

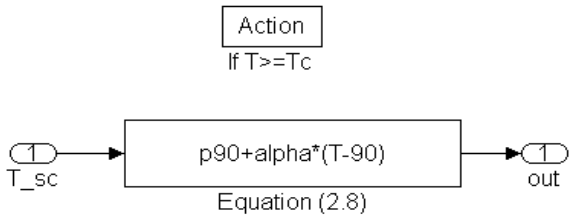

Fig. A.4 – Modeling of the "If ($T >= T_c$) subsystem" block shown in Fig. A.3

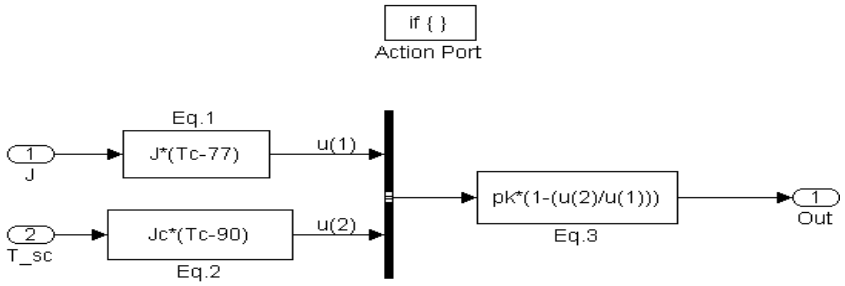

Fig. A.5 – Modeling of the "If ($T < T_c$ & $J > J_c$) subsystem" block shown in Fig. A.3

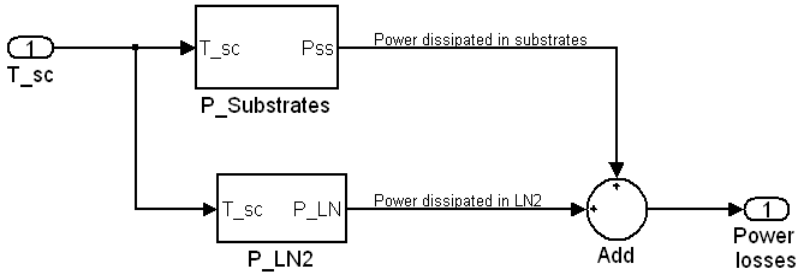

Fig. A.6 – Modeling of the "Power Losses" block shown in Fig. A.2

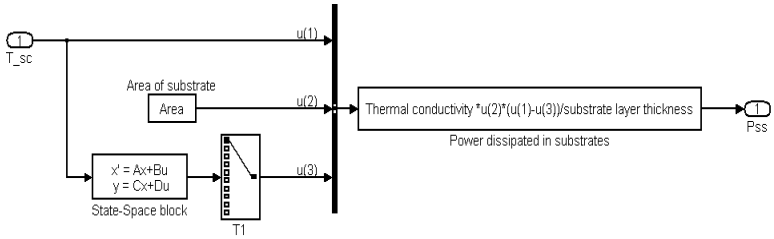

Fig. A.7 - Modeling of the "P_Substrates" block shown in Fig. A.5

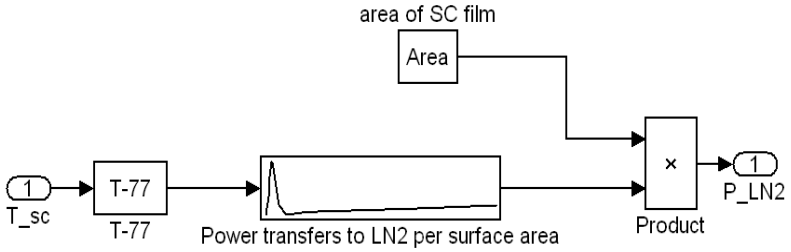

Fig. A.8 - Modeling of the "P_LN" block shown in Fig. A.5

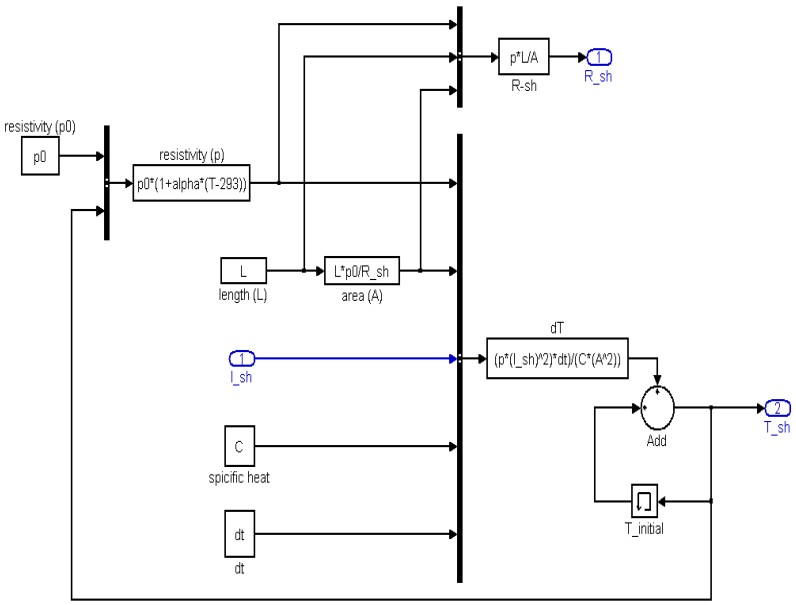

Fig. A.9 – Modeling of the "R-sh" block shown in Fig. A.2

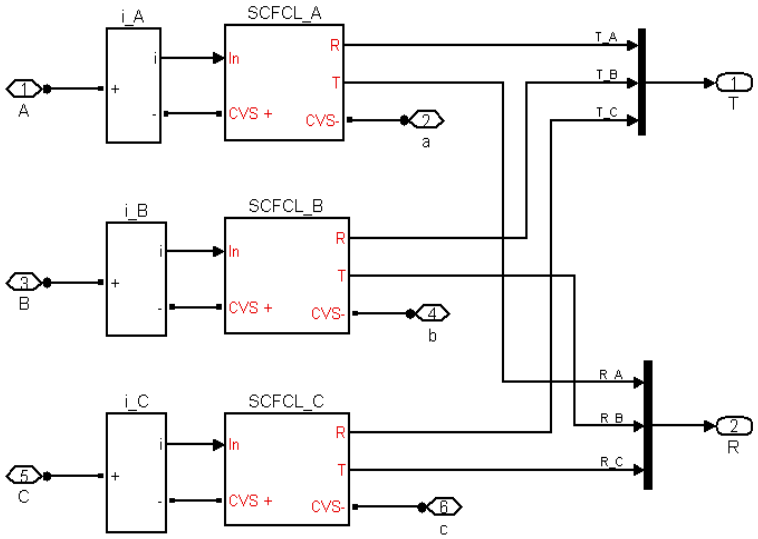

Fig. A.10 – Connection of RSFCL unit in three phase circuits

Table A.1 SC material parameters for RSFCL

Material of SC film	**BI-2212**
Critical current density (J_c) at self field	3×10^6 A/cm^2 at 77K
Critical temperature, T_c	90 K
Sample cross-sectional area	4×10^{-6} cm^2
Cooling liquid	LN2

Table A.2 DFIG parameters

DFIG parameters	
Rated power (MW)	1.5
Rated voltage (V)	575
Rated frequency (Hz)	60
Stator resistance (pu)	0.004843
Rotor resistance (pu)	0.004377
Stator leakage inductance (pu)	0.1248
Rotor leakage inductance (pu)	0.1791
Mutual inductance (pu)	6.77
Transmission line parameters	
Positive sequence resistance (ohm/km)	0.1153
Zero sequence resistance (ohm/km)	0.413
Positive sequence inductance (H/km)	0.00105
Zero sequence inductance (H/km)	0.00332
Positive sequence capacitance (F/km)	11.33e-9
Zero sequence capacitance (F/km)	5.01e-9
Transformer(T1) parameter (Rated power MVA)	12
Impedance (pu)	0.0017+j0.05
Transformer(T2) parameter (Rated power MVA)	47
Impedance (pu)	0.00534+j0.16

APPENDIX (B): Moth Swarm Algorithm (MSA)

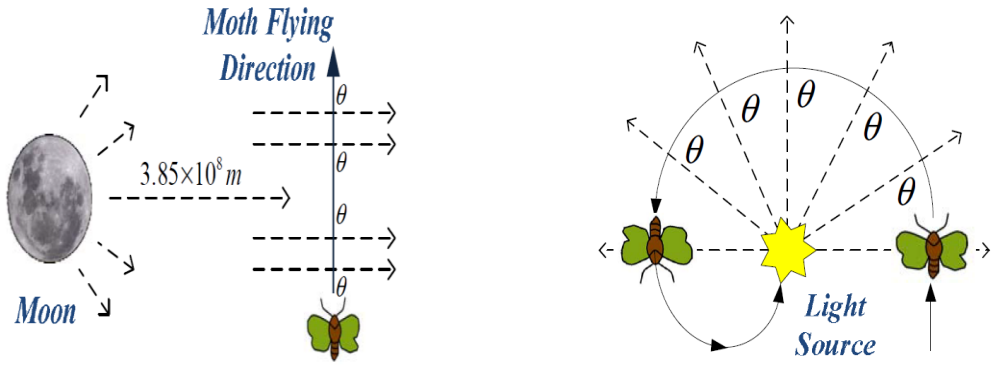

Fig. B.1 Orientation behavior of moth swarm: (a) Moth flying in a spiral path into nearby light source (b) Moth flying in a fixed angle relative to moonlight.

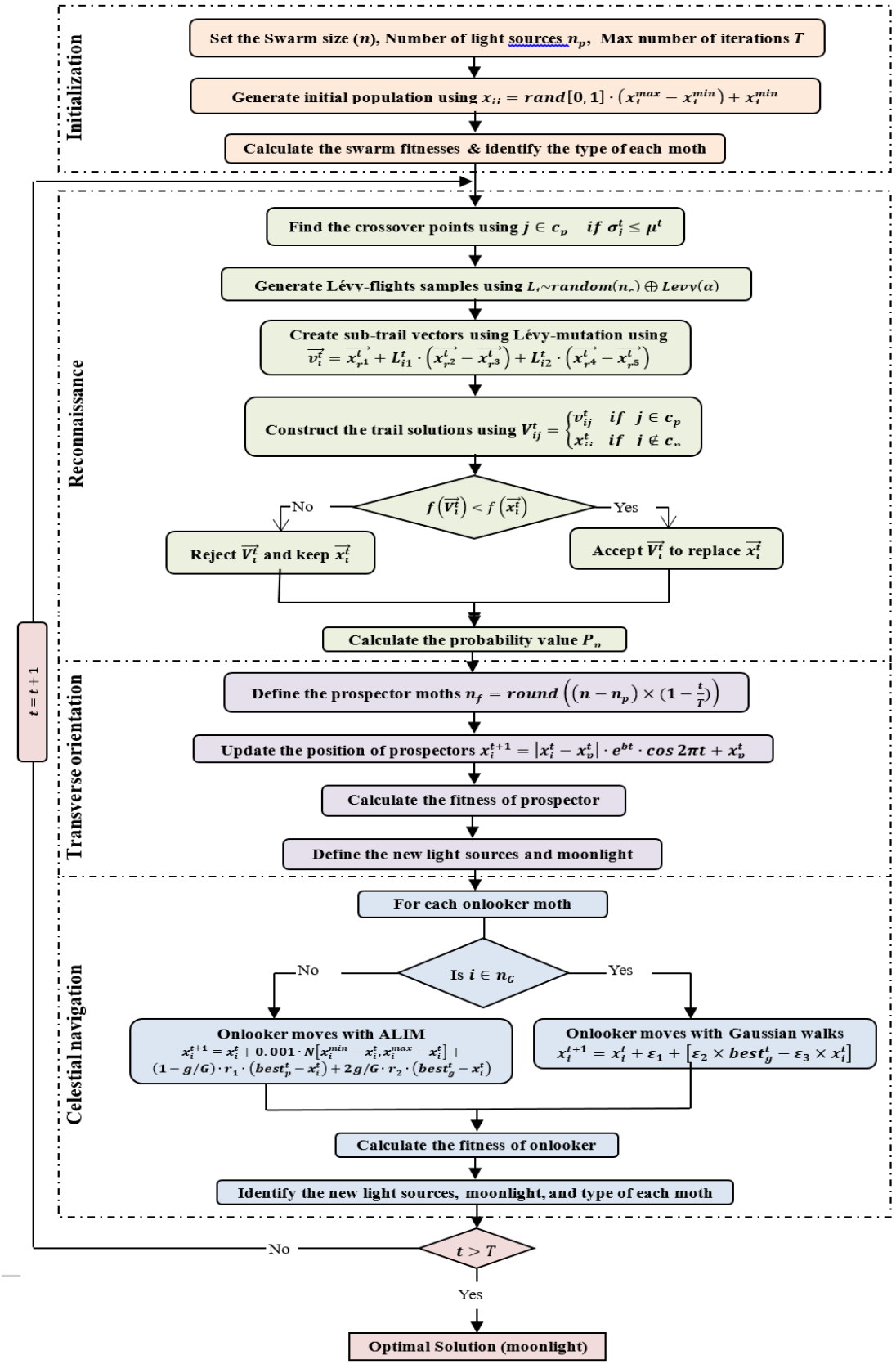

Fig. B.2-Flowchart of MSA

List of Publications

Technical Journal and Transaction

1. **Emad A. Mohamed**, Yaser Qudaih, Yasunori Mitani and Mohamed Ebeed "Study the Different effects of SFCL and Outer Crowbar on Fault Ride-through Capability Enhancement of Wind Farms", *Energy Procedia*, Elsevier, Volume 100, PP.127–136, 2016.

2. **Emad A. Mohamed** and Yasunori Mitani "LFC enhancement of islanded micro-grid considering high wind power penetration using superconducting magnetic energy storage and optimal controller" *Wind Engineering Journal*, 2019.

   DOI: 10.1177/0309524X18824533

3. **Emad A. Mohamed**, Gaber Magdy, Gaber Shabib, Adel Abdel Baset, Yasunori Mitani, "Digital Coordination Strategy of Protection and Frequency Stability for an Islanded Microgrid", *IET Generation, Transmission & Distribution*, Vol. 12, No. 15, pp. 3637-3646, 2018.

4. **Emad A. Mohamed**, Gaber Magdy, Gaber Shabib, Adel Abdel Baset, Yasunori Mitani, "Frequency Stability and Digital Protection Coordination of Multi-Source Power System.", *International Journal of Smart Grid and Clean Energy (SGCE)*, Vol. 7, No. 4, pp. 240-251, 2018.

5. **Emad A. Mohamed**, Eid Gouda, Yasunori Mitani "Impact of SMES integration on the digital frequency relay operation considering High PV/Wind penetration in micro-grid", *Energy Procedia*, Elsevier, Volume 157C, pp. 1292-1304, 2019.

6. **Emad A. Mohamed** and Yasunori Mitani "Enhancement the Dynamic Performance of Islanded Microgrid Using a Coordination of Frequency Control and Digital Protection" *International Journal of Emerging Electric Power Systems*, Vol. 20, No. 1, 2019.

7. Gaber Magdy, **Emad A. Mohamed**, Gaber Shabib, Adel Abdel Baset, Yasunori Mitani "SMES Based a New PID Controller for Frequency Stability of a Real Hybrid Power System Considering High Wind Power Penetration", *IET Renewable Power Generation*, Vol. 12, No. 11, pp. 1304-1313, 2018.

8. Gaber Magdy, **Emad A. Mohamed**, Gaber Shabib, Adel Abdel Baset, Yasunori Mitani, "Microgrid Dynamic Security Considering High Penetration of Renewable Energy", *International Journal of Protection and Control of Modern Power Systems*, Springer, Vol. 3, No. 1, pp. 11-23, 2018.

9. **Emad A. Mohamed**, Al-Attar A. Mohamed, Thongchart Kerdphol, Yasunori Mitani, "Optimization of Reactive Compensation in Distribution Networks Based on Moth Swarm Intelligence for Multi-Load Levels", *International Review of Electrical Engineering*, Vol. 12 (4), pp. 342-352, 2017.

International Conferences

1. **Emad A. Mohamed**, Yaser Qudaih, Yasunori Mitani, "Power system stability improvement using STATCOM and RSFCL during grid faults", *IEEE 19th International Conference on Electrical Machines and Systems (ICEMS)*, pp.1-6, Chiba, Japan, November 2016.

2. **Emad A. Mohamed**, Gaber Magdy, Gaber Shabib, Adel Abdel Baset, Yasunori Mitani, "Coordination of Optimal LFC and Digital Frequency Relay for Multi-Source Power System in Egypt", *IEEE International Conference on Electrical Energy systems (ICEES)*, Chennai, India, February 2018.

3. **Emad A. Mohamed**, Sayed M. Said, Bálint Hartmann, Yasunori Mitani, "An Efficient Fuzzy Logic Controlled-SMES for Isolated-Microgrid System Considering High Wind Power Penetration", *IEEE International Conference on Electric Power and Energy Conversion Systems (EPECS)*, Kitakyushu, Japan, April 2018.

4. **Emad A. Mohamed**, Gaber Magdy, Yasunori Mitani, "Digital Frequency Protection for Micro-Grid Coordinated with LFC Considering High PV/Wind Penetration Level", *IEEE International Istanbul Smart Grids and Cities Congress and Fair (ICSG)*, Istanbul, Turkey, April 2018.

5. Gaber Magdy, **Emad A. Mohamed**, Gaber Shabib, Adel Abdel Baset, Yasunori Mitani, "A Novel Optimal Load Frequency Control Based on Moth Swarm Algorithm with Dynamic Contribution of SMES", *IEEE International Conference on Electrical, Electronics, Communication, Mechanical and Computing (EECCMC)*, Tamil Nadu, India, January 2018.

6. Gaber Magdy, **Emad A. Mohamed**, Gaber Shabib, Adel Abdel Baset, Yasunori Mitani, "Enhancement LFC of a Realistic Multi-Source Power System Concerning Wind Farms Using SMES and New Optimized PID Controller", *IEEE International Conference on Electric Power and Energy Conversion Systems (EPECS)*, Kitakyushu, Japan, April 2018.

Biography of the Author

The author received the B.Eng. with a first class honors and M.Sc. degree in electrical power engineering from Aswan University, Aswan, Egypt in 2005 and 2013, respectively. He is working as an Assistant Lecture in the Department of Electrical Engineering, Aswan Faculty of Engineering, Aswan University, Aswan, Egypt. Currently, he is a Ph.D. student in kyushu Institute of Technology (KIT), Japan. He was in a Master Mobility scholarship at Faculté des Sciences et Technologies - Université de Lorraine, France. The scholarship sponsored by FFEEBB ERASMUS MUNDUS. His research interests are applications of superconducting power devices in power systems, power system stability and protection, and renewable energy issues.

References

1. T. Mai, R. Wiser, D. Sandor, and G. Brinkman, “Renewable electricity futures study volume 1: Exploration of high-penetration renewable electricity futures,” NREL, 2012.

2. Y. C. Chen and A. D. Garcia, “A method to study the effect of renewable resource variability on power system dynamics,” IEEE Transaction Power Systems, vol. 27, no. 4, pp. 1978–1989, 2012.

3. D. Gautam, V. Vittal, and T. Harbour, “Impact of increased penetration of DFIG-based wind turbine generators on transient and small signal stability of power systems,” IEEE Transaction Power Systems, vol. 24, no. 3, pp. 1426–1434, 2009.

4. Mamatha Sandhu, Tilak Thakur, “Issues, Challenges, Causes, Impacts, and utilization of Renewable Energy Sources -Grid Integration” Int. Journal of Engineering Research and Applications., Vol. 4, Issue 3, March 2014, pp. 636-643.

5. R. Teodorescu, M. Liserre, and P. Rodriguez, Grid converters for photovoltaic and wind power systems. [Piscataway, N.J.] : Chichester, West Sussex ; Hoboken, N.J: IEEE ; Wiley, 2011.

6. REN21—Renewables 2016 Global Status Report, 2015. [Online]. Available: http://www.ren21.net/status-of-renewables/global-status-report/.

7. H. Polinder, J. A. Ferreira, B. B. Jensen, A. B. Abrahamsen, K. Atallah, and R. A. McMahon, “Trends in wind turbine generator systems,” IEEE J. Emerg. Sel. Top. Power Electron., vol. 1, no. 3, pp. 174–185, Sep. 2013.

8. M. Aly, E. M. Ahmed, and M. Shoyama, “Thermal and reliability assessment for wind energy systems with D-STATCOM functionality in resilient microgrids,” IEEE Trans. Sustain. Energy, vol. PP, no. 99, pp. 1–1, Dec. 2016.

9. M. Mosa, H. Abu Rub, M. E. Ahmed, and J. Rodriguez, “Modified MPPT with using model predictive control for a multilevel boost converter,” in Proc. IEEE IECON, pp. 5080–5085, 2012.

10. M. E. Ahmed, M. Mousa, and M. Orabi, “Development of high gain and efficiency photovoltaic system using multilevel boost converter topology,” Proc. IEEE PEDG, pp. 898–903, 2010.

11. M. Mohseni and S. M. Islam, “Review of international grid codes for wind power integration: Diversity, technology and a case for global,” Renewable and Sustainable Energy Reviews, vol. 16, no. 1, pp. 3876–3890, 2012.

12. J. Enslin, “Grid impacts and solutions of renewables at high penetration levels,” QUANTA Technology, 2009.

13. Department of Trade and Industry: ‘The energy challenge energy review report’ (DTI, London, 2006).

14. Bevrani, H., Watanabe, M., Mitani, Y.: 'Power System Monitoring and Control' (New Jersey, USA, 2014, John Wiley & Sons)

15. M. Singh and S. Santoso, “Dynamic models for wind turbines and wind power plants”, National Renewable Energy Laboratory, Austin, Texas, 2011.

16. A. H. Moghadasi, A. Islam, and M. Amini, “LVRT capability assessment of FSIG-based wind turbine utilizing UPQC and SFCL,” PES General Meeting, Conference Exposition, IEEE, pp. 1–5, 2014.

17. K. H. Kim, Y. C. Jeung, D. C. Lee, and H. G. Kim, “LVRT scheme of PMSG wind power systems based on feedback linearization,” IEEE Transactions on Power Electronics, vol. 27, no. 5, pp. 2376–2384, 2012.

18. W. Qiao, G. Venayagamoorthy, and R. Harley, “Real-time implementation of a STATCOM on a wind farm equipped with doubly fed induction generators,” IEEE Transactions on Industry Applications, vol. 45, no. 1, pp. 98–107, 2009.

19. W. Qiao, R. G. Harley, and G. K. Venayagamoorthy, “Coordinated reactive power control of a large wind farm and a STATCOM using heuristic dynamic programming,” IEEE Transactions on Energy Conversion, vol. 24, no. 2, pp. 493–503, 2009.

20. Sergey Karabanov, Yury Kukhmistrov, Bogdan Miedzinski, and Zenon Okraszewski, “Photovoltaic systems”, IEEE, Modern Electric Power Systems (MEPS), Proceedings of the International Symposium, September 2010.

21. IRENA- Istrian regional energy agency, “photovoltaic systems”, Rijeka, January 2012.

22. A. Soundarrajan, S. Sumathi, and G. Sivamurugan, “Voltage and frequency control in power generating system using hybrid evolutionary algorithms”, Journal of Vibration and Control: 1077546311404731, 2011.

23. I. 62271-100: “High-voltage switchgear and control gear - part 100: Alternating current circuit-breakers,” Apr. 2008.

24. P. Bousseau, E. Gautier, I. Garzulino, P. Juston, and R. Belhomme, “Grid impact of different technologies of wind turbine generator systems (WTGS),” (Madrid), June 2003.

25. https://www.occto.or.jp/en/pressrelease/2018/180919_hokkaidoearthquake_investigation.html

26. P. Kundur, N.J. Balu, and M.G. Lauby, Power system stability and control. EPRI power system engineering series. McGraw-Hill, 1994. ISBN 9780070359581.

27. P. Kundur, J. Paserba, V. Ajjarapu, G. Andersson, A. Bose, C. Canizares, N. Hatziargyriou, D. Hill, A. Stankovic, C. Taylor, T. V. Cutsem, and V. Vittal, “Definition and classification of power system stability IEEE/CIGRE joint task force on stability terms and definitions,” IEEE Trans. Power Syst. , vol. 19, no. 3, p. 13871401, Aug. 2004.

28. Caixia Wang, James D. McCalley. Impact of wind power on control performance standards. Electrical Power and Energy Systems, 47: 225–234, 2013.

29. N.EL.Y. Kouba, M. Menaa, M. Hasni, M. Boudour. Load Frequency Control in Multi-Area Power System Based on Fuzzy Logic-PID Controller. IEEE, International Conference on Smart Energy Grid Engineering, SEGE’15, UOIT, Oshawa, Canada, August 17-19, pp: 1-6, 2015.

30. N.EL.Y.Kouba, M.Menaa, M.Hasni, B. Boussahoua, M. Boudour. Optimal load frequency control based on hybrid bacterial foraging and particle swarm optimization. IEEE, 11th International Multi-Conference on Systems, Signals & Devices (SSD-PES) Barcelona, Spain; 1-6, 2014.

31. Pieter Tielens, and Dirk Van Hertem, “Grid inertia and frequency control in power systems with high penetration of renewables”, 2012.

32. P. Moutis, S. A. Papathanassiou, and N. D. Hatziargyriou, “Improved load-frequency control contribution of variable speed variable pitch wind generators,” Renewable Energy, vol. 48, pp. 514–523, 2012.

33. B. Hoseinzadeh, F. F. Silva, and C. L. Bak, “Coordination of voltage and frequency feedback in load-frequency control capability of a wind turbine,” IEEE Industrial Electronics Society, IECON14, pp. 5501–5507, 2014.

34. G. Lalor, A. Mullane, and M. O’Malley, “Frequency control and wind turbine technologies,” Power Systems, IEEE Transactions on, vol. 20, no. 4, pp. 1905–1913, 2005.

35. G. Ramtharan, N. Jenkins, and J. Ekanayake, “Frequency support from doubly fed induction generator wind turbines,” IET Renewable Power Generation, vol. 1, no. 1, pp. 3–9, 2007.

36. J. Morren, S. W. de Haan, W. L. Kling, and J. Ferreira, “Wind turbines emulating inertia and supporting primary frequency control,” Power Systems, IEEE Transactions on, vol. 21, no. 1, pp. 433–434, 2006.

37. Z.-S. Zhang, Y.-Z. Sun, J. Lin, and G.-J. Li, “Coordinated frequency regulation by doubly fed induction generator-based wind power plants,” Renewable Power Generation, IET, vol. 6, no. 1, pp. 38–47, 2012.

38. D. Gautam, L. Goel, R. Ayyanar, V. Vittal, and T. Harbour, “Control strategy to mitigate the impact of reduced inertia due to doubly fed induction generators on large power systems,” Power Systems, IEEE Transactions on, vol. 26, no. 1, pp. 214–224, 2011.

39. E. Vittal, M. O’Malley, and A. Keane, “A steady-state voltage stability analysis of power systems with high penetrations of wind,” Power Systems, IEEE Transactions on, vol. 25, no. 1, pp. 433–442, 2010.

40. N. R. Ullah, T. Thiringer, and D. Karlsson, “Voltage and transient stability support by wind farms complying with thee. on netz grid code,” Power Systems, IEEE Transactions on, vol. 22, no. 4, pp. 1647–1656, 2007.

41. E. Vittal, M. O’Malley, and A. Keane, “Rotor angle stability with high penetrations of wind generation,” Power Systems, IEEE Transactions on, vol. 27, no. 1, pp. 353–362, 2012.

42. A. Zertek, G. Verbic, and M. Pantos, “A novel strategy for variable-speed wind turbines’ participation in primary frequency control,” Sustainable Energy, IEEE Transactions on, vol. 3, no. 4, pp. 791–799, 2012.

43. IEEE, “Ieee guide for the application of protective relays used for abnormal frequency load shedding and restoration,” IEEE Std C37.117-2007, Power System Relaying Committee, pp. 1–43, 2007.

44. B. Hoseinzadeh, F. F. Silva, and C. L. Bak, “Decentralized & adaptive load-frequency control scheme of variable speed wind turbines,” The 13th International Workshop on Large-Scale Integration of Wind Power into Power Systems as well as on Transmission Networks for Offshore Wind Power Plants, pp. 747–753, 2014.

45. Hadi, Azah, Hussain and Marjan. Impact of distributed generations on power system protection performance. International Journal of the Physical Sciences Vol. 6(16), pp. 3999-4007, 18 August 2011.

46. Barbier C., Maloyd A. and Putrus G. Embedded controller for LV network with distributed generation. (K/EL/00334/00/REP). UK: Department of Trade and Industry (DTI), 2007.

47. M. T. Doyle, "Reviewing the impacts of distributed generation on distribution system protection," in IEEE Power Engineering Society Summer Meeting, 2002, Chicago, USA, pp. 103-105, 21-25 July 2002.

48. X. Zhen, S. Quanli, S. Haihua, Z. Xing, and Y. Shuying, "High voltage ride through control strategy of doubly fed induction wind generators based on active resistance," in 7th International Power Electronics and Motion Control Conference (IPEMC), 2012, Harbin, China, pp. 2193-2196, 02-05 June 2012.

49. X. Zhen, S. Quanli, S. Haihua, Z. Xing, and Y. Shuying, "High voltage ride through control strategy of doubly fed induction wind generators based on active resistance," in 7th International Power Electronics and Motion Control Conference (IPEMC), 2012, Harbin, China, pp. 2193-2196, 02-05 June 2012.

50. C. Marnay, H. Aki, K. Hirose, A. Kwasinski, S. Ogura and T. Shinji, How two microgrid fared after the 2011 earthquake, IEEE Power Energy Magazine, 13(3), 44-57, 2015.

51. L. Xuan and S. Bin, "Microgrids - an integration of renewable energy technologies," in Electricity Distribution. CICED. China International Conference on, pp. 1-7, 2008.

52. H. Beverani, Y. Mitani, and Y. Watanabe, Power System Monitoring and Control. John Wiley & Sons, New York, Chapter 9, 187-206, 2014.

53. H. Beverani, Y. Mitani, and Y. Watanabe, Microgrid controls. In: H. Wayne Beaty, editor, Standard Handbook for Electrical Engineers, 16th edn, McGraw-Hill, New York, Section 16.9, 159-176, 2013.

54. H. Beverani, and T. Hiyama, Automatic generation control (AGC): fundamentals and concepts. Intelligent Automatic Generation Control, CRC Press, New York, Chapter 2, 11-36, 2011.

55. Ali Khademlahashy, Li Li, Jeremy Every, Jianguo Zhu, "A Review on Protection Issues in Micro-Grids Embedded with Distribution Generations," 12th IEEE Conference on Industrial Electronics and Applications (ICIEA), Siem Reap, Cambodia, 2017.

56. M.Khederzadehi and H.Maleki,“Frequency Control of Microgrids in Autonomous Mode by a Novel Control Scheme Based on Droop Characteristics”. Electric Power Components and Systems, 41:16–30, 2013.

57. A. Arulampalam, M. Barnes, A. Engler, A. Goodwin, and N. Jenkins, Control of power electronic interfaces in distributed generation Microgrids, 2004.

58. Electrical Energy Storage project team, “Electrical energy storage”, International Electrotechnical Commission, IEC, Geneva, Switzerland, 2011.

59. W. Xian, Y. Weijia, Y. Yan and T. A. Coombs, “Minimize frequency fluctuations of the isolated system with wind farm by using power superconducting magnetic energy storage”, International Conference on Power Electronics and Drive Systems (PEDS), Taipei, November 2009.

60. W. Buckles and W. Hassenzahl, “Superconducting magnetic energy storage”, IEEE Power Eng. Rev., Vol. 20, No. 5, pp. 16–20, May 2000.

61. E. Handschin, and Th Stephanblome, “The impact of SC magnet energy storage on power system operation”, Handbook of Applied Superconductivity, Volume 2. Ed. Bernd Seeber. Taylor & Francis, pp. 1735-1756, 1998.

62. M. H. Ali, W. Bin, and R. A. Dougal, “An overview of SMES applications in power and energy systems”, IEEE Transactions on Sustainable Energy, Vol. 1, Issue: 1, pp. 38-47, April 2010.

63. R. W. Boom and H. A. Peterson, “Superconductive energy storage for power systems”, IEEE Transactions on Magnetics., Vol. MAG-8, No. 3, pp. 701–703, September 1972.

64. D. S. Padimiti and B. H. Chowdhury, “Superconducting magnetic energy storage system (SMES) for improved dynamic system performance”, Proc. IEEE Power Engineering Society General Meeting, Tampa, FL, pp. 1–6, 2007.

65. A. K. Kalafala, J. Bascunan, D. D. Bell, L. Blecher, F. S. Murray, M. B. Parizh, M. W. Sampson, and R. E. Wilcox, “Micro superconducting magnetic energy storage (SMES) system for protection of critical industrial and military loads”, IEEE Trans. Magnetics, Vol. 32, No. 4, pp. 2276–2279, July 1996.

66. http://www.climatetechwiki.org/technology/jiqweb-ee, last access on 14/05/2016. http://www.superpower-inc.com/content/superconducting-magnetic-energy-storage-smes, last access on 14/05/2016.

67. N. Koshizuka, F. Ishikawa, H. Nasu, M. Murakami, K. Matsunaga, S. Saito, O. Saito, Y. Nakamura, H. Yamamoto, R. Takahata, Y. Itoh, and M. Tomita, “Progress of superconducting bearing technologies for flywheel energy storage systems”, Physica C: Superconductivity, Vol. 386, pp. 444-450, April 2003.

68. M. Beaudin, H. Zareipour, A. Schellenberglabe, and W. Rosehart, “Energy storage for mitigating the variability of renewable electricity sources: An updated review”, Energy for Sustainable Development, Vol. 14, No. 4, pp. 302-314, December 2010.

69. A. Daneshi, N. Sadrmomtazi, H. Daneshi, and M. Khederzadeh, “Wind power integrated with compressed air energy storage”, IEEE International Conference on Power and Energy (PECON), Kuala Lumpur, pp. 634-639, November/December 2010.

70. Belwin, J., Raja, R.: 'A review on issues and approaches for microgrid protection', Journal of renewable and sustainable energy reviews, 67, pp. 988-997, 2017.

71. Bevrani, H., Watanabe, M., Mitani, Y.: 'Power System Monitoring and Control' (New Jersey, USA, 2014, John Wiley & Sons).

72. Rakhshani, E., Remon, D., Mir, A., et al.: 'Analysis of derivative control based virtual inertia in multi-area high-voltage direct current interconnected power systems', IET Gener. Trans. Distrib., 10 (6), pp. 1458-1469, 2016.

73. Bevrani, H., Ise, T., Miura, Y.: 'Virtual synchronous generators: A survey and new perspectives', Int. J. Elect. Power Energy Syst., 54, pp. 244-254, 2014.

74. Sortomme, E., Venkata S., Mitra, J.: 'Microgrid Protection Using Communication-Assisted Digital Relays', IEEE Trans. on Power Delivery, 25, (4), pp. 2789–2796, 2010.

75. Zamani, M., Sidhu, T., Yazdani, A.: 'A Protection Strategy and Microprocessor-Based Relay for Low-Voltage Micro-grids', IEEE Trans. on Power Delivery, 26, (3), pp. 1873–1883, 2011.

76. Keil, T., ager, J.: 'Advanced Coordination Method for Over-current Protection Relay Using Nonstandard Tripping Characteristics', IEEE Trans. on Power Delivery, 23, (1), pp. 52-57, 2008.

77. Brahma, S., Girgis, A.: 'Development of Adaptive Protection Scheme for Distribution Systems with High Penetration of Distributed Generation', IEEE Trans. on Power Delivery, 19, (1), pp. 56-63, 2004.

78. Juang, C.F., Lu, C.F, Load frequency control by hybrid evolutionary fuzzy PI-controller. IEE Proc. Gener. Transm. Distrib 153(2): 196–204, 2006.

79. Khuntia, S.R., Panda, S, Simulation study for automatic generation control of a multi-area power system by ANFIS approach’.Appl. Soft Comput 12: 333–341. 2012.

80. Yousel, H.A., Kharusi, K.A.L., Albadi, M.H., et al, Load frequency control of a multi-area power system: an adaptive fuzzy logic approach. IEEE Trans. Power Syst 29(4): 1822–1830, 2014.

81. Zeynelgil, H.L., Demiroren, A., Sengor, N.S, Load frequency controls for a power system with reheat steam turbine and governor dead band non-linearity by using neural network controller’, Eur. Trans. Electr. Power 12(3): 179–184, 2002.

82. Raheel Ali, Tarek Hasan Mohamed, Yaser Soliman Qudaih, Y. Mitani, A new load frequency control approach in an isolated small power system using coefficient diagram method. international journal Electrical Power and Energy Systems 56: 110-116, 2014.

83. Princess Garasi, Yaser Qudaih, Raheel Ali, Masayuki Watanabe, and Yasunori Mitani, Coefficient Diagram Method Based Load Frequency Control for a Modern Power System. Journal of Electronic Science and Technology 12(3): 270-276, 2014.

84. Mohamed T. H., H. Bevrani, A. A. Hassan, and T. Hiyama, Decentralized Model Predictive Based Load Frequency Control in an interconnected power system. Energy Convers Manage, 52 (1): 1208-1214, 2011.

85. Patil D.R et al Two area load frequency control with fuzzy gain scheduling of PI controller, parts 1 and 2. IEEE Trans. Sq’st., Man Cybern, 20(2).

86. Edimar J. Oliveira, Leonardo M. Honorio et.al, Linear Programming for Optimum PID Controller Tuning. Applied Mathematics 5: 886-897, 2014.

87. Pretty Neelam Topno, Saurabh Chanana, Load frequency control of a two-area multi-source power system using a tilt integral derivative controller. Journal of Vibration and Control, 241(1): 1–16, 2016.

88. Khodabakhshian A, M. Ezatabadi Pour, R. Hooshmand, Design of a robust load frequency control using sequential quadratic programming technique. Electrical Power and Energy Systems 40: 1–8, 2012.

89. Daneshfar, F., Bevrani, H, Load frequency control: GA-based multi-agent reinforcement learning. IET Gener. Transm. Distrib 4(1): 13–26, 2010.

90. Jiuqi Han, Peng Wang, Xin Yang, Tuning of PID Controller Based on Fruit Fly Optimization Algorithm. IEEE International Conference on Mechatronics and Automation 5 – 8, 2012.

91. Padhan, S., Sahu, R.K., Panda, S, Application of firefly algorithm for load frequency control of multi-area interconnected power system. Electr. Power Compon. Syst 42(13): 1–12, 2014.

92. Gozde, H., Taplamacioglu, M.C, Automatic generation control application with craziness based particle swarm optimization in a thermal power system. Int. J. Electr. Power Energy Syst 33(1): 8–16, 2010.

93. Mohamed T. H, J. Morel, H. Bevrani, and T. Hiyama, Model Predictive Based Load Frequency Control-Design Concerning Wind Turbines. International Journal of Electrical Power & Energy Systems 43(1): 859-867, 2012.

94. Praghnesh Bhatt, Ranjit Roy, S. P. Ghoshal, Dynamic Participation of Doubly Fed Induction Generator in Automatic Generation Control. Renewable Energy 6(1): 1203-1213, 2011.

95. Hasanien, H.M., El-Fergany, A.A, Symbiotic organisms search algorithm for automatic generation control of interconnected power systems including wind farms. IET Gener. Transm. Distrib 11, (7): 1692–1700, 2017.

96. H. Zhao, Q. Wu, S. Hu, H. Xu, and C. N. Rasmussen, “Review of energy storage system for wind power integration support,” Appl. Energy, vol. 137, pp. 545–553, Jan. 2015.

97. W. Wang, C. Mao, J. Lu, and D. Wang, “An Energy Storage System Sizing Method for Wind Power Integration,” Energies, vol. 6, no. 12, pp. 3392–3404, Jul. 2013.

98. S. Vazquez, S. M. Lukic, E. Galvan, L. G. Franquelo, and J. M. Carrasco, “Energy Storage Systems for Transport and Grid Applications,” IEEE Trans. Ind. Electron., vol. 57, no. 12, pp. 3881–3895, Dec. 2010.

99. Kyung Soo Kook, K. J. McKenzie, Yilu Liu, and S. Atcitty, “A study on applications of energy storage for the wind power operation in power systems,” IEEE Power Engineering Society General Meeting, p. 5, 2006 .

100. W. Li and G. Joos, “Comparison of Energy Storage System Technologies and Configurations in a Wind Farm,” in 2007 IEEE Power Electronics Specialists Conference, pp. 1280–1285, 2007.

101. M. Ding and J. Wu, “A Novel Control Strategy of Hybrid Energy Storage System for Wind Power Smoothing,” Electr. Power Components Syst., vol. 45, no. 12, pp. 1265–1274, Jul. 2017.

102. X. Tang, Y. Sun, G. Zhou, and F. Miao, “Coordinated Control of Multi-Type Energy Storage for Wind Power Fluctuation Suppression,” Energies, vol. 10, no. 12, p. 1212, Aug. 2017.

103. J.-S. Yang, J.-Y. Choi, G.-H. A Y.-J. Choi, M.-H. Kim, and D.-J. Won, “Optimal Scheduling and Real-Time State-of-Charge Management of Energy Storage System for Frequency Regulation,” Energies, vol. 9, no. 12, p. 1010, Nov. 2016.

104. J. Shi, W.-J. Lee, and X. Liu, “Generation Scheduling Optimization of Wind-Energy Storage System Based on Wind Power Output Fluctuation Features,” IEEE Trans. Ind. Appl., vol. 54, no. 1, pp. 10–17, Jan. 2018.

105. J. Dang, J. Seuss, L. Suneja, and R. G. Harley, “SoC Feedback Control for Wind and ESS Hybrid Power System Frequency Regulation,” IEEE J. Emerg. Sel. Top. Power Electron., vol. 2, no. 1, pp. 79–86, 2014.

106. J. Y. Yun, G. Yu, K. S. Kook, D. H. Rho, and B. H. Chang, “SOC-based Control Strategy of Battery Energy Storage System for Power System Frequency Regulation,” Trans. Korean Inst. Electr. Eng., vol. 63, no. 5, pp. 622–628, May 2014.

107. Pingping Xie, Yinhong Li, Lin Zhu, Dongyuan Shi, Xianzhong Duan, Supplementary automatic generation control using controllable energy storage in electric vehicle battery swapping stations. IET Gener. Transm. Distrib, 10(4): 1107-1116, 2016.

108. T. Kinjo, T. Senjyu, N. Urasaki, and H. Fujita, “Terminal-voltage and output-power regulation of wind-turbine generator by series and parallel compensation using SMES,” IEE Proc. - Gener. Transm. Distrib, vol. 153, no. 3, p. 276, 2006.

109. M. H. Ali, M. Park, I.-K. Yu, T. Murata, and J. Tamura, “Improvement of Wind-Generator Stability by Fuzzy-Logic-Controlled SMES,” IEEE Trans. Ind. Appl., vol. 45, no. 3, pp. 1045–1051, 2009.

110. P. Bhatt, S. P. Ghoshal, and R. Roy, “Coordinated control of TCPS and SMES for frequency regulation of interconnected restructured power systems with dynamic participation from DFIG based wind farm,” Renew. Energy, vol. 40, no. 1, pp. 40–50, Apr. 2012.

111. S. Said, M. Aly, and M. Abdel-Akher, “Application of Superconducting Magnetic Energy Storage (SMES) to Improve Transient Stability of Multi-Machine System with Wind Power Penetration,” 16th Int. Middle-East Power Syst., 2014.

112. M. M. Aly, M. Abdel-Akher, S. M. Said, and T. Senjyu, “A developed control strategy for mitigating wind power generation transients using superconducting magnetic energy storage with reactive power support,” Int. J. Electr. Power Energy Syst., vol. 83, pp. 485–494, Dec. 2016.

113. S. M. Said, M. M. Aly, and M. Abdel-Akher, “Application of superconducting magnetic energy storage (SMES) for voltage sag/swell suppression in the distribution system with wind power penetration,” in 2014 16th International Conference on Harmonics and Quality of Power (ICHQP), pp. 92–96, 2014.

114. Gaber El-Saady, Y. Mobarak, Mohamed A. A. Wahab, M. M. Hamada, Abdel-Moamen M., A. M. El-Noby, A New Robust Technique LFC of Multi-Area Power System using SMES. International Journal of Control, Automation, and Systems 2, pp. 56-60, 2013.

115. Lin Ye, LiangZhen Lin, and Klaus-Peter Juengst, “Application Studies of Superconducting Fault Current Limiters in Electric Power System,” IEEE Trans. on Applied Superconductivity, Vol. 12, No1, pp. 900−903, March 2002.

116. Thomas P.Sheahen, “Introduction to High-Temperature Superconductivity,” Plenum Press, New York, and London.

117. L. G. Meegahapola, T. Littler, and D. Flynn, “Decoupled-DFIG fault ride through strategy for enhanced stability performance during grid faults,” IEEE Trans. Sustain. Energy, vol. 1, pp. 152–162, Oct. 2010.

118. L. Yang, Z. Xu, J. Ostergaard, Z. Y. Dong, and K. P. Wong, “Advanced control strategy of DFIG wind turbines for power system fault ride through,” IEEE Trans. Power Syst., vol. 27, pp. 713–722, May 2012.

119. J. Vidal, G. Abad, J. Arza, and S. Aurt, “Single-phase DC Crowbar topologies for low voltage ride through the fulfillment of high power doubly fed induction generator-based wind turbines,” IEEE Trans. Energy Convers., vol. 28, no. 3, pp. 768–781, Sep. 2013.

120. Mohamed Ebeed, Omar NourEldeen, and A .A.Ebrahim, “Assessing Performance of Crowbar Protections with The DFIG under Grid Fault” International Journal on Power Engineering and Energy (IJPEE), Vol.4, No.2, April 2013.

121. S. M. Muyeen, M. A. Mannan, M. H. Ali, R. Takahashi, T. Murata, “Stabilization of wind turbine generator system by STATCOM,” IEEJ Trans. Power Energy, vol. 126, no. 10, pp. 1073–1082, Oct. 2006.

122. H. Gaztanaga, I. Etxeberria-Otadui, D. Ocnasu, and S. Bacha, “Real-time analysis of the transient response improvement of fixed-speed wind farms by using a reduced-scale STATCOM prototype,” IEEE Trans. Power Syst., vol. 22, no. 2, pp. 658–666, May 2007.

123. S. Muyeen, M. Ali, T. Murata, and J. Tamura, “Transient stability enhancement of wind generator by a new logical pitch controller,” IEEJ Transactions on Power Energy, vol. 126, p. 742752, 2006.

124. M. J. Hossain, H. R. Pota, V. A. Ugrinovskii, and R. A. Ramos, “Simultaneous STATCOM and pitch angle control for improved LVRT capability of fixed-speed wind turbines,” IEEE Transactions on Sustainable Energy, vol. 1, no. 3, pp. 142–151, 2010.

125. A. Moghadasi, A. Sarwat, and J. M. Guerrero, “A comprehensive review of low-voltage-ride-through methods for fixed-speed wind power generations,” Renewable and Sustainable Energy Reviews, Elsevier, vol. 55, pp. 823–839, 2016.

126. R. A. Ibrahim, M. S. Hamad, Y. G. Dessouky, and B.W. Williams, “A novel topology for enhancing the low voltage ride through capability for grid-connected wind turbine generators,” in Energy Conversion Congress and Exposition (ECCE), IEEE, pp. 2389–2395, 2012.

127. Y. Gui, C. Kim, and C. C. Chung, “Nonlinear control for PMSG wind turbine via the port-controlled Hamiltonian system,” in PowerTech, 2015 IEEE Eindhoven, pp. 1–6, 2015.

128. A. Mullane, G. Lightbody, and R. Yacamini, “Wind-turbine fault ride-through enhancement,” IEEE Transactions on Power Systems, vol. 20, no. 4, pp. 1929–1937, 2005.

129. K. Amei, Y. Takayasu, T. Ohji, and M. Sakui, “A maximum power control of wind generator system using a permanent magnet synchronous generator and a boost chopper circuit,” in Power Conversion Conference, PCC-Osaka 2002. Proceedings of the vol. 3, pp. 1447–1452, 2002.

130. M. Farhadi and O. Mohammed, “Adaptive energy management in redundant hybrid DC microgrid for pulse load mitigation,” IEEE Transactions on Smart Grid, vol. 6, no. 1, pp. 54–62, 2015.

131. F. Deng and Z. Chen, “Adaptive energy management in redundant hybrid DC microgrid for pulse load mitigation,” in Proc. IEEE IECON, p. 621626, 2009.

132. J. Matas, M. Castilla, J. M. Guerrero, L. G. de Vicuna, and J. Miret, “Feedback linearization of direct-drive synchronous wind-turbines via a sliding mode approach,” IEEE Transactions on Power Electronics, vol. 23, no. 3, pp. 1093–1103, 2008.

133. H. Heydari and A. H. Moghadasi, “Optimization scheme in combinatorial UPQC and SFCL using normalized simulated annealing,” IEEE Transactions on Power Delivery, vol. 26, no. 3, pp. 1489–1498, 2011.

134. L. Ye and L. Z. Lin, “Study of superconducting fault current limiters for system integration of wind farms,” IEEE Transactions on Applied Superconductivity, vol. 20, no. 3, pp. 1233–1237, 2010.

135. S. Muyeen, M. Ali, T. Murata, and J. Tamura, “Transient stability enhancement of wind generator by a new logical pitch controller,” IEEE Transactions on Power Energy, vol. 126, p. 742752, 2006.

136. Laghari, J.A., Mokhlis, H., Bakar, A., et al.: 'Application of computational intelligence techniques for load shedding in power systems', a review, Energy Convers. Manag, 75, pp. 130–140, 2013.

137. Hongesombut, K., Tephiruk, N.: 'Modeling of the rate of change of under-frequency relay for microgrid protection'. International Electrical Engineering Congress (iEECON), 2017.

138. Freitas, W., u, W., Affonso, M., et al.: 'Comparative analysis between ROCOF and vector surge relays for distributed generation applications', IEEE Trans. 20, (2), pp. 1315–1324, Apr. 2005.

139. Choi, J., Khalsa, A., Klapp, D. A., Illindala, M., & Subramaniam, K. (2018). Survivability of Synchronous Generator-based Distributed Energy Resources for Transient Overload Conditions in a Microgrid. IEEE Transactions on Industry Applications, 1–1. doi:10.1109/tia.2018.2854622

140. Edwards, W., & Manson, S. (2018). Using protective relays for microgrid controls. 2018 71st Annual Conference for Protective Relay Engineers (CPRE). doi:10.1109/cpre.2018.8349834

141. E. Sortomme, S. S. Venkata, and J. Mitra. “Microgrid protection using communication assisted digital relays.” IEEE Trans. Power Delivery, vol.25, pp. 2789 - 2796, Oct. 2010.

142. Vieira, J., Freitas, W., Xu W., et al. : 'Efficient Coordination of ROCOF and Frequency Relays for Distributed Generation Protection by Using the Application Region', IEEE Transactions on power delivery, 21, (4), pp. 1878 – 1884, Oct. 2006.

143. V. Yaramasu, B. Wu, S. Alepuz, and S. Kouro, “Predictive control for low-voltage ride-through enhancement of three-level-boost and NPC-converter-based PMSG wind turbine,” IEEE Transactions on Industrial Electronics, vol. 61, no. 12, pp.6832–6843, 2014.

144. W. Qiao, G. Venayagamoorthy, and R. Harley, “Real-time implementation of a STATCOM on a wind farm equipped with doubly fed induction generators,” IEEE Transactions on Industry Applications, vol. 45, no. 1, pp. 98–107, 2009.

145. Y. Tang, P. Ju, H. He, C. Qin, and F. Wu, “Optimized control of DFIG-based wind generation using sensitivity analysis and particle swarm optimization,” IEEE Transactions on Smart Grid, vol. 4, no. 1, pp. 509–520, 2013.

146. “Grid connection of wind turbines to networks with voltages below 100 kV,” Regulation TF 3.2.6, Energinet, Frederica, Denmark, 2004.

147. M. Narimani and R. K. Varma, “Application of static var compensator (SVC) with the fuzzy controller for grid integration of wind farm,” in Electrical and Computer Engineering (CCECE), 2010 23rd Canadian Conference on, pp. 1–6, 2010.

148. M. Molinas, J. A. Suul, and T. Undeland, “Low voltage ride through of wind farms with cage generators: STATCOM versus SVC,” IEEE Transactions on Power Electronics, vol. 23, no. 3, pp. 1104–1117, 2008.

149. R. J. Koessler, “Dynamic simulation of static VAr compensators in distribution systems,” in Transmission and Distribution Conference, 1991., Proceedings of the IEEE Power Engineering Society, 1991, pp. 273–279.

150. A. D. Rosso, C. Canizares, and V. Dona, “A study of TCSC controller design for power system stability improvement,” IEEE Transactions on Power Systems, vol. 18, no. 4, pp. 1487–1496, 2003.

151. E. V. Larsen, K. Clark, S. A. Miske, and J. Urbanek, “Characteristics and rating considerations of thyristor controlled series compensation,” IEEE Transactions on Power Delivery, vol. 9, no. 2, pp. 992–1000, 1994.

152. Z. Chen, J. M. Guerrero, and F. Blaabjerg, “A review of the state of the art of power electronics for wind turbines,” IEEE Transactions on Power Electronics, vol. 24, no. 8, pp. 1859–1875, 2009.

153. H. Gaztanaga, I. Etxeberria-Otadui, S. Bacha, and D. Roye, “Fixed-speed wind farm operation improvement by using DVR devices,” in Industrial Electronics, 2007. ISIE 2007. IEEE International Symposium on, pp. 2679–2684, 2007.

154. D. Ramirez, S. Martinez, C. A. Platero, F. Blazquez, and R. M. de Castro, “Low-voltage ride-through capability for wind generators based on dynamic voltage restorers,” IEEE Transactions on Energy Conversion, vol. 26, no. 1, pp. 195–203, 2011.

155. J. A.Wiik, F. D.Widjaya, T. Isobe, T. Kitahara, and R. Shimada, “Series connected power flow control using magnetic energy recovery switch (MERS),” in Power Conversion Conference - Nagoya. PCC ’07, pp. 983–990, 2007.

156. J.Wiik, F.Wijaya, and R. Shimada, “Characteristics of the magnetic energy recovery switch (MERS) as a series FACTS controller,” IEEE Transactions on Power Delivery, vol. 24, no. 2, pp. 828–836, 2009.

157. A. R. Fereidouni, B. Vahidi, and T. H. Mehr, “The impact of solid-state fault current limiter on power network with wind-turbine power generation,” IEEE Transactions on Smart Grid, vol. 4, no. 2, pp. 1188–1196, 2013.

158. H. G. Sarmiento, R. Castellanos, G. Pampin, C. Tovar, and J. Naude, “An example in controlling short circuit levels in a large metropolitan area,” in Power Engineering Society General Meeting, IEEE, vol. 2, 2003, p. 594 Vol. 2, 2003.

159. M. Firouzi and G. B. Gharehpetian, “Improving fault ride-through capability of the fixed-speed wind turbine by using a bridge-type fault current limiter,” IEEE Transactions on Energy Conversion, vol. 28, no. 2, pp. 361–369, 2013.

160. M. Jafari, S. B. Naderi, M. T. Hagh, M. Abapour, and S. H. Hosseini, “Voltage sag compensation of point of common coupling (PCC) using fault current limiter,” IEEE Transactions on Power Delivery, vol. 26, no. 4, pp. 2638–2646, 2011.

161. G. Rashid and M. H. Ali, “A modified bridge-type fault current limiter for fault ride-through capacity enhancement of fixed speed wind generator,” IEEE Transactions on Energy Conversion, vol. 29, no. 2, pp. 527–534, 2014.

162. Y. Salami and M. Firouzi, “Dynamic performance of wind farms with the bridge- type superconducting fault current limiter in distribution grid,” in Electric Power and Energy Conversion Systems (EPECS), 2nd International Conference on, pp. 1–6, 2011.

163. M. T. Hagh, K. M. Muttaqi, D. Sutanto, M. S. A. Hossain, and A. M. A. Haidar, “Improving fault ride-through capability of DFIG based wind generators by using bridge-type superconducting fault current limiter,” in Power Engineering Conference (UPEC), 2015 50th International Universities, pp. 1–6, 2015.

164. N. G. Jayanti, M. Basu, M. F. Conlon, and K. Gaughan, “Rating requirements of the unified power quality conditioner to integrate the fixed speed induction generator-type wind generation to the grid,” IET Renewable Power Generation, vol. 3, no. 2, pp. 133–143, 2009.

165. A. Moghadasi, H. Heydari, and M. Salehifar, “Reduction in VA rating of the unified power quality conditioner with superconducting fault current limiters,” in Power Electronic Drive Systems Technologies Conference (PEDSTC), pp.382–387, 2010.

166. A. Moghadasi and A. Islam, “Enhancing LVRT capability of FSIG wind turbine using current source UPQC based on resistive SFCL,” TD Conference and Exposition, 2014 IEEE PES, pp. 1–5, 2014.

167. P. Huang, M. Moursi, W. Xiao, and J. Kirtley, “Fault ride-through configuration and transient management scheme for self-excited induction generator-based wind turbine,” IEEE Transactions on Sustainable Energy, vol. 5, no. 1, pp. 148–159, 2014.

168. B. Gromoll, G. Ries, W. Schmidt, H.-P. Kramer, P. Kummeth. Neumuller, “Resistive current limiters with YBCO films s,” IEEE Transactions on Applied Superconductivity, vol. 7, no. 2, pp. 828–831, 1997.

169. D. K. Park, M. C. Ahn, S. E. Yang, Y. S. Yoon, B. Y. Seok, C. Lee, H. M. Chang, and T. K. Ko, “Development of 220 v/300 a class non-inductive winding type fault current limiter using 2g HTS wire,” IEEE Transactions on Applied Superconductivity, vol. 17, no. 2, pp. 1863–1866, 2007.

170. H. Shimizu, Y. Yokomizu, M. Goto, T. Matsumura, and N. Murayama, “A study on the required volume of the superconducting element for flux flow resistance type fault current limiter,” IEEE Transactions on Applied Superconductivity, vol. 13, no. 2, pp. 2052–2055, 2003.

171. Mohamed M. Aly, and Emad A. Mohamed, “Enhancement of Multi-Machine Power System Transient Stability Using Superconducting Fault Current Limiters with YBCO and Bi-2212”, International Journal on Power Engineering and Energy (IJPEE), Vol.4, No.2, January 2014.

172. G.s.malhi “Studies of Fault Current Limiters for Power System Protection” Ph.D. thesis, Institute of information sciences and technology, Massey University, 2007.

173. Mohamed Ebeed, Omar NourEldeen, and A .A.Ebrahim, “Assessing Performance of Crowbar Protections with The DFIG under Grid Fault” International Journal on Power Engineering and Energy (IJPEE), Vol.4, No.2, April 2013.

174. W. Guo et al., “LVRT capability enhancement of DFIG with switch type fault current limiter,” IEEE Trans. Ind. Electron., vol. 62, no. 1, pp. 332–342, Jan. 2015.

175. N. Gupta, “Stochastic optimal reactive power planning and active power dispatch with large penetration of wind generation,” J. Renew. Sustain. Energy, vol. 10, no. 2, p. 25902, Mar. 2018.

176. Abraham, R. J., Das D., Patra, A.: 'Automatic generation control of an interconnected hydrothermal power system considering superconducting magnetic energy storage', Int. J. Electr. Power Energy Syst., 2007, 29, (8), pp. 571–579.

177. Al-Attar Ali Mohamed, Yahia S. Mohamed, Ahmed A.M. El-Gaafaryb, Ashraf M. Hemeida, “Optimal power flow using moth swarm algorithm”, Electric Power Systems Research, Vol. 142, pp. 190–206, 2017.

178. Meier, S., Kunsman, S.: 'Protection and control System Impacts from The Digital World', 69th Annual Conf. for Protective Relay Engineers (CPRE), College Station, TX, USA, 2016.

179. Shabib, G.: 'Digital Design of a Power System Stabilizer for Power System Based on Plant-Input Mapping', International Journal of Electrical Power & Energy Systems (IJEPES), 49, pp. 40–46, July 2013.

180. Magdy G.: 'Digital Redesign of Analog Controllers for Power Systems Using PIM' (SIA OmniScriptum Publishing, Riga, Latvia, European Union, pp. 1-164, 2016.

181. Shabib, G., Esam, H., Magdy, G.: 'A New Approach to the Digital Implementation of Analog Controllers for a Power System Control', International Journal of Scientific & Engineering Research (IJSER), 5, (10), pp. 419-427, October 2014.

182. Rabbath, C. A., Lechevin, N., 'Discrete-Time Control System Design with Applications', (New York Heidelberg Dordrecht London, Springer, 2014.

183. Yassin, K., Abd-Raboh, E., Al-Domany, M.: 'Fast Power System Restoration Via Load Shedding Practices in Egyptian Power System', Mansoura Engineering Journal, 17, (1), pp. 1-20, 1992.

184. Bhatt, P., Roy, R., Ghoshal, S.: 'Dynamic Participation of Doubly Fed Induction Generator in Automatic Generation Control', Renewable Energy, 36, (1), pp. 1203-1213, 2011.

185. Kerdphol, T., Rahman, F., Mitani, Y., et al.: 'Virtual inertia Control Based Model Predictive Control for Microgrid Frequency Stabilization Considering High Renewable Energy Integration', Sustainability, Vol. 9, (1), pp. 1-21, 2017.

186. Rizk, Mariam (4 Sep 2014). "Light gradually returns to Egypt after cities-wide blackout". Al-Ahram Weekly. Al-Ahram. Retrieved 5 September 2014.